BASIC AND APPLIED STUDIES WITH

UNSEGMENTED CONTINUOUS

FLOW SYSTEMS

By

SHAOFENG LI

Bachelor of Science

Nankai University

Tianjin, P. R. China

1982

Submitted to the Faculty of the
Graduate College of the
Oklahoma State University
in partial fulfillment of
the requirements for
the Degree of
DOCTOR OF PHILOSOPHY
December, 1995

BASIC AND APPLIED STUDIES WITH

UNSEGMENTED CONTINUOUS

FLOW SYSTEMS

Thesis Approved:

Horacio A Mottola

_____
Thesis Adviser

Ziad El Rassi

_____

Richard A. Bunce

_____

_____

Thomas C Collins

_____
Dean of the Graduate College

ACKNOWLEDGMENTS

TABLE OF CONTENTS

LIST OF TABLES

LIST OF FIGURES

CHAPTER I

INTRODUCTION TO UNSEGMENTED

CONTINUOUS FLOW

Unsegmented Continuous Flow

Unsegmented continuous flow (UCF) is a sample/reagent(s) processing technique in

the field of automatic analytical methods. It has been widely used in most areas of

analytical chemistry, such as pharmaceutical, food, environmental, clinical, biochemical

and agricultural analysis, because of its simplicity, reproducibility, small sample size

requirement, low cost, high sampling rate, and extreme versatility.

From the late 1960's to the mid 1970's much pioneering work in UCF was done

[1,2,3,4,5]. Conventionally, the history of UCF is traced back to the work of Ruzicka and

Hansen [6], as well as Stewart et al. [7] in the mid 1970's, in which UCF was called "flow

injection analysis" (FIA). Their work made UCF recognized and accepted by analytical

chemists and stimulated the further studies of its theory and applications. At that time, "all

these contributions directly or indirectly tried to provide alternatives to achieve the goals

for automatic wet chemical analysis already cited: more determinations per unit of time

and less expensive determinations" [8].

1

In the early time of UCF history, a large number of chemistries and techniques, such as liquid-liquid extraction [9], hydride generation [10], gas diffusion [11], immunoassays [12], and determinations with immobilized enzymes [13] were integrated into an UCF system and found many useful applications. With the development of UCF and the growth of its applications, it has been realized that UCF is not only an automatic tool or an interface for analysis, but also a generally applicable solution sample/reagent(s) processing technique [14,15]. It can be used to enhance the sensitivity and selectivity of some analytical techniques, to control and monitor kinetic aspects of automated analysis [16], and to measure the rate coefficient(s) of a physicochemical process that is taking place in the UCF system [17]. Since the mid 1970s, more than 5000 papers have been published on UCF (or FIA) studies.

As an automated analytical technique, UCF presents the following essential features:

1. The flow is not segmented.

2. The introduced sample plug is carried along the system, and a physicochemical process (chemical reaction, dialysis, extraction, etc.) may take place in addition to the mass transport process.

3. The partial dispersion of the analyte throughout its transport can be controlled by changing the geometric and hydrodynamic characteristics of the system.

4. Neither physical nor chemical equilibrium needs to be attained when the signal is detected.

5. Because measurements can be made under non-equilibrium conditions, the operational time must be highly reproducible.

Basic Scheme of an UCF System

A basic UCF system, shown in Figure 1, consists of four basic parts: the propelling unit, the sample introduction system, the flow path, and the sensing unit.

The propelling unit generates a constant flow of solution, containing a dissolved reagent or acting as a carrier of the reagent or analyte. The flow is usually laminar. Peristaltic pumps, gas-pressure systems or even gravitation can be used as propelling units.

The sample introduction system makes the reproducible introduction of an accurately measured sample volume into the flow system. In early work, hypodermic syringes were used to inject the sample into the stream [6]. That is why UCF is also called "flow injection analysis" (FIA). Presently, rotary valves are the most commonly used devices for sample introduction.

The flow path can be made of a straight, coiled, or knotted tubing, with or without a reactor. Sample transport and chemical reaction(s) can take place in this part. The sample concentration profile is dependent on the transport process in the tubing. The reactor can be a mixing chamber or a tube packed with a chemically active material, like a redox or ion-exchange resin, immobilized enzymes, etc. In the first part of the work described in this dissertation, for example, a coiled tubing was used for the basic study of

propelling unit   sample   flow path   sensing unit
introduction
system

sample   detector

pump   tubing/reactor   waste

readout

carrier/reagent
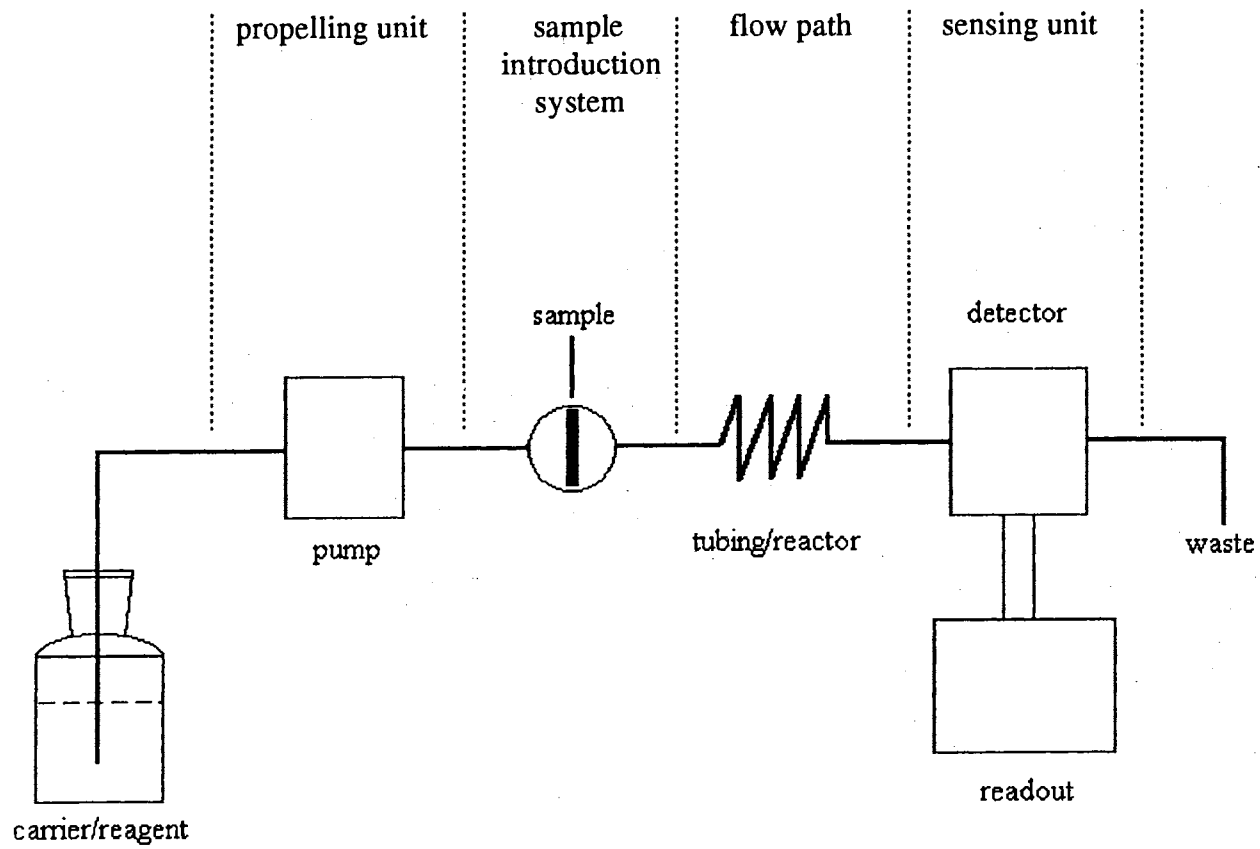
Figure 1. Schematic Representation of a Basic UCF System.

the diffusion process in an UCF system. In the second and third parts of this dissertation, integrated rotating bioreactors/detector units with immobilized enzymes were employed for the determination of substrate or an inhibitor concentrations in enzyme catalyzed bioreactions, respectively. Therefore, by modifying the flow path in the UCF system, extreme versatility can be achieved.

In the sensing unit a flow-through cell is positioned in the detection system such as a photometer, a fluorimeter, or an electrochemical cell. This unit can be integrated with a reactor in the flow path to directly monitor the process within the reactor. The detector transduces the physical or chemical property which is proportional to the analyte concentration and feeds electrical information into a readout device, such as a recorder or a computer, to display the analytical information.

Usually the flow emerging from the sensing unit goes to waste, but sometimes it is recirculated through a pump, such as the closed-loop system used for the determination of glucose by Bergmeyer and Hagen [3].

In a basic UCF system a computer or microprocessor with an interface is needed for automation and to obtain greater reproducibility in a given determination. Many computerized UCF instruments are commercially available today.

Unsegmented Continuous Flow Signals

Because sample transport, chemical reaction, and signal measurement in a UCF system are time-dependent, the response of the detection unit is in the form of a transient signal [18]. This signal is commonly recorded as a peak on a recorder chart or a computer display. A typical UCF signal is shown in Figure 2. This is a plot of the analytical signal

t_R: residence time
h: peak height
Δt_b: baseline-to-baseline peak width
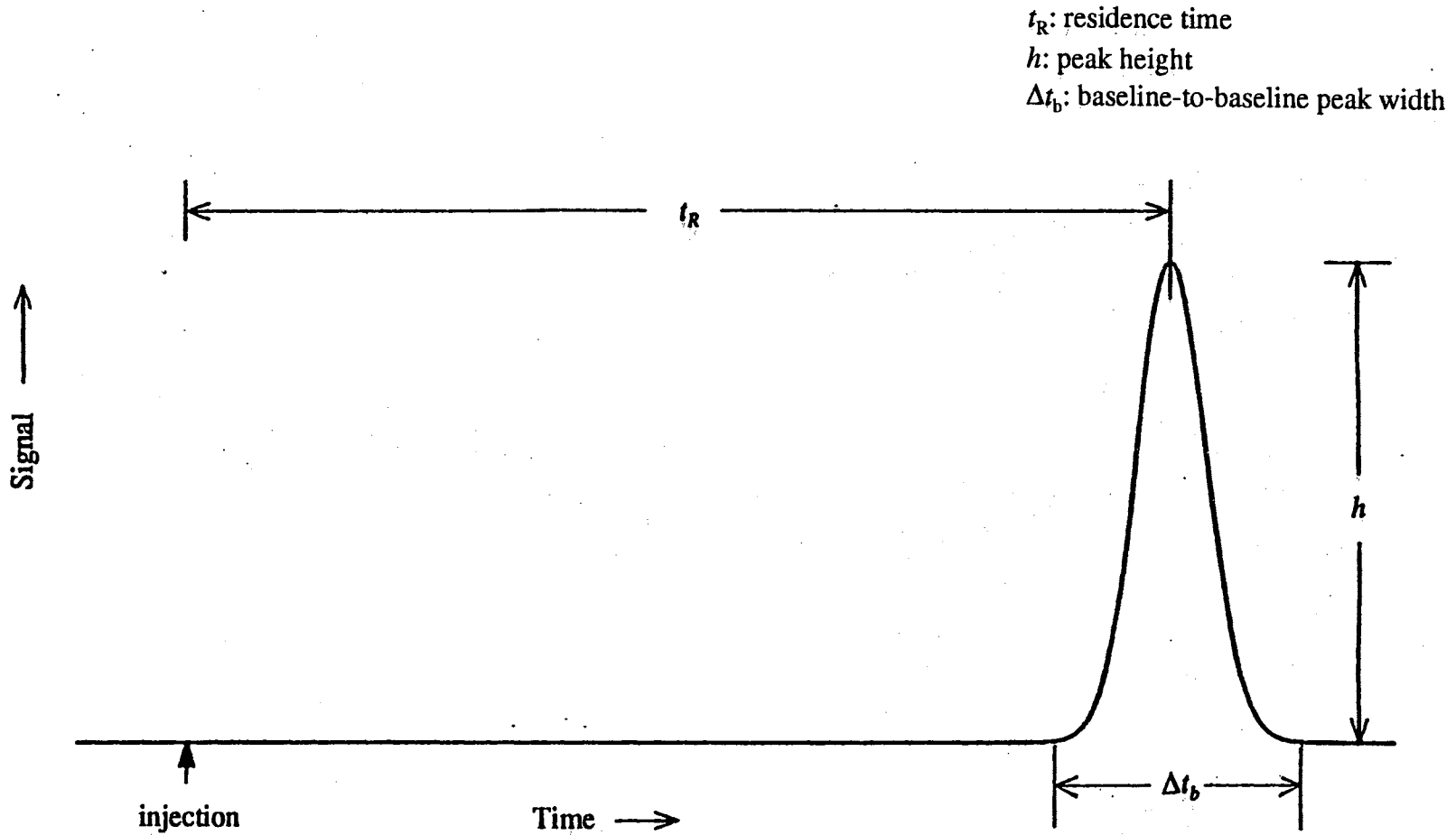
Figure 2. UCF Signal

(e.g., absorbance, fluorescence intensity, electrode potential or electrical current) as a function of time. The signal profile (or curve shape) is influenced by the chemical reaction(s) in the flow path and by the dispersion of the species under study in the injected sample. The detail of the relationship between reaction rate or dispersion of analyte and the signal profile will be discussed in the following chapters. From a UCF signal, the following features can be obtained for interpreting the analytical information:

1. Peak height, h, which is related to the concentration of the component being determined in the injected sample. The peak area can also be used to determine the concentration if integration is performed.

2. Residence time, t_R, which is the time elapsed from injection until the maximum signal is attained. It is related to the length of the flow path between the injection point and the detection site, as well as the flow rate.

3. Baseline-to-baseline time, Δt_b, is the interval between the start of the signal and its return to the baseline. As it will be discussed in the next chapter, this parameter is a measure of the dispersion of the analyte-containing sample plug.

4. If the stopped-flow method is used [19], a chemical reaction rate can be represented by the slope of the leading part of an UCF peak. That is, the transient signal shows the kinetic characteristics of the reaction taking place in the flow-through cell.

Because of the characteristics described previously, UCF can be used in many sophisticated processes. One example is the application of UCF in biosensor studies. In studies of biosensors, UCF can provide very accurate time control for some of the specific

7

steps involved, such as incubation time and the time to obtain maximum response. Also, the volumes of substrate, cofactor and dye used in some biosensor studies can be handled very accurately by using a UCF system. For some analytical tasks, it is hard to imagine how to collect accurate and reproducible results without the help of UCF to manage the processing of the sample and reagent(s).

The research described in this dissertation encompasses basic as well as applied studies with UCF systems. In Chapter 2, based on the study of the fundamental characteristic of UCF, that is, the control of dispersion, the determination of the molecular diffusion coefficients of some Fe(II) complexes with ligands containing the $=N-C=C-N=$ moiety was investigated. In Chapters 3 and 4, the concentration of glucose in serum and phosphate in water samples was determined by using integrated bioreactor/detector units and the stopped-flow approach. Glucose acts as the substrate in an oxidation reaction catalyzed by glucose oxidase [EC 1.1.3.4], and phosphate acts as an inhibitor of alkaline phosphatase [EC 3.1.3.1] which catalyzes the hydrolysis of a phosphate ester. Both enzyme-catalyzed reactions were implemented in UCF systems by immobilizing the enzymes on inert surfaces and incorporating the enzyme preparation into rotating reactors.

CHAPTER II

DETERMINATION OF THE MOLECULAR

DIFFUSION COEFFICIENT OF

SOME Fe(II) COMPLEXES

Background

Fick's Laws and the Stokes-Einstein Relation

The transport of mass from one location to another in solution takes place in many chemical processes. The molecular scale mass transport is called diffusion and the bulk motion is known as convection. Many chemical reactions in solution have elementary steps that are diffusion-controlled [20]. In many analytical methodologies diffusion is the most important mechanism of mass transport. In chromatography, diffusion has a significant effect on the efficiency and resolution of separations [21]. The diffusion of electroactive species to electrodes is a critical step in electroanalysis [22] because it controls the intensity and dynamic range of the signal transduced from the electrode. Knowledge of the diffusion coefficient of macromolecules is very important in biochemical and biophysical analysis because this quantity is related to the mass and shape of these substances [23]. As will be discussed later, diffusion greatly contributes to dispersion in UCF sample/reagent processing.

Like the transfer of heat from a point of higher temperature to a point of lower temperature in a thermoconductor, diffusion is the mass transfer of matter from a region of higher concentration to a region of lower concentration in a solution. The heat transfer is forced by the temperature gradient in the thermoconductor, and the concentration gradient (or chemical potential gradient in dilute solution) drives the mass diffusion in the solution. This similarity between heat transfer and diffusion was discovered by Fick [24], who argued by analogy with Fourier's treatment of heat conduction, that one could simply replace the temperature gradient in Fourier's equation (Eq. 2. 1) with the concentration gradient to propose what is now known as his first law of diffusion [25] (Eq. 2. 2).

$$J_q = - k(dT/dx) \quad \text{(Fourier's law)} \tag{2.1}$$

$$J_i = - D(dC_i/dx) \quad \text{(Fick's first law)} \tag{2.2}$$

The fluxes, J_q and J_i, are the amount of heat and mass of i passing through a defined reference plane perpendicular to the direction of flow with unit area, A, per unit time in their media; k and D are the thermoconductivity and the diffusion coefficient, respectively; dT/dx and dC_i/dx are the temperature gradient and the concentration gradient, respectively, in the dimension of x. The negative sign in the equations means that the flows are opposite to the direction of the gradients.

The gradient is time dependent, e.g. the concentration is a function of time and position. As shown in Figure 3, for the diffusion of a component i in solution across the reference planes of unit area, A, placed normal to the flow at x and x + δx, the fluxes are given by J_i and $J_i + (\partial J_i/\partial x)\delta x$. The component i accumulates in the volume element of

10

A: reference plane (unit area)

J_i: amount of component i passing through

the reference plane per unit time

δx: the thickness of the volume

x: the dimension of the flow of i
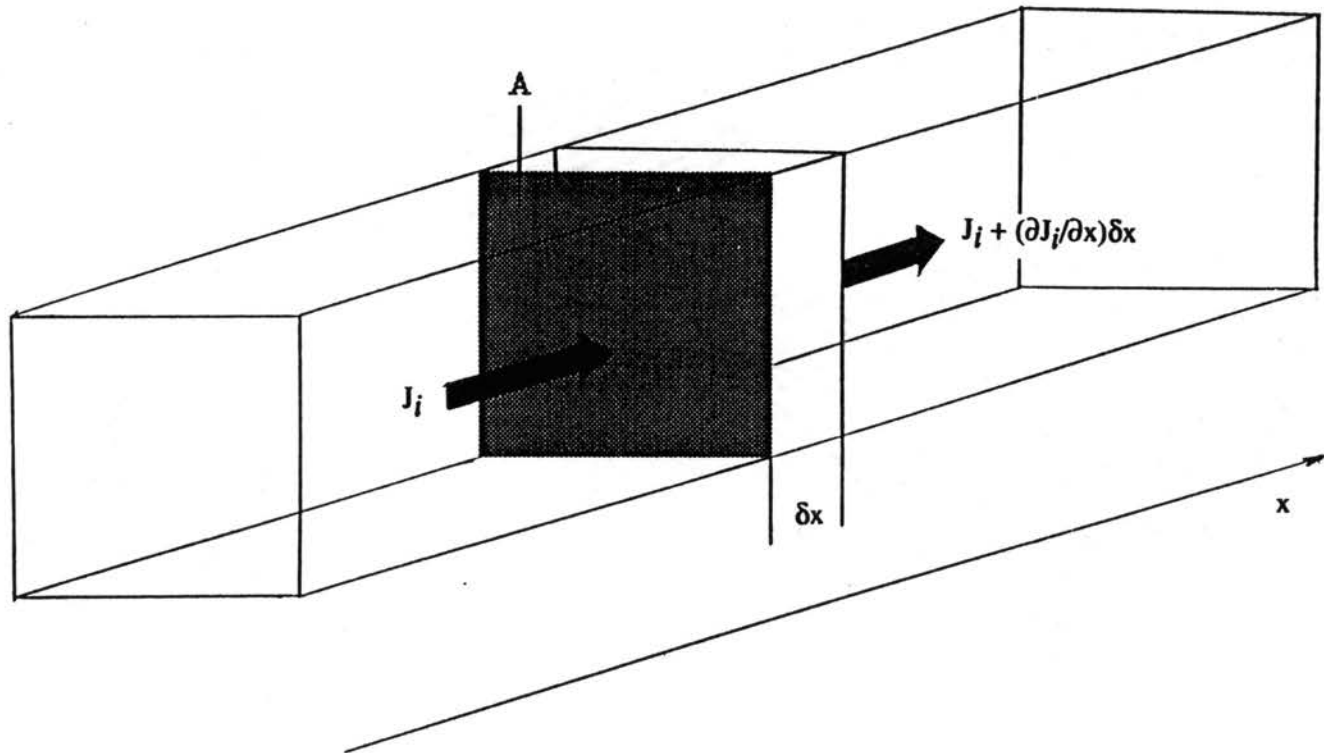
Figure 3. Flow of Species i in Dimension x

unit cross-section and thickness δx. This accumulation causes an increase in the concentration of i within this volume element. The increase is given by:

$$\partial C_i / \partial t = \{J_i - [J_i + (\partial J_i / \partial x)\delta x]\}/\delta x = -\partial J_i / \partial x \qquad (2.3)$$

Using Fick's first law:

$$J_i = -D_i(\partial C_i / \partial x)$$

$$\partial J_i / \partial x = -\partial [D_i(\partial C_i / \partial x)]/\partial x \qquad (2.4)$$

If D_i is independent of x,

$$\partial J_i / \partial x = -D_i(\partial^2 C_i / \partial x^2) \qquad (2.5)$$

Combining equation (2.3) and (2.5) gives:

$$\partial C_i / \partial t = D_i(\partial^2 C_i / \partial x^2) \qquad (2.6)$$

Equation (2.6) is called Fick's second law of diffusion. It is of considerable importance, as is his first law, in the interpretation of experimental work in a system with diffusion. Also from such experimental work, the diffusion coefficient, D_i, can be determined by solving these two equations (2.2) and (2.6) which are subject to the boundary conditions appropriate to the particular experimental arrangement.

The process of diffusion may be modeled by a sphere moving in a fluid. The motion of the sphere is slowed down by collisions with the fluid. The repeated collisions with the fluid translate into a frictional force from the fluid which retards the motion of the sphere. According to Einstein [26] the diffusion coefficient is inversely proportional to the frictional coefficient ζ:

$$D = \kappa T/\zeta \qquad (2.7)$$

12

where κ is the Boltzmann constant and T is the temperature.

Stokes [27] has shown that, if the diffusing particle is considered very large in comparison to the fluid particle, the frictional force is proportional to the solvent viscosity, η, and the radius of the diffusing sphere, r:

$$\zeta = 6\pi\eta r \tag{2.8}$$

Combining equations (2.7) and (2.8) the Stokes-Einstein equation can be obtained:

$$D = \kappa T/6\pi\eta r \tag{2.9}$$

This equation shows that the diffusion coefficient of a species is inversely proportional to its radius. That is, the plot of D vs. $1/r$ should give a straight line for different species in the same medium and at the same temperature.

Experimental Methods for the Determination of D

There are several methods that can be used for the determination of diffusion coefficients [28], such as the diaphragm cell method [29], NMR spin-echo [30], electrochemical methods [31,32], and UCF methods based on the original work of Taylor [33].

Diffusion coefficients for the species of relevance in analytical chemistry are frequently determined by electrochemical methods (e.g. polarography, chrono-potentiometry, chronoamperometry, and chronocoulometry) and only occasionally by a UCF method [34]. In comparison with other methods, the UCF approach has following advantages:

1. It is faster (diaphragm cell methods, for instance, require 1 to 3 days for a measurement).

2. The instrument, measurement, and calculations are simple.

3. Different types of detection can be used.

4. The cost is low.

As it will be seen in the next section, the disadvantage is that this method may require a reference standard in order to calibrate the UCF system.

Determination of *D* with an UCF System

According to hydrodynamics, for a liquid flowing under laminar flow conditions through a narrow tube, there is a parabolic distribution of velocity over any cross-section normal to the tube axis. The liquid at the center of the tube moves at twice the average flow velocity. As first observed by Griffiths [35], when a plug of liquid of different chemical composition is intercalated into the laminar stream, the plug shape is spread by the stream into a parabolic bolus after a given time, t. Taylor [33] later explained the band spreading as the result of both convection and diffusion contributing to mass transport. As shown in Figure 4, The initial expansion is predominantly due to convection. However, after a longer time, convection and diffusion govern the band spreading which is called convection-diffusion controlled (or Taylor) dispersion. The shape of the UCF signal is significantly affected by the dispersion processes.

Taylor has solved his equation which describes the convection and diffusion under laminar flow conditions within a narrow round tubing by using Fick's laws, and he has shown that under convection-diffusion control, if the time after the introduction of the

Sample plug   concentration profile

a. Injection

b. Convection

c. Convection-diffusion

d. Diffusion

t = 0   Time
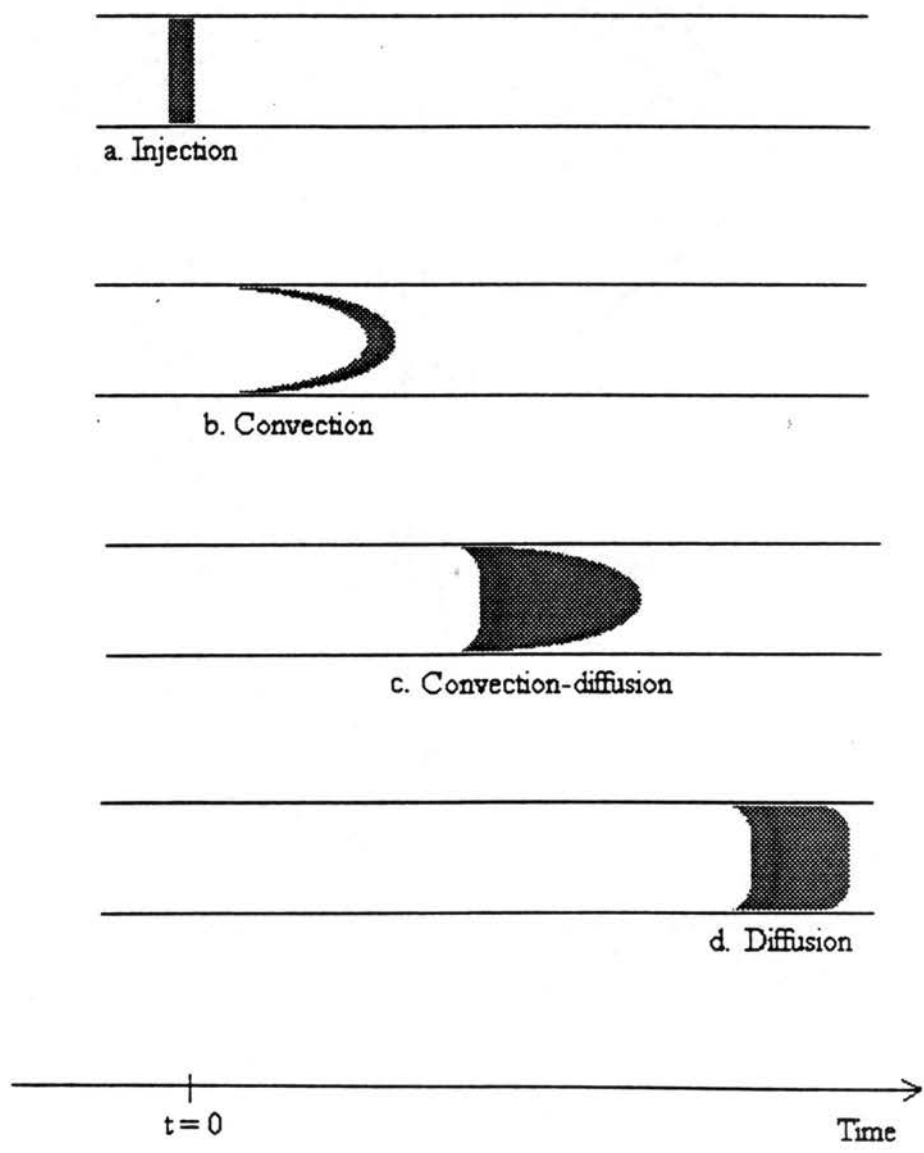
Figure 4. Dispersion in Laminar Flow.

15

sample plug is long enough, diffusion is responsible for the majority of the band spreading. He also stated that if

$$L/u \downarrow [2r^2/(3.8)^2D] \qquad (2.10)$$

where L is the tube length, u is the average flow velocity, r is the tube radius, and D is the diffusion coefficient of the species in the intercalated plug, the radial diffusion controls the dispersion of the species out of the plug boundaries. In such a case the concentration distribution with time in the region defined by the leading and tailing fronts of the plug should be, ideally, Gaussian (as shown in Figure 5) and characterized by a variance:

$$\sigma^2 = (2Dt/u^2) + (r^2 t/24D) \qquad (2.11)$$

in which t is the time elapsed from the point of intercalation to the point of detection of the maximum concentration in the distribution, that is the residence time in an UCF system. Usually, the values of D for solutes are in the order of 10^{-5} cm^2 s^{-1} or even less in liquid solutions. If in a given experiment, u is sufficiently low (long residence time) and r is very small, the first term in equation (2.11) can be neglected, and:

$$\sigma^2 = r^2 t/24D \qquad (2.12)$$

Since in a perfectly Gaussian peak, the peak width at half height, $w_{1/2}$, corresponds to 2.354σ, we have:

$$\sigma^2 = (w_{1/2})^2/5.54 \qquad (2.13)$$

Combining equations (2.11) and (2.12), the following is obtained:

$$(w_{1/2})^2 = 5.54r^2 t/24D \qquad (2.14)$$

diffusion coefficient: $D_1 > D_2$

residence time: $t_1 < t_2$

variance: σ

peak width at half height: h

t_1

t_2

$w_{1/2}$

4σ
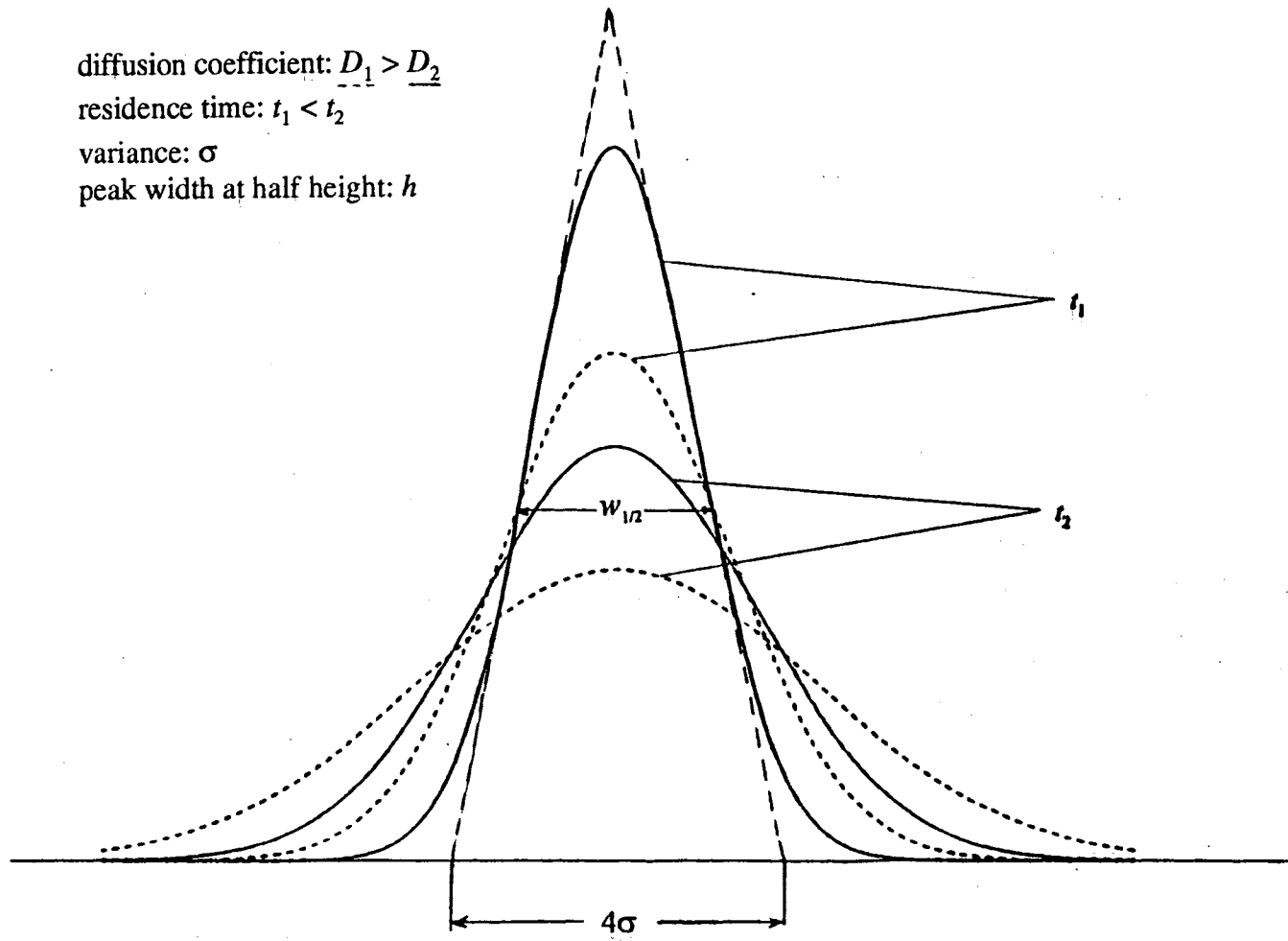
Figure 5. Diffusion-Controlled Concentration Distribution in UCF System

17

Experimentally, t and $w_{1/2}$ can be estimated by changing the flow rate, and a plot of $(w_{1/2})^2$ vs. t allows the calculation of D from the slope of the resulting straight line. The calculation of D, however, requires a knowledge of r, a value that can be obtained by direct measurement or by calibration against standards. The method with direct measurement of r is an absolute method [37], but the relative method that uses standards is more commonly used [38,39,40,41] because of its accuracy and simplicity.

In an effort to reduce the experimental time, solutions to the Taylor's convection-diffusion equation for high flow rate have been provided [42,43]. These solutions are solved using numerical analysis of the observed peak using high flow rates under specific experimental conditions. One such significant contribution to the numerical treatment was done by Vanderslice et al. [44,45] who adapted the approach of Ananthakrishnan et al. [43,46] by numerically solving Taylor's convection-diffusion equation to account for the dispersion occurring at both boundaries of an injected sample plug at high flow rate. The numerical solution is based on the method of alternating direction implicit finite difference approximation [47]. In Vanderslice's first paper [44], the following empirical equation can be found which permits the determination of D by the UCF method at high flow rate:

$$\Delta t_b = (35.4 r^6 f / D^{0.36})(L/u)^{0.64} \tag{2.15}$$

where Δt_b is the baseline-to-baseline peak width of the Gaussian peak and f is a correction factor (concentration and detector sensitivity factor). If in the experiments r, L, f, and u are kept constant, equation (2.14) reduces to :

$$\Delta t_b = X / D^{0.36} \tag{2.16}$$

18

where X is a calibration factor that can be obtained with the help of a standard. If X is

known, an unknown D can be calculated by using:

$$D = (X/\Delta t'_b)^{2.778} \tag{2.17}$$

in which $\Delta t'_b$ is the baseline-to-baseline peak width for the species under study. Equation

(2.16) is valid if

$$0.002 \leq 30\pi DL/u \tag{2.18}$$

[48] and all experimental parameters used to calculate X with a standard are duplicated in

determining D for the species of interest.

Gerhardt and Adams [49] used the above approach to determine diffusion

coefficients for biogenic amine neuro-transmitter related compounds. In their experiment,

they calibrated the UCF system with a substance whose diffusion coefficient was known.

They also found that the peak heights must be reproduced to within 5% to obtain accurate

values of the diffusion coefficients.

In the experimental determination of D with a UCF system, the measurement of Δt_b

is usually done with a ruler, but $w_{1/2}$ for a peak can be measured automatically with an

electronic integrator. To use an integrator for his work, Robinson [50] related Δt_b with $w_{1/2}$

as follows:

$$\Delta t_b = (4w_{1/2})2.355 \tag{2.19}$$

In this part of the dissertation, Vanderslice's method was employed (with n UCF

system described in the next section) for the determination of molecular diffusion

coefficients in solution of a series of Fe(II) complexes with ligands containing the

chelating moiety =N-C=C-N= present in 1,10-phenanthroline, its substituted derivatives,

and some other analytical ligands. These determinations were prompted by the need for

such diffusion coefficient values in a study on the characterization of chemically modified

conducting surfaces. Two detection methods, amperometric and photometric, were

employed, and the results are compared. The reference standard used for the

determination was Solochrome Violet RS . The value of D for this chemical species in the

same medium was determined by polarography.

Experimental

Reagents and Solutions

All reagents used were of AR grade, except as noted. All ligands, L, form complexes

with Fe(II) in a 3:1 ligand-metal ion ratio and were purchased from GFS Chemicals

(Columbus, OH). Solochrome Violet RS was from K&K Labs (Cleveland, OH). The

complexes containing perchlorate as counterion were prepared by mixing

stoichiometrically an aqueous solution of $Fe(NH_4)_2(SO_4)_2$ with the ligand dissolved in

acetone and then precipitating the perchlorate salt, $FeL_3 \cdot 2ClO_4$ by addition of $NaClO_4$.

Other complexes were directly purchased from GFS Chemicals and used as received.

The water used for solution preparation was deionized and further purified by

distillation in an all-borosilicate-glass still with a quartz immersion heater. The carrier

solution, 0.036 M in H_2SO_4, was prepared with acetonitrile-water (74.6 : 25.4).

Acetonitrile was required to solubilize some of the rather high molecular weight ligands

and at the same time to provide a suitable conducting medium for the electrochemical

detection. All injected samples (4.20 μL) of Fe(II) complexes were 1.00×10^{-3} M in complex and used the carrier as solvent. The 0.0040 M Cd^{2+} solution was prepared with $CdCl_2$ in 0.20 M HCl.

Apparatus

A block diagram of the single-line UCF system used in this work is shown in Figure 6. In this system, the pump (Model 396, Laboratory Data Control/Milton Roy, Riviera Beach, FL) was used to feed the carrier solution from the reservoir into the delivery bottle, which propelled the solution by gravitational flow (typically at a rate of 0.30 ml min^{-1}), through the feed line. The overflow line was used to keep the liquid level in the delivery bottle, and correspondingly the flow into the following units, constant. Gravitational flow provides a very effective pulse-free flow, essential for the preservation of the laminar flow conditions, and helps to eliminate detection artifacts with amperometric detection. The flow path (defining the residence time) was 400 cm long and was provided by a coiled tubing (25 cm coil diameter). All tubing was PTFE and had an i.d. of 0.06 cm (Cole-Parmer, Chicago, IL).

Photometric detection was accomplished with a Spectronic 21 spectrophotometer (Bausch and Lomb, Rochester, NY) equipped with a quartz ultra-micro flow cell with a volume of 20 μL (NSG Precision Cells, Farmingdale, NY). The wavelengths used for detection are listed in Table I. Amperometric detection (applied potentials also listed in Table I) was accomplished with a thin-layer cell equipped with a glassy carbon sensing surface (Bioanalytical Systems, West Lafayette, IN) in a three-electrode system [51].

21
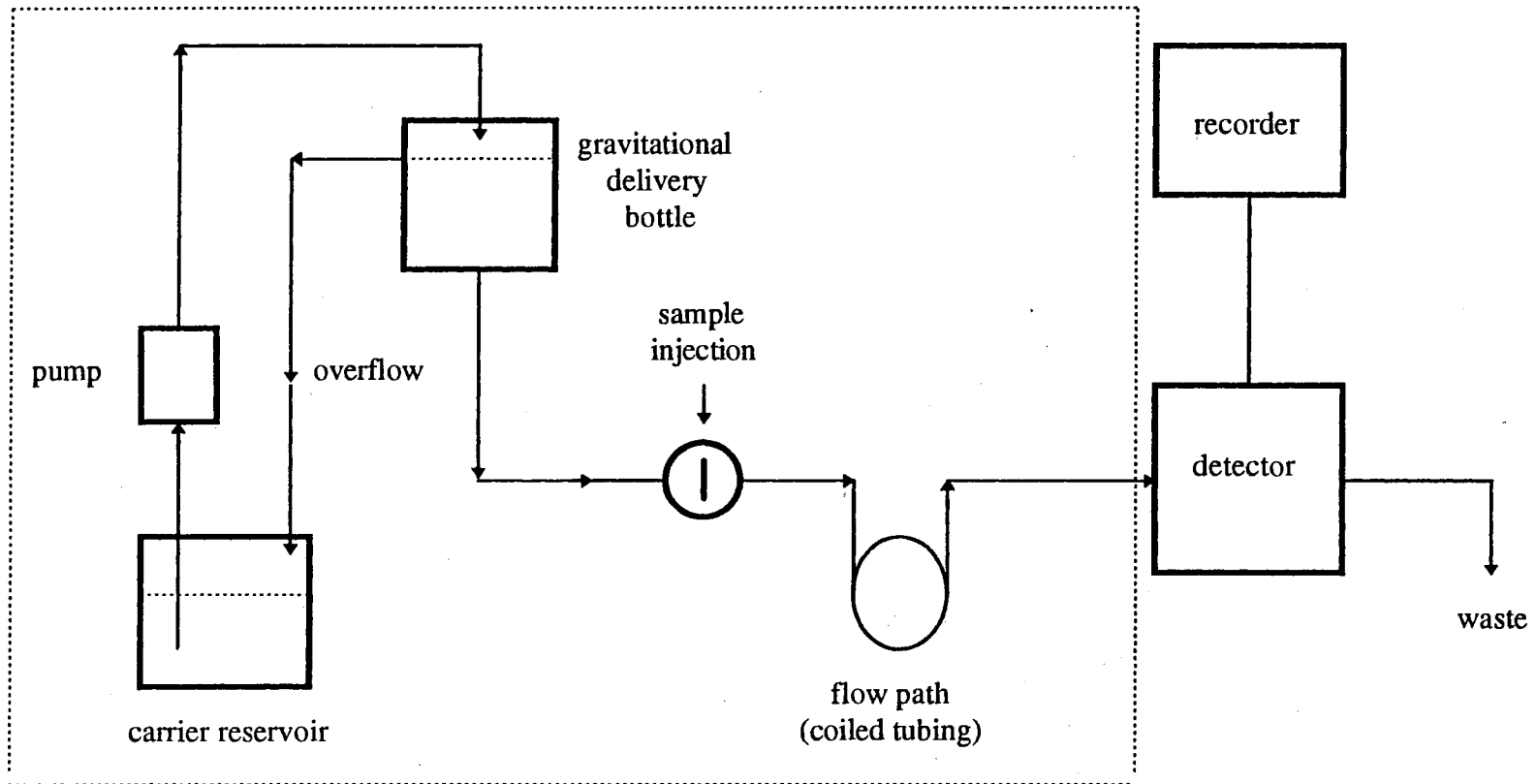
Figure 6. Single-line UCF System Used for the Determination of Molecular Diffusion Coefficient

Cyclic voltammetric data obtained with a BAS 100 unit (Bioanalytical Systems) were used to select the applied potentials listed in Table I. Some of the cyclic voltammograms for choosing the applied potentials are shown in Figure 7.

Sample injection was performed with a rotary four-way valve, Rheodyne Type 50 (Rheodyne, Cotati, CA). Recording conditions (Hewlett Packard HP 7128 strip chart recorder) were adjusted so as to obtain peaks with heights of 21.6 ± 1.3 cm to keep the correction factor, f in equation (2.12), constant. The components within the area delimited by the broken line in figure 6 were thermostated by use of a thermostat-water circulator, Lauda K-2/R (Brinkman Instruments, Westbury, NY). All measurements were then performed at $25.0 \pm 0.1\,^{\circ}\text{C}$.

Determination of D for Solochrome Violet RS

Current-potential data were obtained with a Metrohm Herisau Polarecord E 506 equipped with an E 505 polarographic stand. A mercury pool electrode was used as reference and a platinum wire as auxiliary electrode in determining D for Solochrome Violet RS. A saturated calomel electrode (SCE) was used as reference in the determination of D for Cd^{2+}.

Polarographic measurements were performed using a 0.0040 M Cd^{2+} solution prepared from a $CdCl_2$ stock solution diluted with 0.20 M HCl as supporting electrolyte. An aliquot of the resulting solution was subject to $N_2(g)$ bubbling for 15 min and the polarogram was recorded between -0.20 and -1.10 V vs. SCE at a sensitivity of 2.5×10^{-7} A mm^{-1}.

TABLE I

WAVELENGTH AND APPLIED POTENTIAL USED
FOR EACH OF THE Fe(II) COMPLEXES
WITH THE LISTED LIGANDS

(in 0.036M H_2SO_4-CH_3CN-H_2O)

Ligand	Wavelength (nm)	Applied potential (V)
1,10-Phenanthroline	520	1.000
5-Mehtyl-1,10-phenanthroline	524	1.000
5-Chloro-1,10-phenanthroline	510	1.150
5-Nitro-1,10-phenanthroline	510	1.300
5-Nitro-1,10-phenanthroline (in 1.00 M KCl)	510	1.000
5-Phenyl-1,10-phenanthroline	512	1.100
3,4,7,8-Tetramethyl-1,10-phenanthroline	512	0.800
4,7-Diphenyl-1,10-phenanthroline	532	1.000
4,7-Diphenyl-1,10-phenanthroline disulfonate	549	0.950
3-(2-Pyridyl)-5,6-diphenyl-1,2,4-triazine, PDT	560	1.300
3-(2-Pyridyl)-5,6-bis(4-phenylsulfonic acid)-1,2,4-triazine, Ferrozine	560	1.300
Solochrome Violet RS*	532	0.800
Hexacyanoferrate(III)*	410	0.180

* Data for species other than Fe(II) complexes
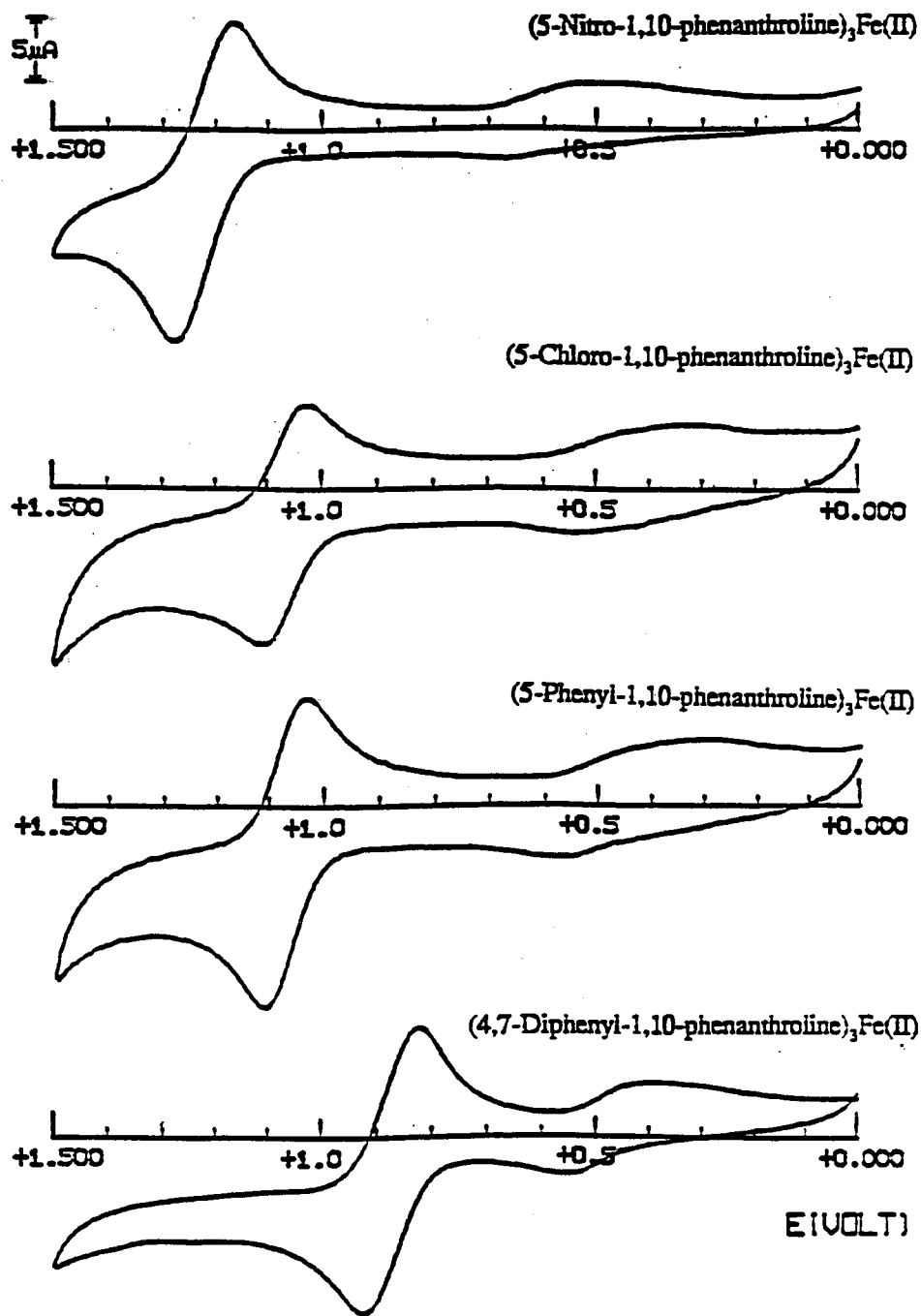
Figure 7. Some of the Cyclic Voltammograms for Selecting Applied Electrode Potentials

Aqueous solutions containing 0.271 mM Solochrome Violet RS were prepared in

0.072 M and 0.037 M H_2SO_4 as supporting electrolyte. A volume of 0.40 ml of a

0.0050% Triton X-100 was added per 100 ml of each dye solution. An aliquot of the

resulting solutions was subjected to $N_2(g)$ bubbling for 15 min and polarograms were

obtained between 0 V and -0.60 V vs. a mercury pool electrode at a sensitivity of 1.5×10^{-8} A mm^{-1}. The determination in acetonitrile-H_2SO_4-H_2O was performed similarly.

The values of D were extracted from Ilkovic's equation:

$$I = 708.3\ Z_iD_i^{1/2}\ t^{1/3}\ w^{2/3}\ C_i \qquad\qquad (2.20)$$

The measurements of w (the flow rate of Hg), t (the drop time of Hg), and the average

diffusion current, I, were performed between -0.30 V and -0.50 V. The number of

electron equivalents per molar unit, Z_i, has the value of 2 for both Cd^{2+} and for

Solochrome Violet RS. C_i is the bulk concentration for the species under study. All

measurements were then performed at $25.0 \pm 0.1^\circ$C.

Results and Discussion

Diffusion Coefficients for Reference Standard

of Solochrome Violet RS

Solochrome Violet RS (as the sodium salt of 5-sulfo-2-hydroxy[α]benzene-azo-2-

naphthol) was chosen as reference standard. It can be detected by both the photometric

and the electrochemical methods. Values of D for this chemical species in different

supporting electrolytes are available in the literature [52] and were used to validate the

determination in the media used in this dissertation. Table II summarizes the results obtained in experiments described in the Experimental section. The D value of $6.20 \pm 0.20 \times 10^{-6}$ cm^{2}s^{-1} was used as the standard value to calibrate the UCF system used for the determination of the diffusion coefficients of the metal chelates under study. The polarographic system was previously "calibrated" by determining D for Cd^{2+} in 0.20 M HCl as supporting electrolyte. A value of $0.65 \pm 0.01 \times 10^{-5}$ cm^{2}s^{-1} was obtained which coincides with a literature value [53] of 0.65×10^{-5} cm^{2}s^{-1}.

Determination of D for a Series of Fe(II) Complexes

Table III summarizes the values of the diffusion coefficients determined by use of Vanderslice's approach and as described above. Figure 8 displays the correlation of the D values listed in Table III with the molecular weight of the Fe(II) complexes. In most cases, higher values were obtained with amperometric detection than with photometric detection. Verification of this trend was further established by determining the D for the Fe(II) complex with 5-nitro-1,10-phenanthroline in aqueous medium and using hexacyanoferrate(III) as the standard (see Table III). The values of the diffusion coefficients obtained with both detection approaches are exponentially related to the molecular weight and decrease according to: $D = 244$ (molecular weight)$^{-0.58}$, with photometric monitoring, and $D = 513$ (molecular weight)$^{-0.67}$, with amperometric monitoring. Excluded from these plots are the values for 5-phenyl-1,10-phenanthroline as ligand since the difference between values obtained with amperometric and photometric detection differ considerably more than with the other ligands.

TABLE II

DIFFUSION COEFFICIENTS FOR SOLOCHROME
VIOLET RS AT $25 \pm 1^{O}C$

Supporting electrolyte in H_2O/CH_3CN (25 : 75)	Literature [a] $D \times 10^6 \ cm^2 s^{-1}$	Experimental [b] $D \times 10^6 \ cm^2 s^{-1}$
0.0720 M H_2SO_4	4.06	4.00 ± 0.10
0.0370 M H_2SO_4	4.25	4.20 ± 0.05
0.0360 M H_2SO_4		6.02 ± 0.20

[a] Values taken from Reference 15.

[b] Uncertainties based on 10 replicate measurements.

TABLE III

DIFFFUSION COEFFICIENTS FOR A SERIES OF Fe (II) COMPLEXES WITH THE LISTED LIGANDS [a]

Ligand	$D \times 10^6$ cm²s⁻¹ Photometric detection	$D \times 10^6$ cm²s⁻¹ Amperometric detection
1,10-Phenanthroline	6.13±0.40	5.56±0.06
5-Methyl-1,10-phenanthroline	5.66±0.02	6.17±0.13
5-Chloro-1,10-phenanthroline	5.49±0.28	6.41±0.26
5-Nitro-1,10-phenanthroline	5.24±0.28	7.62±0.30
5-Phenyl-1,10-phenanthroline	5.01±0.17	10.2±0.10
3,4,7,8-Tetramethyl-1,10-phenanthroline	5.16±0.43	6.54±0.24
4,7-Diphenyl-1,10-phenanthroline	4.24±0.08	5.85±0.12
4,7-Diphenyl-1,10-phenathroline sulfonate	3.25±0.09	3.23±0.01
3-(2-Pyridyl)-5,6-diphenyl-1,2,4-trizine, PDT	4.45±0.18	4.22±0.64
3-(2-Pyridyl)-5,6-bis(4-phenyl sulfonic acid-1,2,4-triazine), Ferrozine	3.59±0.03	3.45±0.11
5-Nitro-1,10-phenanthroline[b] (in 1.00 M KCl)	2.13±0.01	3.46±0.08

[a] Solochrome Violet RS as standard at 25.0±0.1°C
0.036 M H_2SO_4 in 25.4:74.6, v/v, H_2O-CH_3CN
Uncertainties based on 6 to 12 replicate measurements.
[b] Hexacyanoferrate(III) as standard.
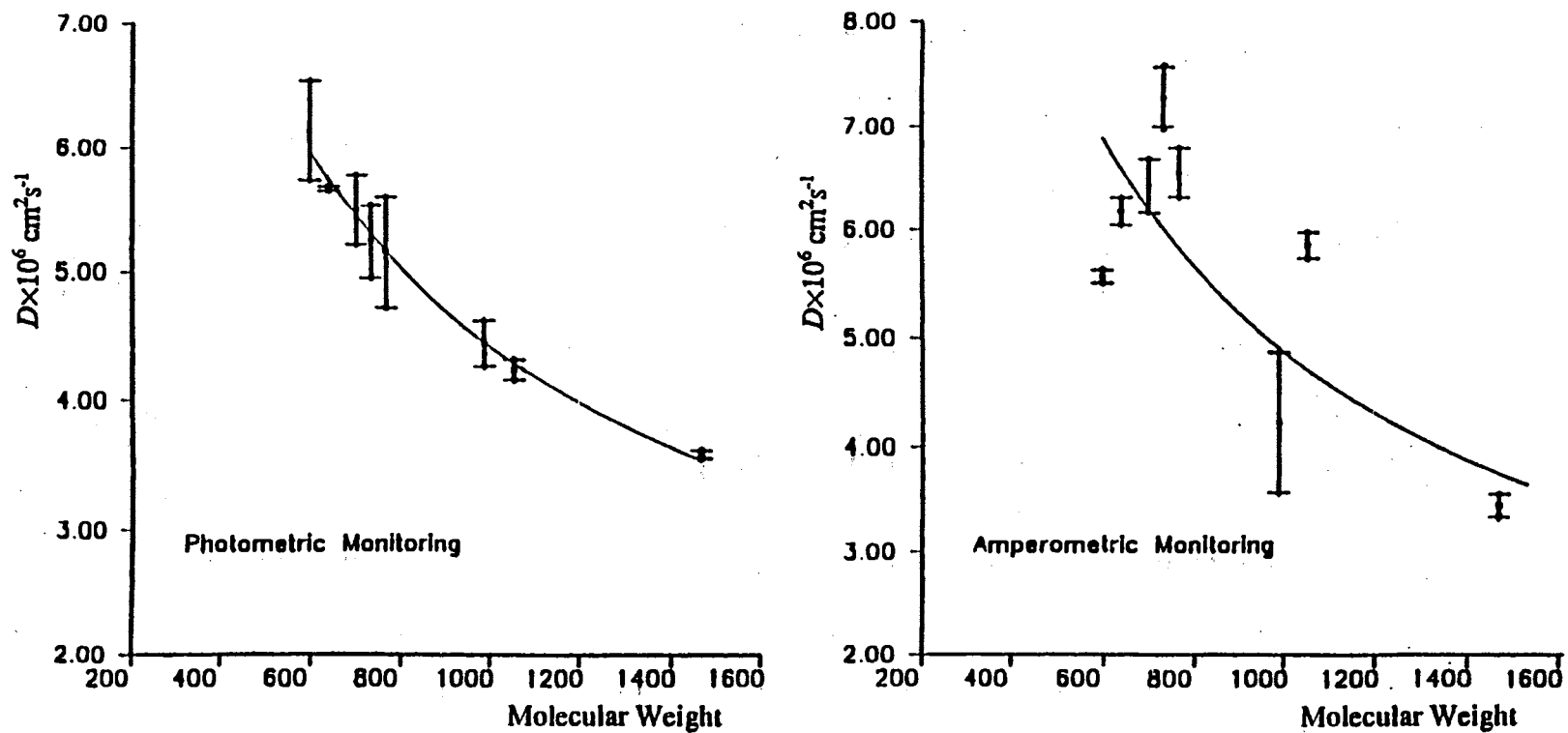
Figure 8. Correlation of D Values with Molecular Weight of Fe(II) Complexes

The reason for the doubling in the values of D obtained by amperometric detection is probably due to the strong adsorption of the analyte on the surface of the electrode. In amperometry, the intensity of the signal, measured as the electrode current, is proportional to both the concentration of the species adsorbed on the electrode surface and its diffusion coefficient. If the species is strongly adsorbed on the electrode surface, the apparent diffusion coefficient could be higher than if determined by the photometric method.

The overall trend observed with the relative values obtained seems in agreement with the Stokes-Einstein relation (Eq. 2.9) if the radius of the unsolvated complexes are considered to be directly proportional to their molecular size. Figure 9 illustrates the trend and is a plot of diffusion coefficients (obtained using photometric detection) as a function of the reciprocal of the cross sectional radius for the unsolvated complexes of the 1,10-phenanthroline family used in this work. The value of the radius for each complex was obtained by molecular computer graphics (Poly Graf from Molecular Systems, Burlington, MA).

The typical residence times ranged from 180 to 200 seconds. Triton X-100, used as the surface suppressor in the polarographic work, was found to have no effect on the determination of D values for the Fe(II) complexes with the UCF approach.

Conclusions

In this experiment, the UCF signals for the determination of D values of Fe(II) complexes were of Gaussian shape (see Figure 10). This means that the UCF system used

D: diffusion coefficient
r: radius of complex
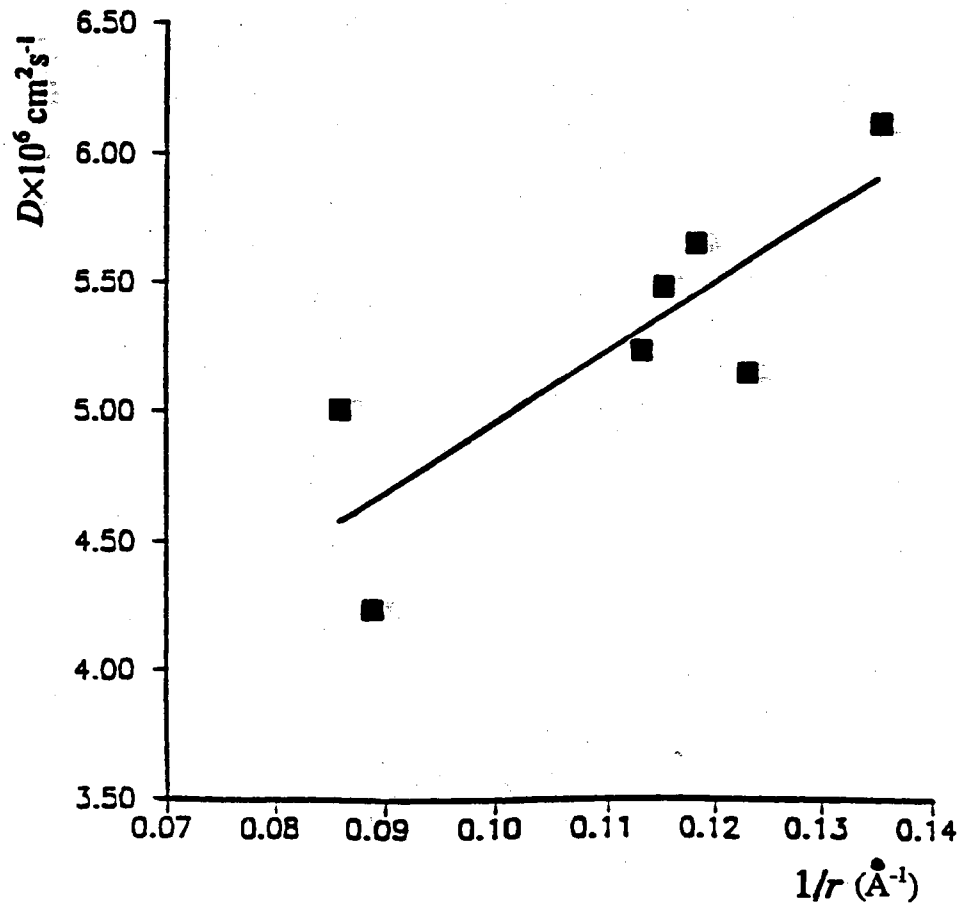
Figure 9. Stokes-Einstein Plot
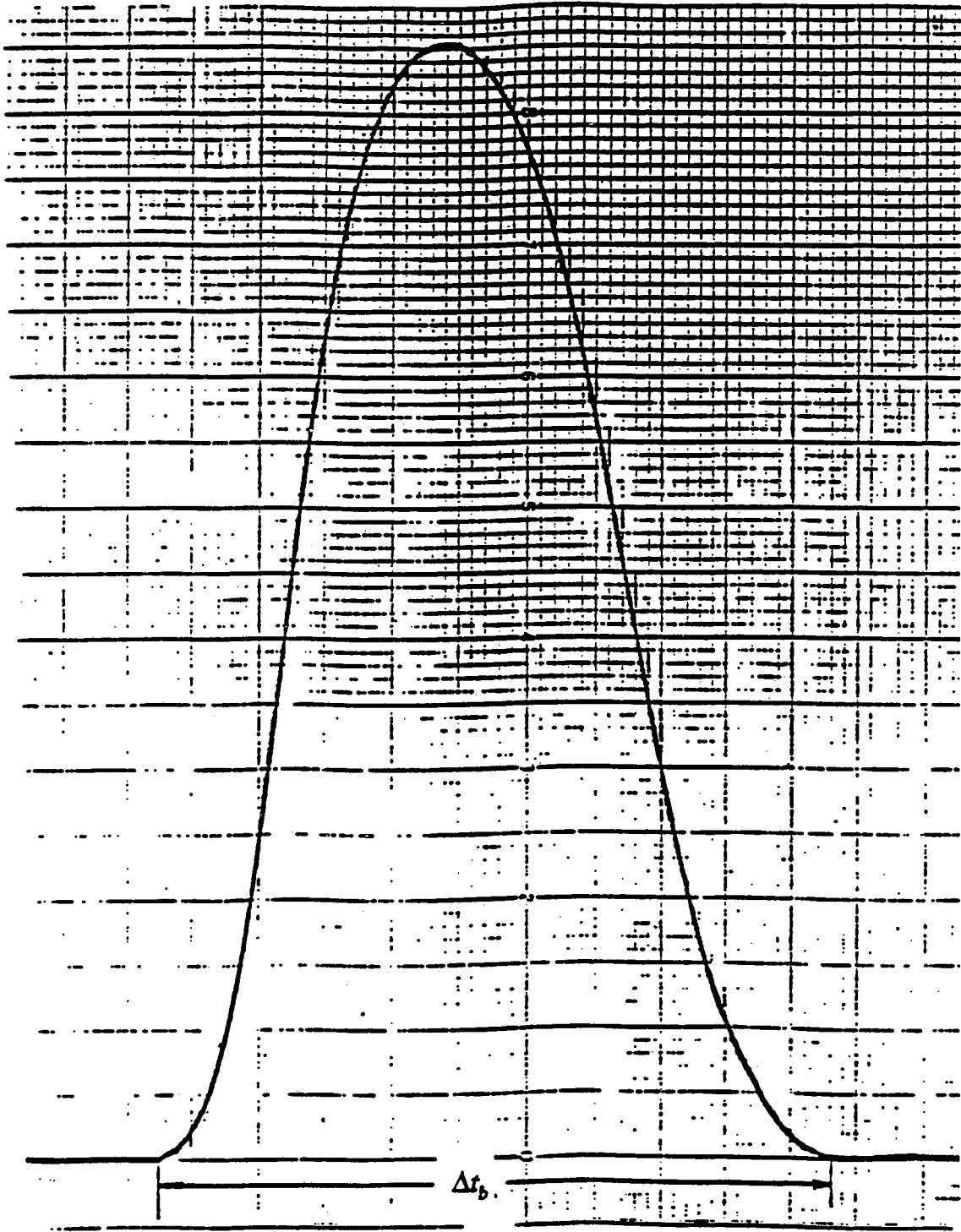
Figure 10. Typical UCF Signal for the Determination of D in this Work

satisfied the conditions stated by Taylor. The gravitational flow used in this UCF system provided a very effective pulse-free laminar flow which ensured smooth signal peaks in this work.

The results presented here point to the relative validity of the data obtained within a family of related complexes rather than in the validity of absolute values, as well as to the sensitivity of the approach to changes in detection means. The data with photometric detection appear more reliable than the data obtained with amperometric detection as evidenced by the correlation observed in Figure 8. Although the in-method precision is comparable with the two detection modes, adsorption of the complexes on the glassy carbon surface and redox reaction of impurities (all the oxidation currents measured required relatively high positive potentials) may be responsible for the greater scatter of values obtained with electrochemical detection (Figure 7). The data trend is in qualitative agreement with the Stokes-Einstein relationship, Equation (2.9).

This work confirms that use of UCF for determination of molecular diffusion coefficients is faster, more accurate, simpler, and lower in cost. The results of this work have been used in a study of fractal dimension of electrode surfaces [54].

CHAPTER III

DETERMINATION OF GLUCOSE CONCENTRATION

IN SERUM SAMPLES WITH AN INTEGRATED

BIOREACTOR/PHOTOMETRIC CELL

Background

The Role of Unsegmented Continuous Flow in Kinetic

Aspects of Analytical Chemistry

In analytical chemistry, chemical reactions are employed to represent the origin and justify the name of the subdiscripline. Regardless of the complexity of a reaction, the rate of a chemical reaction can be profiled as shown in Figure 11. Before the forward rate (R_f) and the reverse rate (R_r) get to equality, the system is within the kinetic region. When the rates are equal, the system reaches the equilibrium region The kinetic and the equilibrium regions illustrated in this figure reflect the two main approaches in analytical methodology:

1. the thermodynamic approach, in which signal measurements are made with the system at equilibrium.

2. the kinetic approach, in which signal measurements are made with the system approaching equilibrium.

kinetic region

equilibrium region

R_f (forward rate)

R_r (reverse rate)
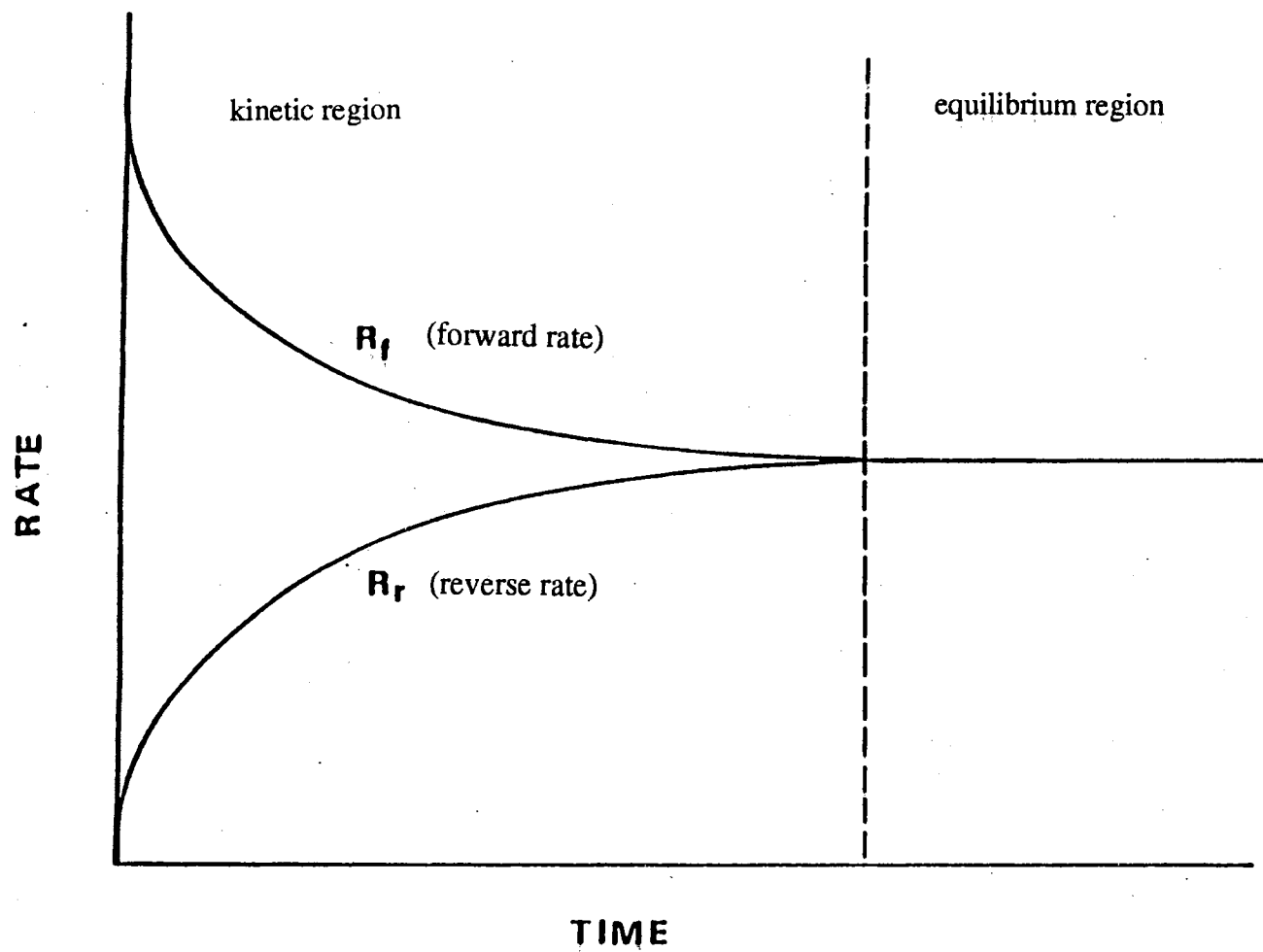
RATE

TIME

Figure 11. Reaction Rate - Time Profile

In comparison with the thermodynamic approach, the kinetic approach has the following advantages:

- it is faster because for the measurement there is no need to wait until the system reaches equilibrium for the measurement.

- it can be more selective. For example, a kinetic measurement using an enzyme as a biocatalyst adds selectivity to the determination of substrate.

Thermodynamic approaches, however, are more traditional than kinetic approaches, because the reliable instrumentation needed for sample processing, continuous determination of changes in the reaction system, and data processing were not available for the use of kinetic methods until the middle of the 1960's.

In the development of kinetic methods in analytical chemistry, UCF plays an increasing role, not only because of its inherent kinetic nature, but also because of its utility in providing a uniquely convenient way to automate kinetic determinations. The impact of UCF (or FIA) on kinetic approaches in analytical chemistry was clearly seen during the First International Symposium on Kinetics in Analytical Chemistry as singled out in a 1984 review in the journal, *Analytical Chemistry* [55].

This chapter gives an example in which the application of UCF is illustrated with the kinetic determination of glucose in serum samples. This work provides a model UCF system for enzymatic analysis together with coupled reaction systems. The real contribution of this work to the UCF is the design of a photometric cell in which coupled enzymatic reactions occur with rotation of one of the reactors to improve the existing

approaches using the same biochemical catalysts. Therefore, the emphasis of this project is on the design and characterization of an integrated bioreactor/detector unit.

Coupled Reactions

Coupled reactions are very often used to indicate or amplify the change of the reactions involved in the determination of substrate concentration or enzyme activity. For example, the determination of serum glutamic-oxaloacetic transaminase [EC 2.6.1.17] (GOT) by:

$$\alpha\text{-ketoglutarate} + \text{aspartate} \xrightleftharpoons{\text{GOT}} \text{glutamate} + \text{oxalocetate}$$

$$\text{oxalocetate} + \text{NADH} \xrightleftharpoons{\text{MDH}} \text{malate} + \text{NAD}$$
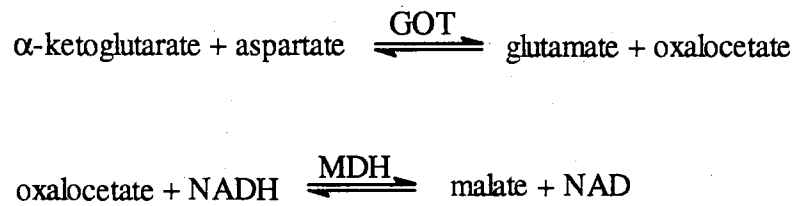
where NAD is nicotinamide adenine dinucleotide, and NADH is its reduced form; MDH is the enzyme malic dehydrogenase [EC 1.1.1.37]. The rate of decrease in absorbance of NADH at 340 nm is directly proportional to the GOT activity. An example of the amplification approach using coupled reactions is the determination of L-lactate by exploiting substrate cycling as illustrated below:
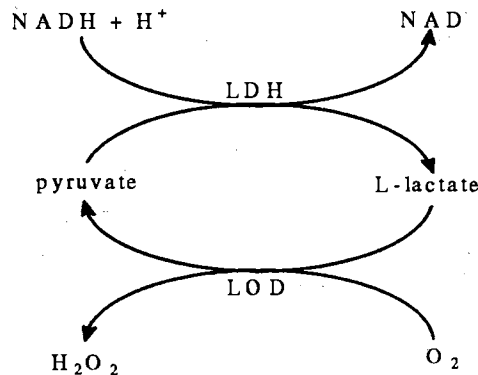
where LOD and LDH are the enzymes lactate oxidase [EC 1.1.3.x] and lactate dehydrogenase [EC 1.1.1.27], respectively. The L-lactate can be determined by amperometrically monitoring the formation of H_2O_2 in the reaction catalyzed by LOD. Consequently, H_2O_2 can be built up as a result of repeated cycling of the L-lactate substrate using another reaction catalyzed by LDH. As a result of the catalytic cycling, a chemical amplification of 10^9 is in operation and the H_2O_2 accumulation results in enhanced signals affording a very low limit of detection for L-lactate (ca. 10^{-16} M) [56].

Coupled reaction systems which involve an indicator reaction, like that in the first example cited above, are very commonly used in enzymatic analysis, and are very important in bioanalytical chemistry and in clinical chemistry. The usefulness of such determinations, however, is dictated by the type of UCF system and by the design of bioreactors. Packed-column reactors, by far the most widely employed type of reactor in continuous-flow configurations, require either a very high enzyme loading for effective use or a large residence time in the reactor (long columns), which is detrimental for effective accumulation of products to obtain enhanced signals at the detecting unit located downstream. Moreover, these situations favor an increase in the dispersion of the sample plug, which causes a "dilution effect". Therefore, it is of significance to work with a model system for this type of determination in the development of a different type of reactor. Glucose oxidase is the best biocatalyst to be used for such a purpose, because:

1. it is commercially available with high purity and at relatively low price,

2. its stability is competitive with other enzymes, and

3. it has been well-studied and documented in the analytical literature.

For this reason, a UCF system is described in this chapter for a kinetic-based measurement of glucose concentration in serum samples utilizing a coupled reaction system which involves glucose oxidase [EC 1.1.3.4] and horseradish peroxidase [EC 1.11.1.7]. The emphasis of this work is on the design, characterization, and application of an integrated bioreactor/detector unit that makes the kinetic measurement with a coupled reaction system more efficient and more sensitive than with other methods. The kinetics of the enzyme-catalyzed bioreactions involved in the determination, the design of the integrated bioreactor/detector unit, the description of the UCF system, the experimental techniques, and the collected results are presented in the following sections.

Kinetic Method for Determination of Glucose

β-D-glucose (glucose, briefly in this presentation) is a very important analyte not only in clinical chemistry where it is one of the most frequently determined species, but also in the food and beverage industry. Glucose metabolism provides the human body with the energy to keep it alive. The normal levels of glucose in blood are in the range of 65-95 mg/dL, and in serum this range is 70-105 mg/dL. A high blood glucose level (hyperglycemia) and a low blood glucose level (hypoglycemia) are both dangerous to human life.

With glucose oxidase (GOD) / glucose system is commonly used as a model reagent for the development of glucose determination. The following enzyme-catalyzed reaction is commonly employed in bioanalytical systems, such as the so-called "biosensors":

$$glucose + H_2O + O_2 \xrightleftharpoons{GOD} gluconic\ acid + H_2O_2$$

With this reaction, the glucose concentration can be determined using a kinetic approach

by amperometrically monitoring the rate of oxygen consumption [57,58],

potentiometrically monitoring the formation of gluconic acid (pH stat method [59]), or

also amperometrically monitoring the formation of H_2O_2 [19]. The rate of H_2O_2 formation

can be also measured by coupling with another enzyme-catalyzed reaction employing, for

instance, the enzyme peroxidase (POD):

$$H_2O_2 + \text{dye (reduced form)} \xrightleftharpoons{\text{POD}} \text{dye (oxidized form)} + H_2O$$

In this reaction, the dye (usually *o*-dianisidine [60]) is oxidized to a colored form which

absorbs light of a given wavelength. Therefore, the rate of the first reaction, which is

called the main reaction in the coupled reaction system, can be determined by

spectrophotometrically monitoring the rate of the second reaction, which is called the

indicator reaction. As discussed in the next section, the glucose concentration only affects

the rate of the main reaction, and the indicator reaction should go faster than the main

reaction to ensure that the main reaction controls the overall rate of the coupled reaction

system.

Kinetics of Enzyme-Catalyzed Reactions

A general, simplified, mechanism for enzyme-catalyzed reactions can be illustrated

as follows:

$$E + S \underset{k_{-1}}{\overset{k_1}{\rightleftharpoons}} ES \xrightarrow{k_2} P + E$$

41
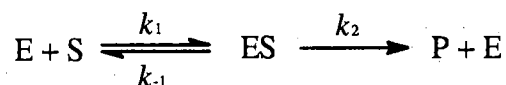
where E, S, ES, and P symbolize the enzyme, the substrate, the enzyme-substrate complex, and the product, respectively. According to this model, when the substrate concentration becomes high enough to entirely convert the enzyme to the ES form, the second step of the reaction becomes rate limiting and the overall reaction rate becomes insensitive to further increases in substrate concentration. The general expression for the velocity or rate of this reaction is:

$$\upsilon = \frac{d[\text{P}]}{dt} = k_2[\text{ES}] \tag{3.1}$$

The overall rate of production of [ES] is:

$$\frac{d[\text{ES}]}{dt} = k_1[\text{E}][\text{S}] - k_{-1}[\text{ES}] - k_2[\text{ES}] \tag{3.2}$$

With the steady-state assumption proposed in 1925 by Briggs and Haldane [61], after the first milliseconds of mixing the enzyme and substrate, we have:

$$\frac{d[\text{ES}]}{dt} = 0 \tag{3.3}$$

and equation (3.2) can be rewritten as follows:

$$k_1[\text{E}][\text{S}] = k_{-1}[\text{ES}] + k_2[\text{ES}] = (k_{-1} + k_2)[\text{ES}] \tag{3.4}$$

Since the total enzyme concentration is given by:

$$[\text{E}]_{\text{T}} = [\text{E}] + [\text{ES}] \tag{3.5}$$

equation (3.4) can be simplified to:

$$k_1([\text{E}]_{\text{T}} - [\text{ES}])[\text{S}] = [\text{ES}](k_{-1} + k_2) \tag{3.6}$$

which upon rearrangement becomes:

$$[\text{ES}] = \frac{[\text{E}]_{\text{T}}[\text{S}]}{K_{\text{M}} + [\text{S}]} \tag{3.7}$$

where K_M, which is known as the Michaelis-Menten constant, is defined as:

$$K_M = \frac{k_{-1} + k_2}{k_1}$$ (3.8)

Then the initial velocity of the reaction can be expressed as:

$$\upsilon_0 = \left(\frac{d[P]}{dt}\right)_{t=0} = k_2[ES] = \frac{k_2[E]_T[S]}{K_M + [S]}$$ (3.9)

The use of the initial velocity, which is usually the velocity measured before more than about 10% of the substrate has been converted to product, minimizes complicating factors such as the effects of reversible reactions, the inhibition of the enzyme by product, and the progressive inactivation of the enzyme.

The maximum velocity of an enzyme-catalyzed reaction, V_{max}, occurs at high substrate concentrations when all active sites of the enzyme are saturated, that is, when the enzyme is entirely in the ES form; then,

$$V_{max} = k_2[E]_T$$ (3.10)

Therefore, combining equations (3.9) and (3.10) we obtain:

$$\upsilon_0 = \frac{V_{max}[S]}{K_M + [S]}$$ (3.11)

This expression is called the Michaelis-Menten equation. In this equation, if $[S] = K_M$, $\upsilon_0 = V_{max}/2$ so that K_M can be defined as the substrate concentration at which the reaction velocity is half-maximum. If an enzyme has a small value of K_M, it achieves maximum catalytic efficiency at relatively low substrate concentrations. In an enzymatic method, lower values are preferred to obtain a high initial rate at low substrate concentration, when sensitivity is of concern.

The magnitude of K_M varies widely with the identity of the enzyme and the nature of the substrate. It is also a function of temperature and pH. From equation (3.8), it can be seen that if $k_{-1} >> k_2$, $K_M = k_{-1}/k_1$, and the Michaelis-Menten constant becomes the dissociation equilibrium constant for the enzyme-substrate complex ES. On the other hand, if $k_{-1} << k_2$, $K_M = k_2/k_1$, and it should be considered as a kinetic constant.

As mentioned previously, K_M is equal to the value of [S] when $v_0 = V_{max}/2$, therefore the value of the Michaelis-Menten constant can be obtained from a plot of initial rate vs. substrate concentration as shown in Figure 12. Because very high substrate concentrations are required to reach V_{max}, it is difficult to determine K_M and V_{max} by using the hyperbolic relationship of equation (3.11). However, other forms of the Michaelis-Menten equation are more useful in plotting experimental data to obtain the values for K_M and V_{max}. A widely used linear transformation of the Michaelis-Menten equation (3.11) is the Lineweaver-Burk equation [61]:

$$\frac{1}{v_0} = \frac{K_M}{V_{max}} \cdot \frac{1}{[S]} + \frac{1}{V_{max}} \qquad (3.12)$$

A plot of $1/v_0$ vs. $1/[S]$ is a straight line with a slope of K_M/V_{max} and an intercept of $1/V_{max}$ as shown in Figure 13. Therefore, the values of K_M and V_{max} can be obtained from this plot.

It can be seen from Figure 12 that the plot of initial rate vs. substrate concentration has the shape of a rectangular hyperbola. At low substrate concentrations the Michaelis-Menten equation (3.11) reduces to a linear form:

44

υ_0: initial rate
[S]: substrate concentration
K_M: Michaelis-Menten constant
V_{max}: maximum rate

$\upsilon_0 = \left(\dfrac{V_{max}}{K_M}\right)[S]$

$\upsilon_0 = V_{max}$

$\upsilon_0 = V_{max}/2$

$\upsilon_0 = \dfrac{V_{max}\,[S]}{K_M + [S]}$

[S] = K_M
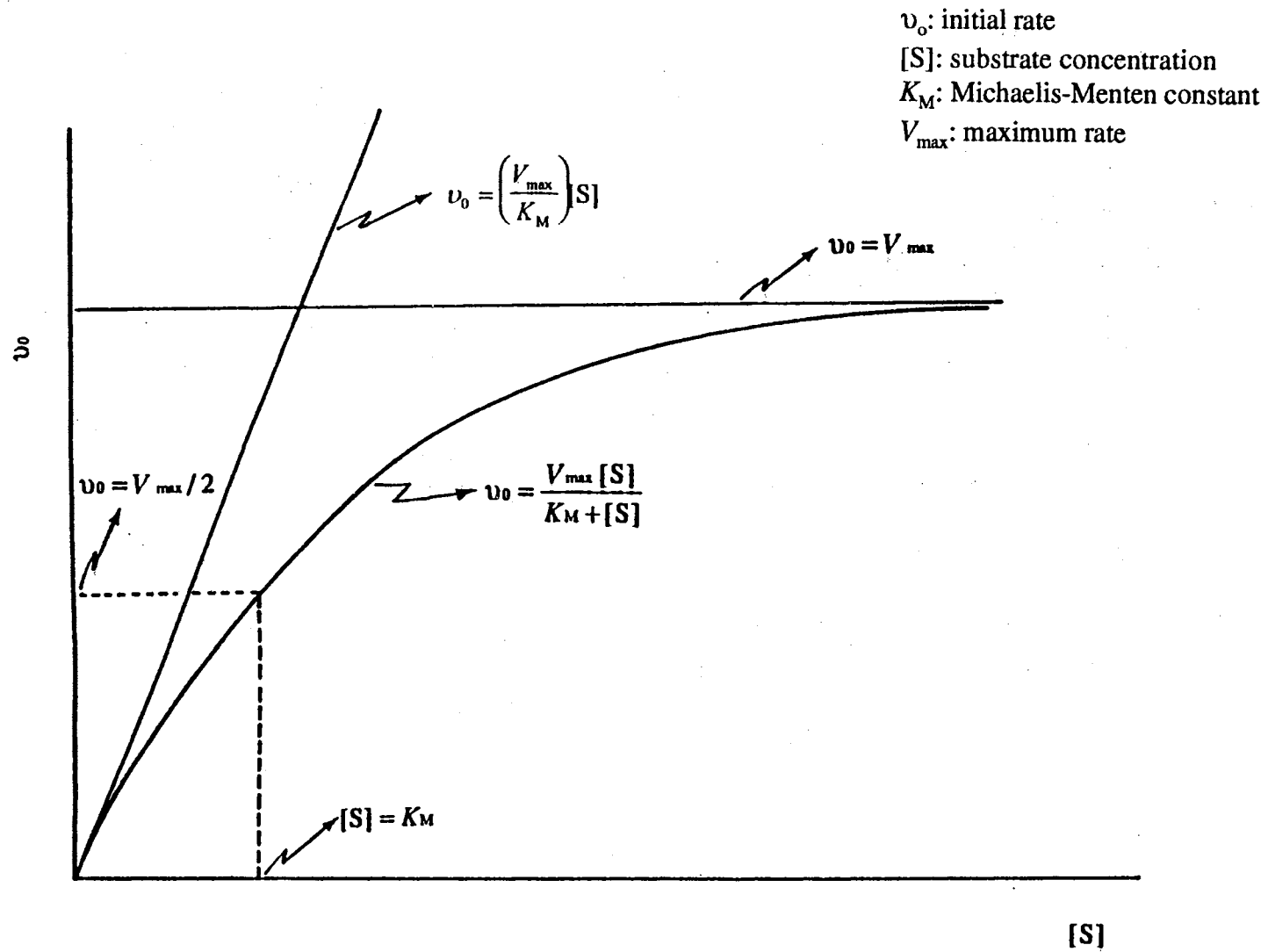
Figure 12. Plot of Initial Rate vs. Substrate Concentration

υ_o: initial rate
[S]: substrate concentration
K_M: Michaelis-Menten constant
V_{max}: maximum rate

K_M/V_{max}

$1/V_{max}$

$1/\upsilon_o$

$1/[S]$ ⟶
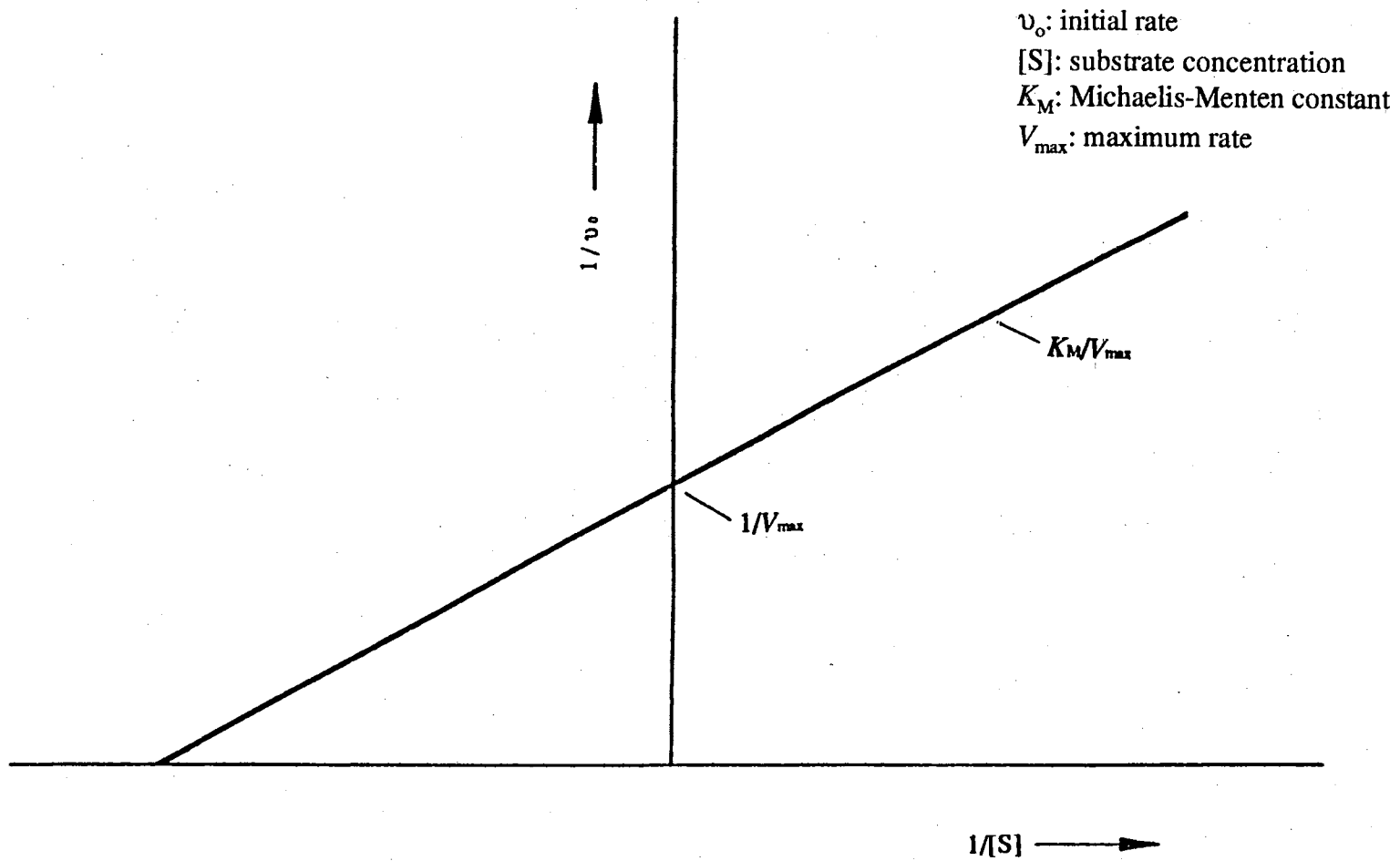
Figure 13. Lineweaver-Burk Plot

$$\upsilon_0 = (\frac{V_{max}}{K_M})[S] \qquad\qquad (3.13)$$

That is, the initial rate is directly proportional to the substrate concentration and first-order kinetics apply. On the other hand, at very high substrate concentration, the Michaelis-Menten equation reduces to another linear form:

$$\upsilon_0 = V_{max} \qquad\qquad (3.14)$$

That is, the initial rate is no longer dependent on substrate concentration and zero-order kinetics applies at constant enzyme concentration. Between these two rather extreme conditions, the complete equation is required and the reaction order is mixed. Obviously, for the enzymatic determination of a substrate in a one-substrate system by a kinetic method, as is the case in this work, the first condition is preferred. Therefore, the linear region at low substrate concentration in the plot of initial rate vs. substrate concentration is employed.

As can be predicted from the Michaelis-Menten equation (3.11), the initial rate, υ_0, is proportional to the total enzyme concentration (activity), $[E]_T$, at a given substrate concentration $[S]$. However, sometimes it is found that there is a falling off from linearity at high enzyme concentration. This does not indicate a true decrease in the activity of the enzyme but represents limitations, such as constraints due to diffusion of the substrate to the enzyme active site or a relatively slow indicator reaction. This usualy gives an apparently higher Michaelis-Menten constant. Therefore, the Michaelis-Menten constant determined experimentally should be always qualified as an apparent constant, K'_M.

47

In using the simplified Michaelis-Menten equation (3.13), the greater the value of (V_{max}/K'_M), the higher the sensitivity of the kinetic method; this can be obtained by increasing V_{max} (e.g. by using as a high $[E]_T$ as possible, because $V_{max} = k_2[E]_T$), and/or by decreasing K'_M. In this research a spectrophotometric cell comprising parallel rotating and stationary bioreactors was designed and used with a UCF system in order to satisfy these conditions.

Another important aspect of this work is the use of immobilized enzymes in the bioreactor/photometric cell. Immobilization in this work is referred to as the localization of the enzyme in such a manner that it remains physically separated from the substrate solution and the products of the enzyme-catalyzed reactions. The biocatalyst is in an insoluble form in the medium, and heterogeneous biocatalysis occurs in a restricted space. There are four commonly used methods of enzyme immobilization [63]:

1. Containment by a membrane;

2. Entrapment in a polymeric gel matrix;

3. Surface immobilization by physical adsorption; and

4. Surface immobilization by covalent binding.

For use in a continuous-flow system, the last method is the most commonly employed, and was also used here. The use of an insoluble immobilized-enzyme provides some advantages that overcome limitations encountered when using soluble enzymes in solution for example:

1. there is some increase in the retention of enzyme activity with time;

2. easy separation and recovery is accomplished with minimum (if any) contamination of the enzyme preparation by reactants and products;

3. the insoluble enzyme preparation is ubiquitous in the design of reactor/sensor units and is adaptable to continuous-flow sample and reagents processing;

4. the "concentration" of immobilized enzyme can be made relatively higher than that of free soluble enzyme if the volume of the reaction system is small enough;

5. the insoluble enzyme does not enter into the bulk of the solution and does not affect the spectrophotometric measurement.

In this work, all these advantages have been exploited. The procedure for the preparation of the immobilized enzymes and the effects of use of the immobilized enzymes are discussed in the following sections.

Experimental

Design of the Integrated Bioreactor/Photometric Cell

To perform sensitive and accurate determinations of glucose by using coupled enzyme-catalyzed reactions and rate measurements, a UCF system was employed, and the following objectives were taken into consideration:

1. to increase V_{max};

2. to decrease K'_M, and

3. to maximize the signal.

As mentioned previously, the value of V_{max} can be increased by increasing the total enzyme activity $[E]_T$. The approach doing this is to immobilize the enzyme in the reactor

and to make the volume of the reaction space as small as possible. Because the amount of immobilized enzyme is constant in the reactor, decreasing the volume of the reaction space is equivalent to increasing $[E]_T$.

One of the main effects on the value of K'_M is the diffusional constraint for the substrate to approach the enzyme active site and for the products to exit it, especially when the enzyme is immobilized. An efficient way to reduce this diffusional constraint is to effectively stir the reaction mixture in order to speed up the substrate transfer to the active site of the enzyme and the release of product from the same site.

If the indicator reaction is slower than the main reaction in a coupled reaction system, the indicator reaction controls the overall rate. This results in an apparently higher value for the K'_M of the main reaction. One approach to overcome this problem is to directly rotate the reactor with the enzyme that catalyzes the indicator reaction.

To obtain enhanced signals in a UCF system, a high concentration of the monitored species is needed, as well as optimum detection conditions. This is because the signal (such as electrode current or light absorbance) is directly proportional to the concentration of the species. In this work, the product of the main reaction, H_2O_2, was detected via the coupled indicator reaction; therefore, dilution of H_2O_2 and the colored dye needed to be avoided or at least minimized. To achieve this, the coupled reactions must take place in the same defined space. In this way, the dilution caused by dispersion during the transport of H_2O_2 from the main reaction to the indicator reaction is avoided. If the reaction system is integrated with the detector, the dilution of the colored dye caused by dispersion during transport from the reaction system to the detector is eliminated. Also, a small volume for

the reaction system favors relatively high concentrations of both H_2O_2 and the colored dye.

Combining all the facts mentioned above, an integrated bioreactor/photometric cell was designed, as shown in Figure 14, and was evaluated with the determination of glucose using the coupled reactions mentioned earlier. In this design, glucose oxidase is immobilized on the top of the cell and the horseradish peroxidase is immobilized on the top of the rotating disk A magnetic stirring bar is embedded inside the disk, so that the disk can be driven by a magnetic stirrer. Rotation of the disk stirs the reaction system inside the cell to reduce diffusion constraints. The sample enters the cell through the "flow in" tube, reactions take place in the cell, and the absorbance of light passing through the cell is measured. After the measurement, the solution inside the cell is flushed out with carrier solution via the "flow out" tube.

As has been already discussed, a small cell volume is preferred in order to have relatively high concentrations of enzymes and monitored species. But, to obtain a stronger signal from an integrated detector, a larger cell volume is required so that more photons can pass through the cell to reach the photometric detector. In this design, the trade-off between high concentrations and more photons was approached by sliding the lower part (C) of the cell, which is made of borosilicate glass, up or down to optimize the cell volume.

measurements in millimeter (mm)

flow in   flow out

upper part

54

O-ring

intermediate cell body

13

6.5

glucose oxidase   O-ring

lower pert

10

peroxidase

rotating disk

12

magnetic stirring bar
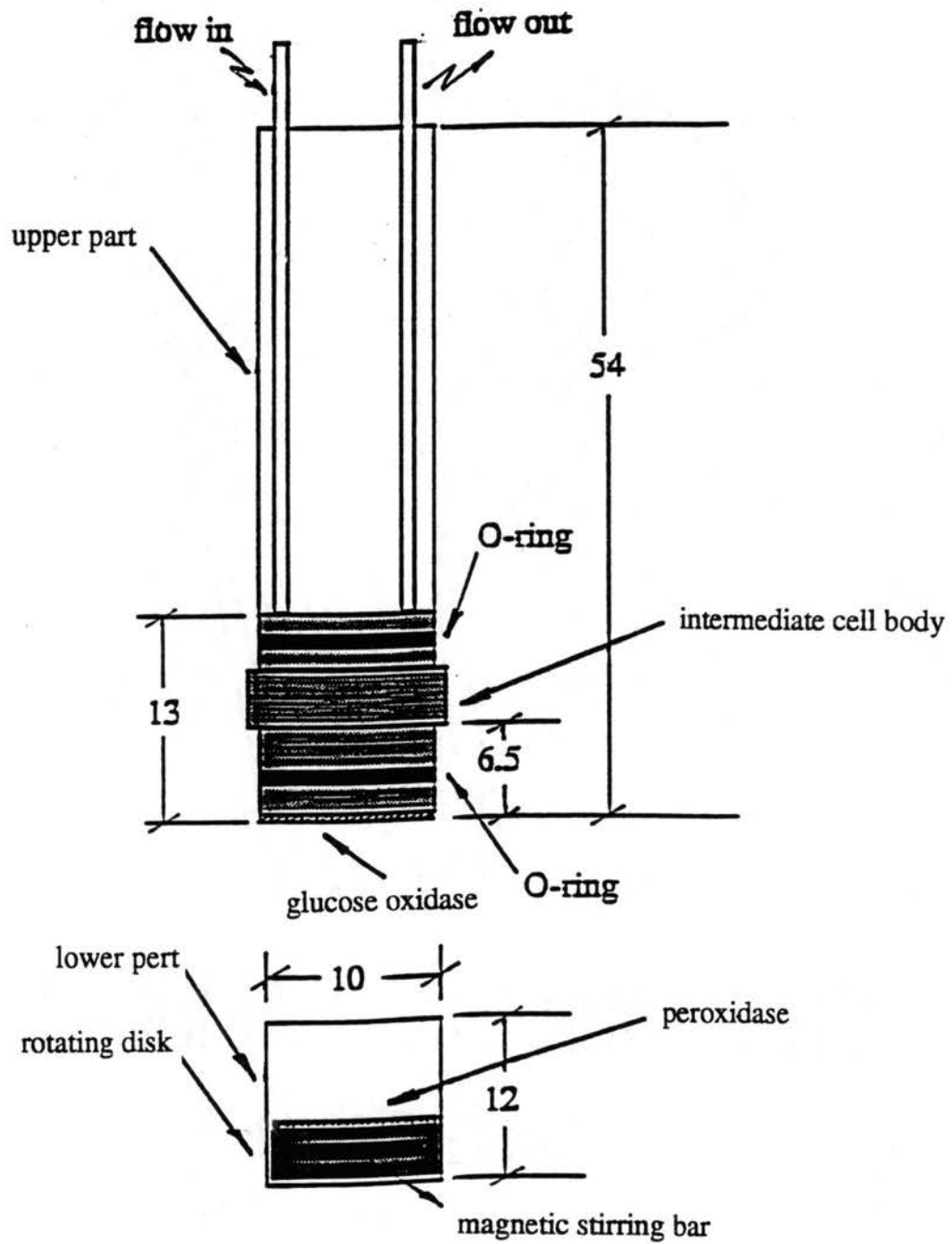
Figure 14. Schematic Representation of the Bioreactor/Photometric Cell

The intermediate cell body and the rotating disk were made of black Delrin. The upper part of the cell was made of Plexiglass. All measurements in Figure 14 are in millimeters (mm).

The Unsegmented Continuous Flow System

The overall configuration of the UCF system is schematically illustrated in Figure 15. A FIAtron SHS-200 microprocessor-controlled solution handling unit (FIAtron System, Milwaukee, WI) was used for pumping, sample introduction, and for controlling the flow. The bioreactor/photometric cell was located in the cell compartment of the spectrophotometer (Spectronic 21, Bausch and Lomb, Rochester, NY). A magnetic stirrer (Dayton 3M247, Dayton Electric, Chicago, IL) was located underneath the spectrophotometer to drive the rotating disk inside the cell. The rotation velocity was controlled by means of a variable transformer [5]. A strip-chart recorder (HP 7128A, Hewlett-Packard, St. Diego, CA) was used as readout. The pump tubing used in the FIAtron SHS-200 unit was made of Tygon (Fisher AccuRated 1.0 mm i.d., Fisher Scientific, Pittsburgh, PA). The tubing for connecting the rest of the components in the UCF system was 1.0 mm i.d., PTFE (Cole Parmer, Chicago, IL).

Reagents and Solutions

The water used for solution preparation was deionized and further purified by distillation in a borosilicate glass still with a quartz immersion heater. All reagents used, except as noted, were of analytical grade. Glucose oxidase [EC 1.1.3.4] from *Aspergillus*
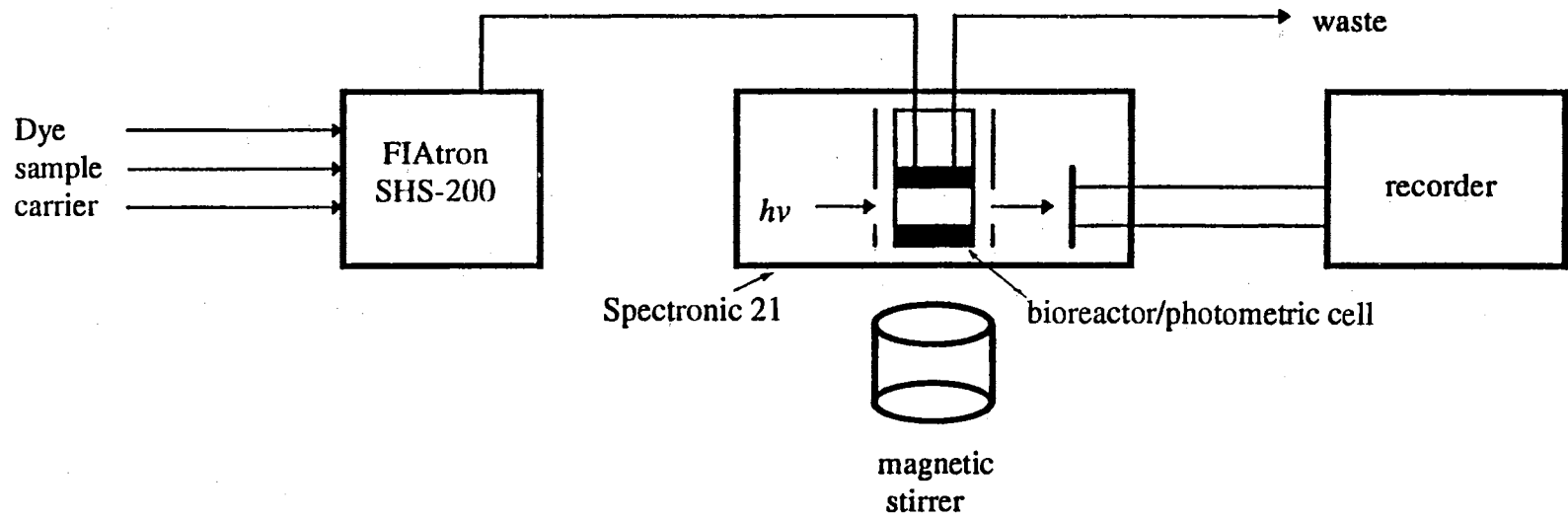
Figure 15. Diagram of the UCF System with the Bioreactor/Photometric Cell

niger (Type VII, 125 I.U. per mg of solid) and horseradish peroxidase [EC 1.11.1.7]

(Type VI, 250-330 I.U. per mg of solid) were purchased from Sigma (St. Louis, MO).

Anhydrous D-(+)-glucose (dextrose, corn sugar), *N,N*-dimethylaniline, 4-aminophenazone,

Accutrol™ (normal and abnormal lyophilized preparation control standards), and the *o*-

dianisidine glucose determination kit (Catalog No. 510-DA) were also from Sigma.

Glutaraldehyde (25% w/w aqueous solution) was from Aldrich (Milwaukee, WI). 3-

Aminopropyl-modified controlled-pore glass (APCPG) powder, 1400 A mean pore

diameter and 24 m^2g^{-1} surface area, was from Electro-Nucleonics (Fairfield, NJ) and

contained 48.2 μmol g^{-1} of amino groups.

Enzyme Immobilization

The enzyme reactors were prepared by immobilizing glucose oxidase and peroxidase

on APCPG glass, respectively. The APCPG was smoothly spread on one side of a double-

sided tape (Scotch double-coated tape 665, 3M, St. Paul, MN), was allowed to react with

an aqueous solution of 5% w/w glutaraldehyde at pH 10.00 (0.20 M carbonate) for 2

hours at room temperature to form a thin layer of cross-linked polymer on the top of the

APCPG. After being washed with purified water and 0.10 M phosphate buffer of pH 7.00,

the glucose oxidase (10.0 mg of enzyme preparation in 0.50 ml of 0.10 M phosphate

buffer, pH 7.00) or peroxidase (5 mg of enzyme preparation in 0.25 ml of 0.10 M

phosphate buffer, pH 7.00) were coupled to the residual aldehyde groups on the cross-

linked polymeric layer in phosphate buffer (0.10 M, pH 7.00) overnight at 5°C. The

immobilized enzyme preparations were finally washed with phosphate buffer (0.10 M, pH

7.00), and the tapes with the immobilized enzymes were affixed on to the reactors for experimental use. The mechanism of the immobilization with glutaraldehyde is complicated [64]. A simplified scheme of the immobilization is illustrated in Figure 16. The immobilized glucose oxidase and horseradish peroxidase preparations were perfectly stable for at least four and two weeks of daily use, respectively.

Preparation of Serum Samples

Blood samples were taken from Angus x Hereford cattle via venipuncture. To each 10 ml of sample was added 1.25 mg of oxalic acid, and the mixtures were placed on ice. Upon arrival at the laboratory (and no more than 4 hours after extraction), the samples were ultracentrifuged (3000 $\times$ g for 20 min.) in a Sorvall RC 3 ultracentrifuge (Du Pont, Wilmington, DE), and the plasma was decanted and stored at -20°C. Before the determination of glucose, 1.80 ml of purified water and 1.0 ml of 0.60 M aqueous barium hydroxide were added to an aliquot of 0.20 ml of the serum. After mixing, 1.0 ml of 0.30 M zinc sulfate was added. After thorough mixing and 2 or more min. of standing, the mixture was centrifuged. The supernatant liquid constituted a 1:20 protein-free solution ready for the determination of glucose.

Measurement of Initial Rate

For the measurement of the initial rate of reaction, a continuous-flow/stopped-flow/continuous-flow operation technique was used with the UCF system. In the continuous-flow step, the carrier solution (0.10 M phosphate buffer, pH 6.00) was passed

$$\Big|\quad +\ \textcircled{\tiny{A}}\!-\!NH_2 \quad\longrightarrow\quad \Big|\textcircled{\tiny{A}}\!-\!NH_2$$

double-sided tape   APCPG

$$\Big|\textcircled{\tiny{A}}\!-\!NH_2 \ +\ \overset{O}{\overset{\|}{H\!C}}(CH_2)_3\overset{O}{\overset{\|}{C}}H \xrightarrow{\ pH\ 10.0\ } \Big|\textcircled{\tiny{A}}\!-\!N\!=\!CH(CH_2)_3\overset{O}{\overset{\|}{C}}H$$

glutaraldehyde

$$\Big|\textcircled{\tiny{A}}\!-\!N\!=\!CH(CH_2)_3\overset{O}{\overset{\|}{C}}H \ +\ H_2N\!-\!E \xrightarrow{\ pH\ 7.0\ } \Big|\textcircled{\tiny{A}}\!-\!N\!=\!CH(CH_2)_3CH\!=\!N\!-\!E$$

enzyme   immobilized enzyme
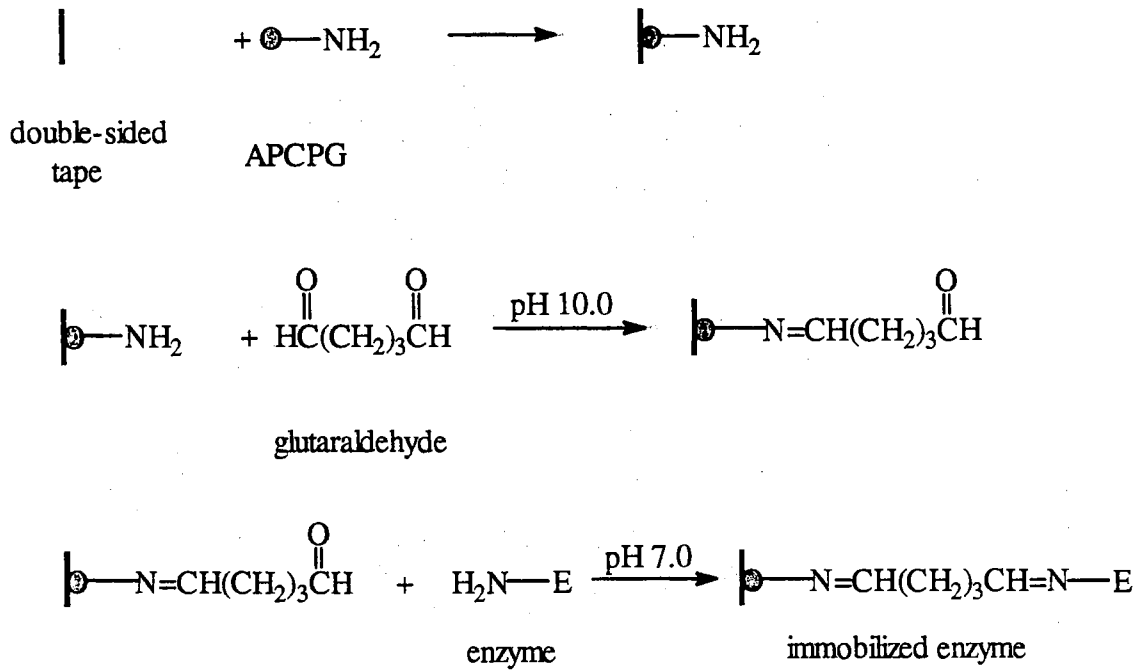
Figure 16. Scheme of Enzyme Immobilization

through the system. Meanwhile the sample and the dye solutions were loaded, mixed, and transported by the carrier solution to the optimum position in the reactor/detector cell. In the stopped-flow step, the pump of the SHS-200 unit was stopped to ensure that there was enough residence time for the reaction to take place inside the cell, and for the levels of absorbance caused by the monitored species to be detectable. The following continuous-flow step delivered the carrier solution to flush the reactor/detector cell and the whole system in order to prepare the following measurement cycle. The typical time intervals used in this continuous-flow/stopped-flow/continuous-flow operation with the FIAtron SHS-200 unit are listed in Table IV. The flow rate provided by this unit was 2.28 ml min^{-1}.

The measurement of the initial rate of the main reaction was performed by measuring the signal from the spectrophotometer. This signal was produced by the change of absorbance with time, and was displayed as a peak on the recorder chart paper. The rate of reaction, or the rate of response, was determined by measuring the slope of the leading part of the peak (as shown in Figure 17), which is responsible for the rate of reaction under stopped-flow (for 1 min.) and rotating conditions (840 rpm). A kinetic study [65] shows that the main reaction catalyzed by glucose oxidase has a first-order behavior at different glucose concentrations during the first 5 min interval. Therefore, the rate of response for the first minute can be used as the initial rate of the main reaction.

TABLE IV

TIME INTERVALS TYPICALLY USED IN THE CONTINUOUS-FLOW/STOPPED-FLOW /CONTINUOUS-FLOW OPERATION AS PROGRAMMED VIA THE SHS-200 UNIT

time interval (s)	operating condition	pump
60	carrier passed through system until sample introduction	ON
10	sample loading	ON
30	sample transported by carrier to optimum position in reactor/detector cell	ON
90	stopped flow	OFF
	cycle repeated for introduction of next sample	

Rate of Response = h (mm)/t (mm)
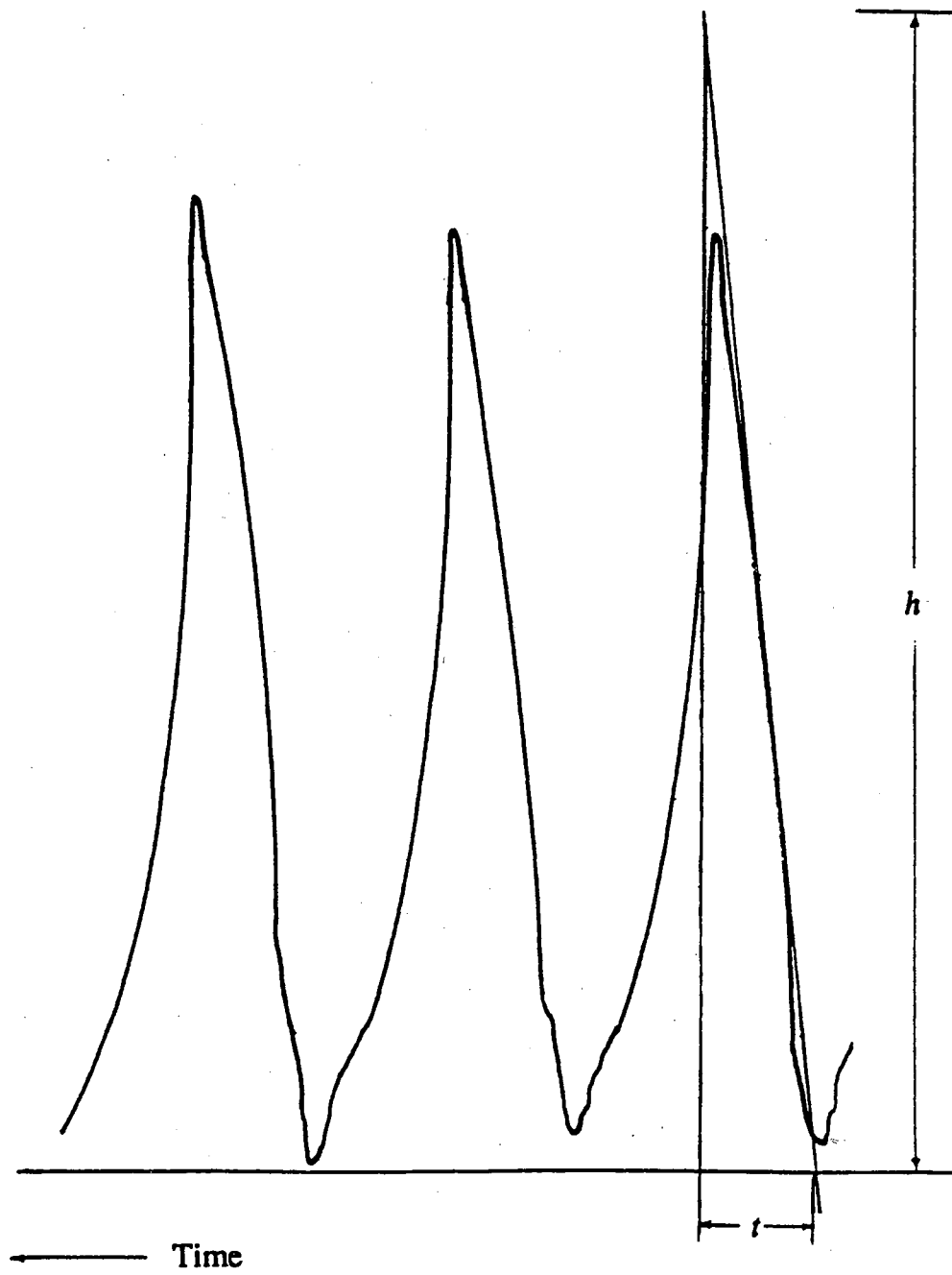
Figure 17. Measurement of Rate of Response from UCF Signal

Effect of Dye

As already mentioned, the coupled reaction system for the determination of glucose generally employs *o*-dianisidine as the dye in the indicator reaction. The oxidized form of the dye has a maximum absorbance at 460 nm. It was found, however, that *o*-dianisidine strongly adsorbed onto the immobilized-enzyme-controlled pore glass layer, impairing the biocatalytic action of the enzymes. 4-Aminophenazone, on the other hand, has been reported to be free of adsorption problems [65], and this was confirmed in this work. In the presence of a *N,N*-(disubstituted) aniline, 4-aminophenazone is oxidized to a purple colored complex in the indicator reaction:

$$H_2O_2 + N,N\text{-(substituted) aniline} + 4\text{-aminophenazone}$$

$$\xrightarrow{\text{Peroxidase}} H_2O + \text{colored complex}$$
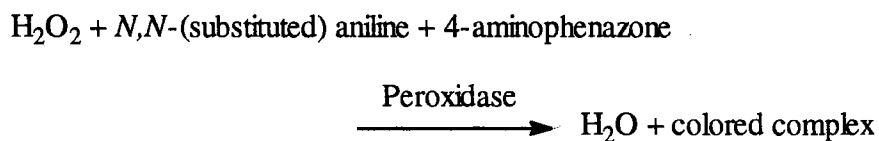
The colored complex shows a broad absorption band with absorbance maximum at 555 nm and with a molar absorptivity of 2.6×10^4 M^{-1} cm^{-1} based on the possible structure illustrated below [66]:
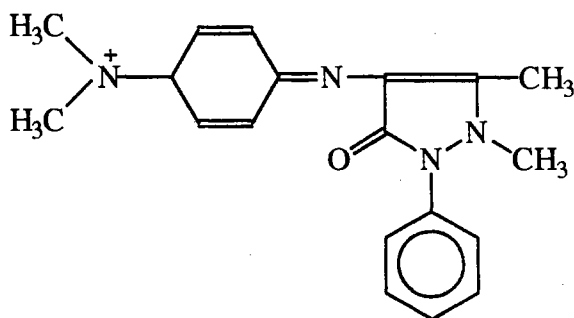
Effect of Lower Reactor Rotation and Continuous-

Flow/Stopped-Flow Operation

As shown in Figure 18, if the lower reactor is devoid of rotation at point A, the response is lower because diffusional limitations control the enzyme-catalyzed reaction. When the rotation of the lower reactor (the rotator disk with immobilized peroxidase) was restored at point B (at 840 rpm), comparatively larger responses were regained. In this figure, i, s, and f symbolize the points of injection of sample, stopping of the flow, and continuation of the flow, respectively.

However, if the lower rotating reactor contains immobilized glucose oxidase and the preparation containing immobilized peroxidase is affixed at the top of the cell, the response is about 90% lower (Figure 19B) than when the enzymes are placed in the opposite configuration (Figure 19A). This suggests that the indicator reaction is slower than the main reaction under the conditions used in this work. Rotating the reactor with immobilized peroxidase lowers the apparent Michlaelis-Menten constant for the rate controlling indicator reaction more efficiently, and the overall rate of the coupled reaction system is more dependent on the rate of the main reaction.

Under continuous-flow conditions (Figure 20A) there is no noticeable response because the mean residence time in the cell is not sufficient for the indicator reaction to proceed to levels of detectable absorbance with the instrumentation and flow conditions used in this work. Very low flow rates (detrimental with regard to dispersion) provide detectable signals; these, however, cannot compare with signals obtained by stopping the flow and rotating the lower reactor (Figure 20B). In

i: injection
s: stop flow
f: flush the cell
A: stop rotation
B: rotation restored
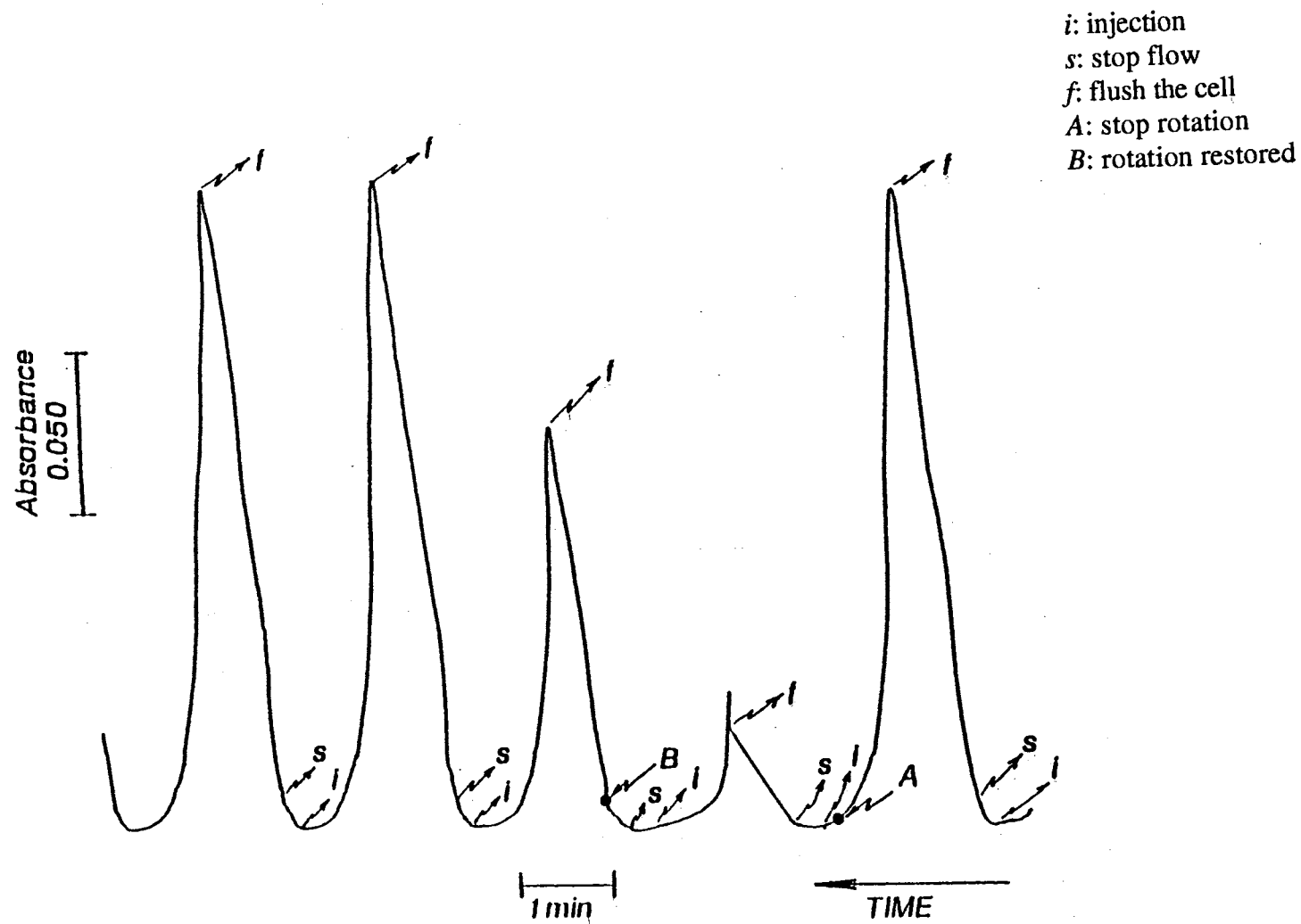
Figure 18. Effect of Reactor Rotation under Stopped-Flow Condition

i: injection
s: stop flow
f: flush the cell
A: peroxidase on the rotating disk
B: glucose oxidase on the rotating disk
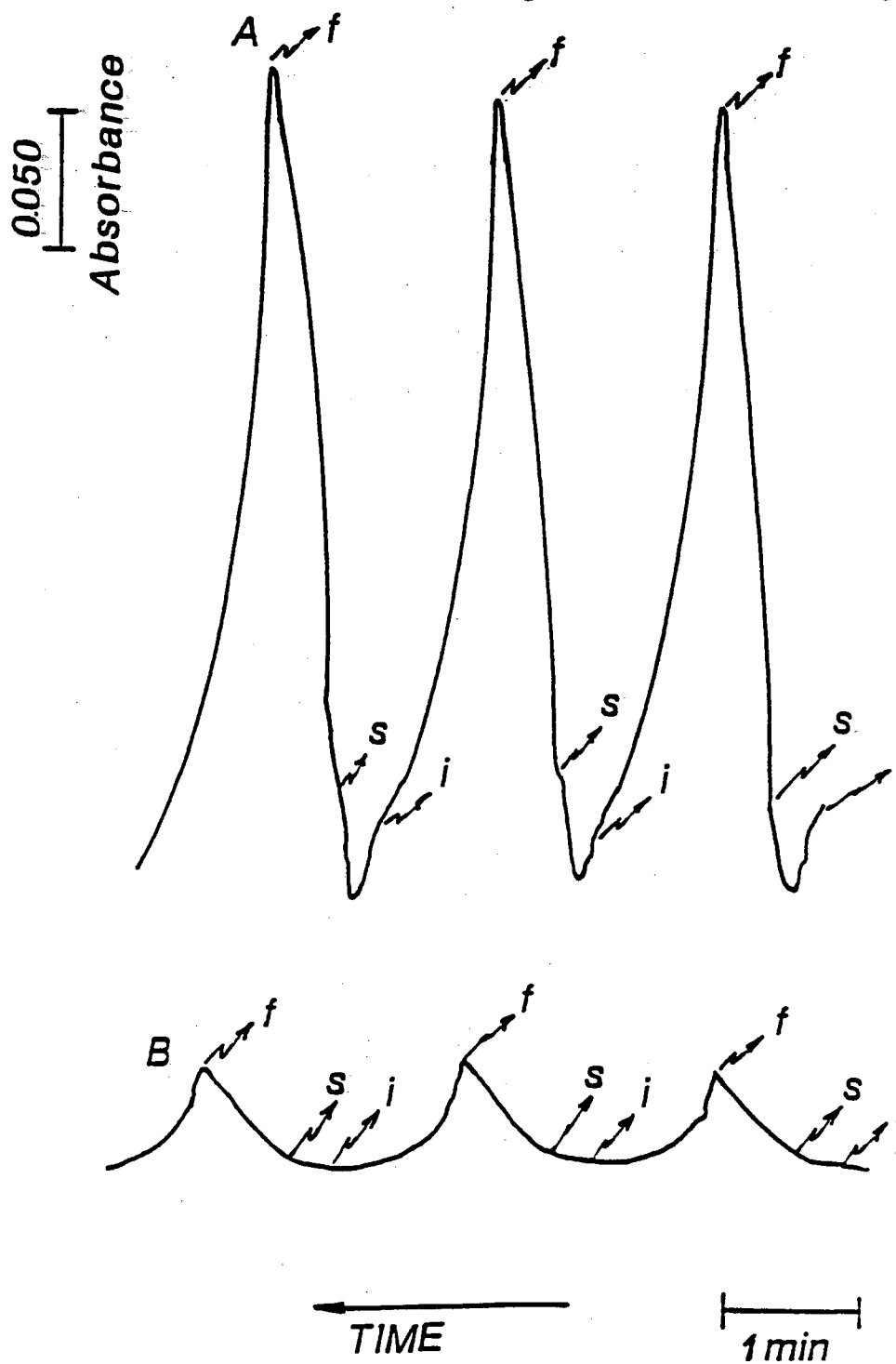
Figure 19. Effect of Inverting Reactors
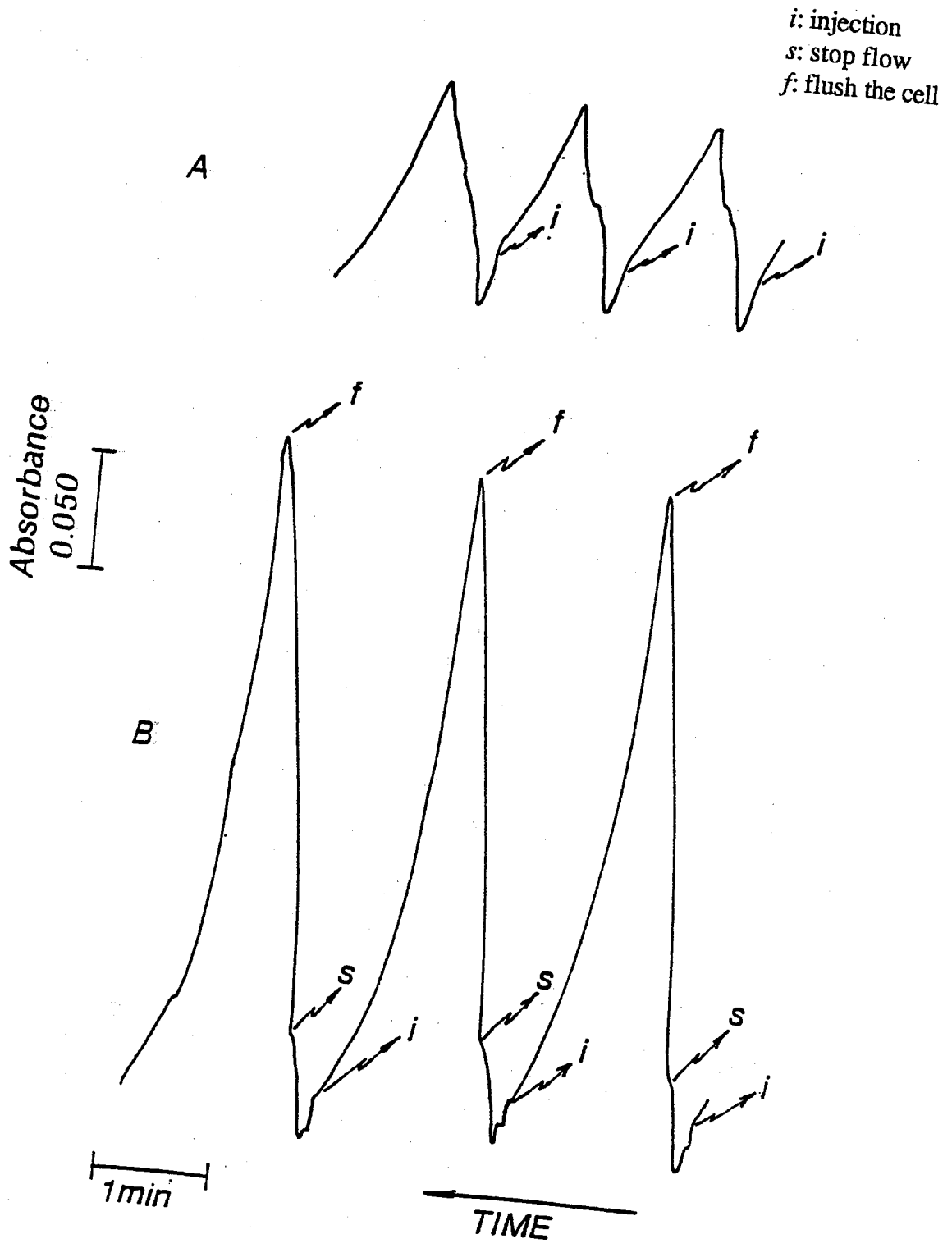
Figure 20. Response under Continuous-Flow (A) and Stopped-Flow (B) Conditions

this work, all the rates of reaction were determined under this continuous-flow/stopped-flow operation.

Effect of Cell Volume and Sample Size

The volume of the cell was changed by sliding the lower part of the cell up or down. As expected, the rate of response decreased with increasing cell volume because of the dilution effect on the enzyme concentration and the absorbance response to the bulk concentration of the colored complex. Considering the trade off between the dilution effect and the signal value, a cell volume of 330 μl (volume comprising the area between the reactors with immobilized enzymes) was used in all measurements.

As expected, the rate of response increased with increasing the sample size until the cell was filled with the sample solution. In this work a sample size of 73.3 μl was obtained by setting the sample loading time at 10 seconds on the FIAtrron SHS-200 unit, and this sample size was used to evaluate other parameters.

The Apparent Michaelis-Menten Constant

Table V summarizes the value of the apparent Michaelis-Menten constant, K'_M, for a given enzyme preparation. These ware obtained at three different rotation velocities and by stopping the flow for 90 seconds. The calculation of K'_M was performed by using the Lineweaver-Burk plot under conditions in which $[S] > K'_M$. The value of K'_M was then obtained from the slope and the intercept of the corresponding plot.

TABLE V

VALUES OF APPARENT MICHAELIS-MENTEN
CONSTANT FOR THE GOD/POD
SYSTEM AT 20±1°C

rotation velocity (rpm)	K_M^* (mM)	linear regression standard deviation
240	0.90	±0.07
420	0.36	±0.08
840	0.21	±0.05
free enzymes in solution**	5.22	±0.11

* each value based on triplicate of six different substrate concentrations.

** estimated by using the o-dianisidine glucose determination kit (Sigma, St. Louis, MO)

As expected, the value of K'_M in Table V decreases as the velocity of rotation increases, and this confirms that rotation of the lower reactor minimizes the diffusional constraints observed when using immobilized enzymes. However, when the rotation velocity was higher than 840 rpm, vibration of the lower reactor, introducing optical artifacts, was observed. Therefore, no measurement was performed at a rotation velocity higher than 840 rpm.

Effect of pH and Glucose Concentration

Most enzymes are active over a limited range of pH and in most cases a definite pH optimum is observed. This pH optimum might be due to a number of effects:

1. the effect of pH on the stability of the enzyme, which may become irreversibly destroyed on one or both sides of the optimum pH;

2. the effect on the V_{max};

3. the effect on the affinity of the enzyme for its substrate;

4. the effect of pH on the indicator reaction.

For the development of an analytical procedure with coupled reactions, the pH dependence of the total enzyme system should be determined experimentally, and the optimum pH should be used for determination. In this work, as shown in Figure 21, the rate of response under stopped-flow conditions was practically independent of pH between pH 6.00 and 6.50. It has been reported that using the same coupled reactions, but using free enzymes, the optimum pH is 7.00 [61]. The difference in the pH profile is probably due to changes in properties of the biocatalysts as a result of immobilization. The immobilization may shift the optimum pH depending upon the nature of the carrier,
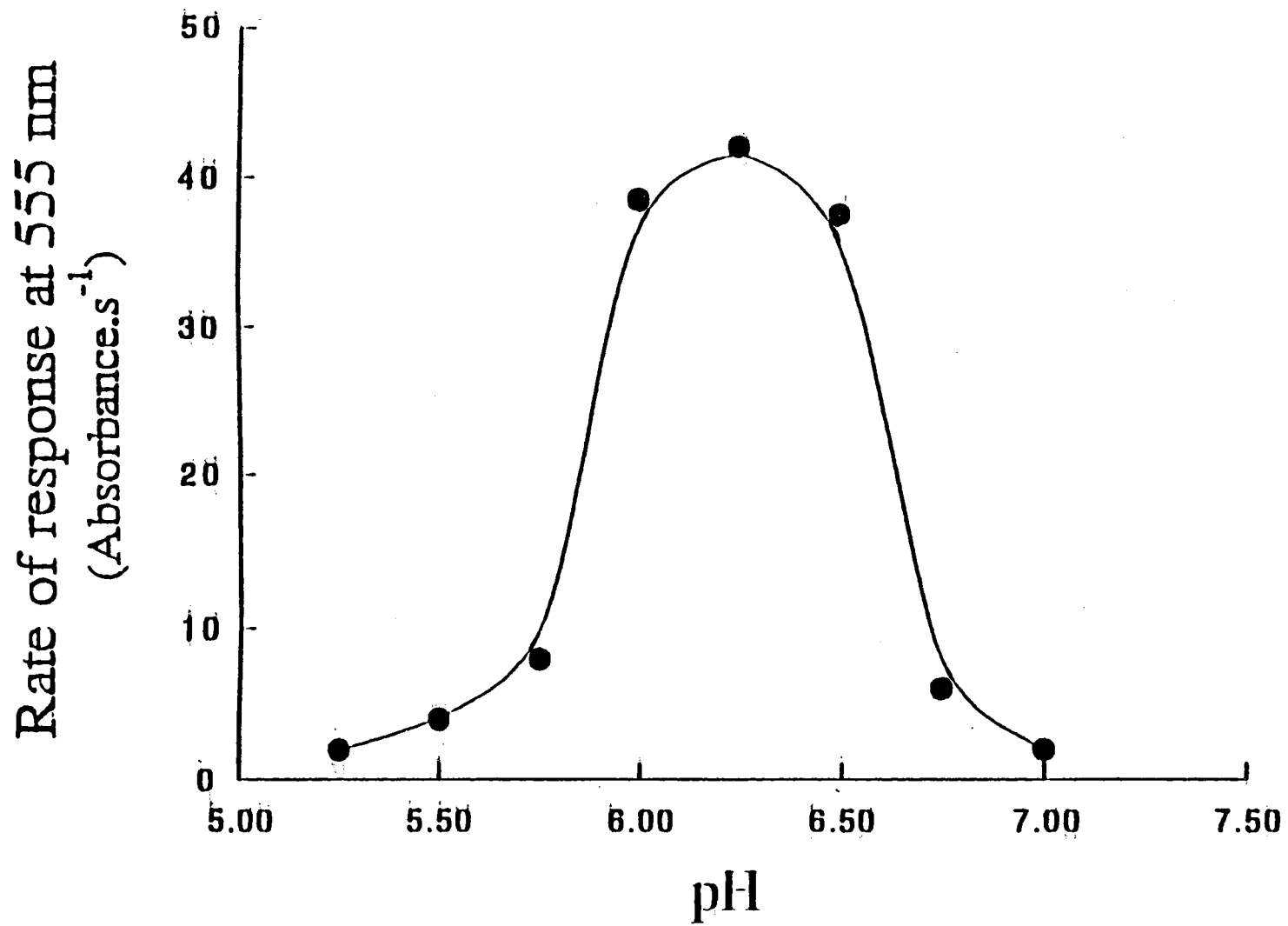
Figure 21. Effect of pH on Rate of Response

chemical modification of the enzyme, the type of enzymatic reaction, and the buffer capacity in the vicinity of enzyme active site [68,69]. In this work, the pH used to evaluate other variables was 6.00 for the convenience of preparation of 0.10 M phosphate buffer.

As shown in Figure 22, a linear relationship was observed between the rate of response and the glucose concentration in the range of 0.010 mM and 0.50 mM (rotation at 840 rpm):

$$\text{Rate of response (at 555 nm)} = 1.16 + 51.89[C_{glucose}, \text{mM}]$$

The linear regression coefficient for this type of plot was typically 0.9991, the standard deviations of slope and intercept were 0.91 and 0.18, respectively. Based on 3 times the sample standard deviation of blank readings, the limit of detection was estimated to be 0.010 mM. The relative standard deviation for six successive measurements using a 0.070 mM glucose solution was typically 0.78%.

Determination of Glucose in Serum Samples

Glucose concentration was determined in two (normal and abnormal) serum standards (Accutrol™) and in fifteen samples of bovine blood serum. The results are shown in Table VI. The samples were deproteinized because they arrived at the laboratory markedly colored and turbid. A volume of 0.50 ml of each sample (1:20 protein-free) was diluted to 5.00 ml with phosphate buffer (0.10 M total phosphate, pH 6.00). The resulting solution was intercalated into the UCF system, as shown in Figure 15.
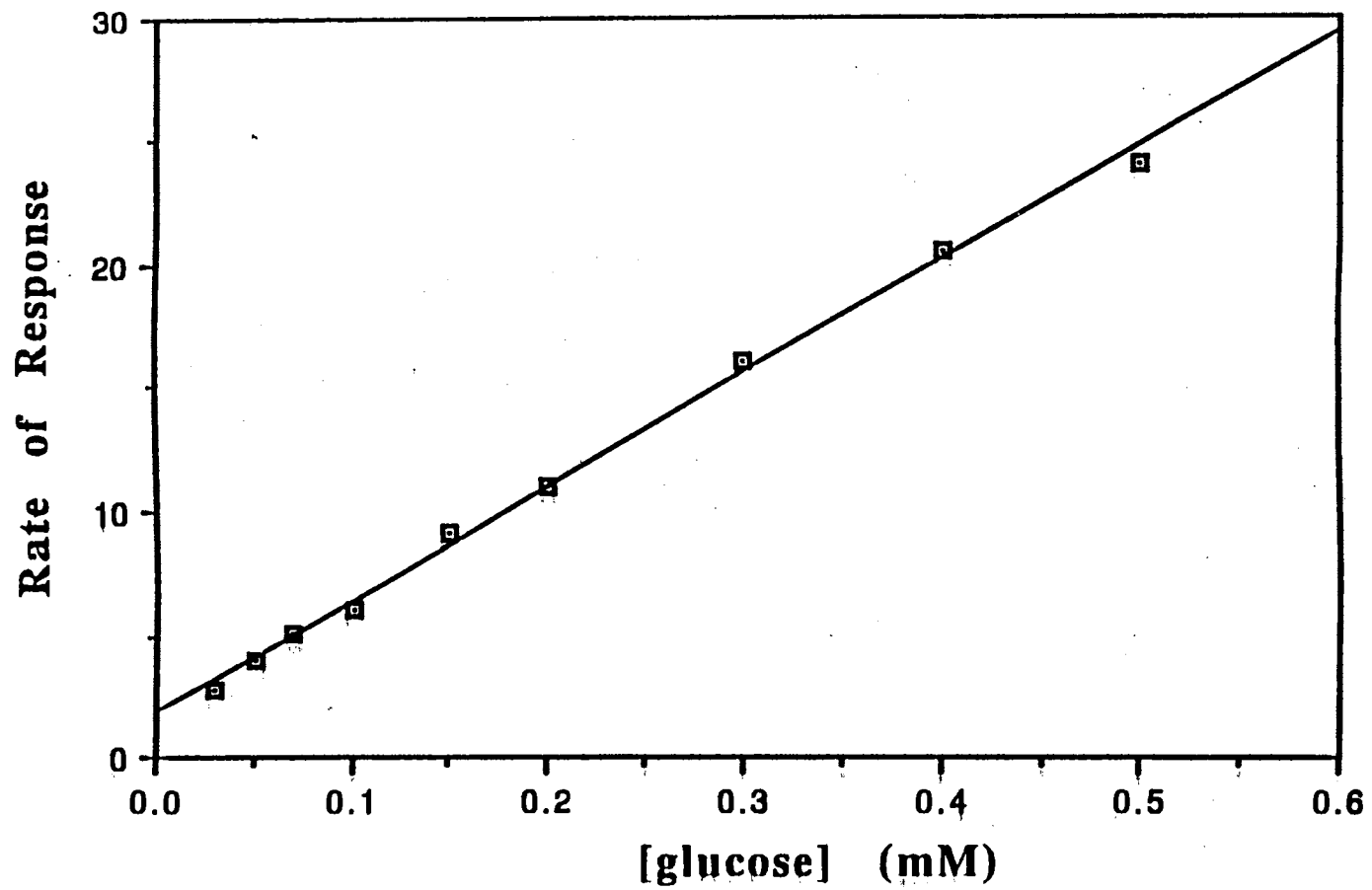
Figure 22. Linear relationship between the Rate of Response and Glucose Concentration

TABLE VI

GLUCOSE CONCENTRATION
IN SERUM SAMPLES

blood serum sample	[glucose] (mg/dL) o-dianisidine method	[glucose] (mg/dL) proposed method
normal*	80.83	84.16
abnormal*	291.75	297.04
serum 1	68.15	72.25
serum 2	74.15	70.12
serum 3	67.80	63.06
serum 4	67.40	66.14
serum 5	47.65	49.01
serum 6	70.85	73.35
serum 7	65.32	69.08
serum 8	70.50	74.00
serum 9	69.95	70.00
serum 10	65.30	67.00
serum 11	71.00	73.00
serum 12	64.60	64.00
serum 13	60.70	62.00
serum 14	65.70	58.00
serum 15	52.70	50.00

* standard human serum samples (Accutrol™ from Sigma, St. Louis, MO)

Although several chemical species (e.g. urate, ascorbate, bilirubin, and gluathione) interfere in the reaction involving horseradish peroxidase in the determination with *o*-dianisidine [61], such interferences were not observed in the direct determination of glucose in this work. The reasons probably are:

1. immobilized enzymes had less affinity for these interferences, and

2. the concentration of these interferences were very low in the serum samples analyzed.

Figure 23 correlates the results obtained by applying the *o*-dianisidine determination with the kit mentioned in the experimental section and by applying the method developed in this work. The *o*-dianisidine method used was an equilibrium approach using free glucose oxidase and peroxidase. In this approach, *o*-dianisidine is used as the dye in the indicator reaction, and the concentration of glucose is determined by measuring the total color change of the reaction system after the overall reaction reaches equilibrium. Between these two methods, the standard error of the difference [70] was estimated to be 1.08, and the Pearson's correlation coefficient was calculated to be 0.998 with the help of the following equation [71]:

$$r = \frac{\sum X_i Y_i - \sum X_i \sum Y_i}{\{[n\sum X_i^2 - (\sum X_i)^2][n\sum Y_i^2 - (\sum Y_i)^2]\}^{1/2}} \qquad (3.15)$$

where r is the correlation coefficient, n is the number of observations, and X_i and Y_i are the individual values of the concentrations of glucose determined by these two different methods.
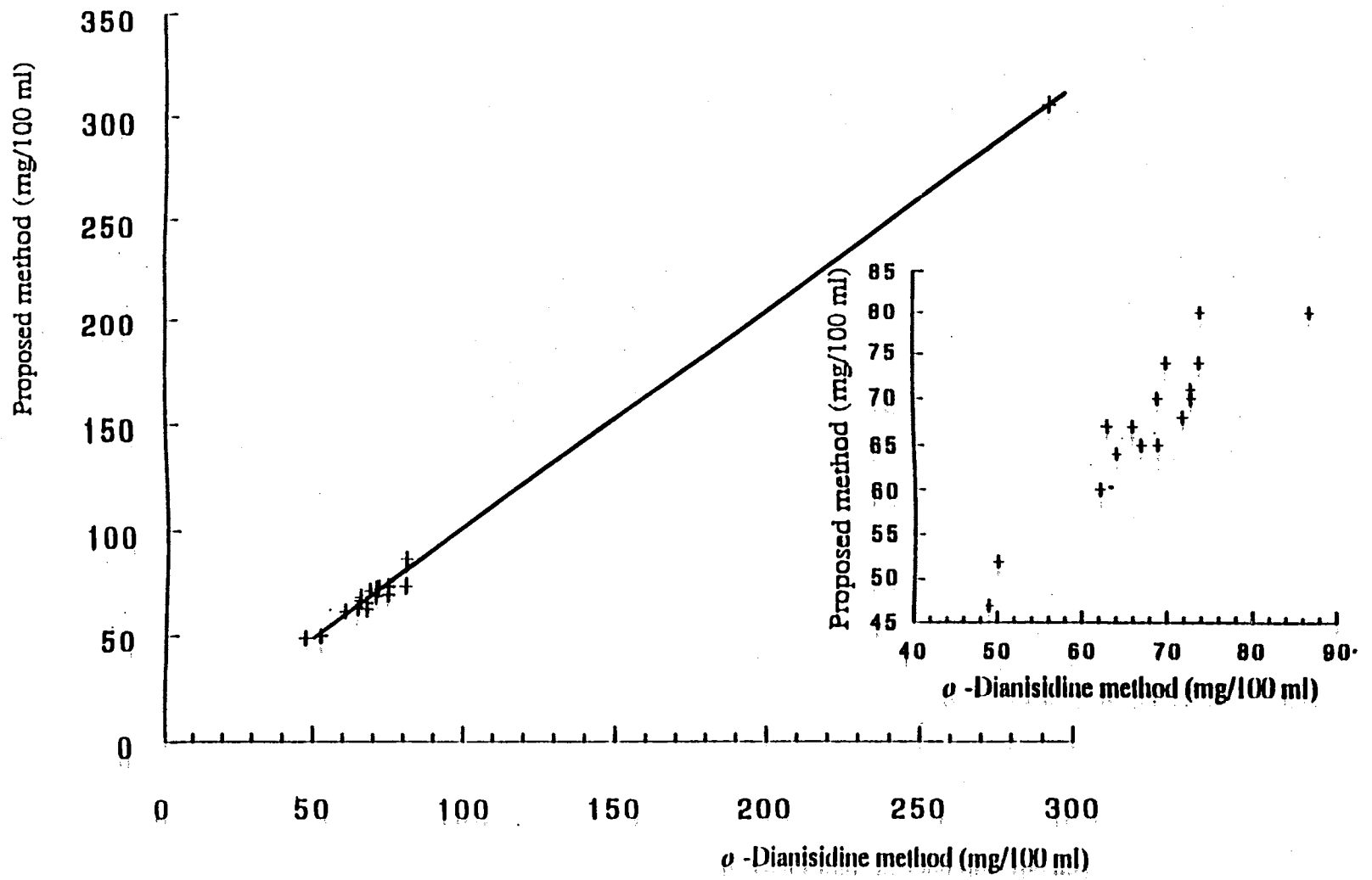
Figure 23. Comparison of Results from this Method and o-Dianisidine Method

If a minimum measurement time of about 90 seconds is considered, together with the sample transport time and a cell-flushing time of 30-60 seconds, the sum of these times gives a figure of about 20 for the number of samples which can be processed in 1 hour.

Conclusion

The research reported in this chapter, as in the previous chapter, illustrates an example of a UCF system for applying kinetic methods in analytical chemistry. The emphasis was, however, on the implementation of chemical coupling of two enzyme-catalyzed reactions (main reaction and indicator reaction) in a specially designed flow-through bioreactor/photometric cell. The cell comprises parallel bioreactors facing each other, with the lower reactor rotating and the upper reactor fixed. The overall approach was shown to conveniently implement the chemical coupling utilizing very small amounts of biocatalysts. This is because the imposed rotation to one of the reactors minimizes diffusional constraints that slow down the process of substrates reaching the active site of biocatalysts and also slow down the release of products from the same site. Immobilized enzymes were used in this research to prepare the bioreactors, and these bioreactors were re-used under flow conditions for long periods. Also, the continuous-flow/stopped-flow/continuous-flow operation employed in this UCF system provided a fast, accurate, sensitive approach for the determination of glucose in serum samples. The main relevance of the work reported here is that this approach can be used with any of the commonly used main enzyme-catalyzed/secondary (indicator) reactions with spectrophotometric monitoring.

CHAPTER IV

INDIRECT ENZYMATIC DETERMINATION

OF PHOSPHATE

Introduction

Inorganic phosphate, PO_4^{3-}, is important in many products, such as detergents, cola drinks, dental abrasives, and flame retardants. It is an essential nutrient for plants and animals, but when it becomes a waste product, whether in sewage, fertilizer run-off, or detergent effluent, it can cause "algal bloom" in lakes, rivers, and even in coastal sea waters, leading to oxygen depletion and fish kills. This eutrophication has led to the banning of phosphate detergents in some states in the USA. According to the Quality Criteria for Water from the United States Environmental Protection Agency (EPA) [72], " to prevent the development of biological nuisances and to control accelerated or cultural eutrophication, total phosphate as phosphorus (P) should not exceed 50 μg/L in any stream at the point where it enters the lake or reservoir, nor exceed 25 μg/L within the lake or reservoir."

For the determination of phosphate in water samples, various methods, based on the spectrophotometric determination of molybdophosphate derived from the Fiske and Subbarow method [73], have been widely used. These methods generally require

pretreatment of the sample, the use of hazardous chemicals, and they are time-consuming and complicated. The monitoring of pollution and environmental control cannot be achieved easily with such methods. Therefore, the design of highly selective determinations that are easy to handle, give a fast response, and are suitable for continuous use is relevant in the search for alternatives.

Because of the high selectivity and low environmental impact, enzymatic methods hold the promise of ideal alternatives. In 1975, Guilbaut and Nanjo [74] reported an indirect enzymatic method for the determination of phosphate with the electrochemical detection of oxygen. In their work, the following coupled reactions were involved:

$$\text{Glucose-6-phosphate} \xrightarrow{\substack{\text{alkaline} \\ \text{phosphatase}}} \text{glucose} + \text{phosphate}$$

$$\text{glucose} + O_2 \xrightarrow{\substack{\text{glucose} \\ \text{oxidase}}} \text{gluconic acid} + H_2O_2$$

The competitive inhibition by added phosphate causes a decrease in the consumption of dissolved oxygen by the second reaction. The added phosphate can be detected with a limit of detection of 1.0×10^{-4} M by using amperometric detection.

Five years later Cornell et al. [75] reported a direct enzymatic method for the determination of phosphate using the following reactions:

$$\text{fructose 1,6-diphosphate} \underset{}{\overset{\text{aldolase}}{\rightleftharpoons}} \text{dihydroxyacetone phosphate} \\ + \text{glyceraldehyde 3-phosphate}$$

$$\text{glyceraldehyde 3-phosphate} + \text{phosphate} + NAD^+ \underset{}{\overset{\substack{\text{gyceraldehyde} \\ \text{3-phosphate} \\ \text{dehydrogenase}}}{\rightleftharpoons}} NADH^+ \\ + \text{1,3-diphosphoglycerate} + H^+$$

$$\text{1,3-diphosphoglycerate + ADP} \xrightleftharpoons{\text{phosphoglycerate kinase}} \text{3-phosphoglycerate + ATP}$$

$$\text{ATP + glucose} \xrightleftharpoons{\text{hexokinase}} \text{ADP + glucose 6-phosphate}$$

where NAD^+ and $NADH$ are the oxidized and reduced form of nicotinamide adenine dinucleotide, and ADP and ATP are adenosine diphosphate and adenosine triphosphate, respectively. The first reaction provides the glyceraldehyde 3-phosphate for the second (indicator) reaction. The third reaction forces equilibrium toward the right and causes phosphate to be reacted completely. Adenosine diphosphate, ADP, used in the third reaction, is regenerated in the fourth reaction and serves to drive the third one. Therefore, the phosphate can be determined photometrically by monitoring the absorbance change at 340 nm caused by $NADH$ formation. The limit of detection obtained by this approach was 1.0×10^{-4} M. Because so many enzymes and reactions are involved in this method, and because the limit of detection is not better than in those using fewer enzymes, it has attracted little practical interest.

Other enzymes and reaction systems can be used for the determination of phosphate. Alkaline phosphatase (AP), for example, is a very stable enzyme and can catalyze a group of hydrolysis reactions of phosphate esters to give inorganic phosphate and a phenolic leaving group, as illustrated below:

The formation of this phenolic moiety has been followed by absorption spectrophotometry using phenylphosphate [76] or *p*-nitrophenylphosphate [77], by chemiluminescence using dioxitanephosphate [78], and by amperometry using *o*-hydroxyphenylphosphate [79] or *p*-aminophenylphosphate [80]. Therefore, there are many detection approaches that can be employed to determine phosphate on the basis of its inhibition of the enzyme.

Because only one enzyme is needed and different means of detection can be selected, the approach based on the inhibition of phosphate on alkaline phosphatase catalyzed hydrolysis reactions was studied to indirectly determine phosphate in aqueous solution. As shown in the previous chapters, by combining rotating bioreactor/detector units with an UCF system, the diffusional constraints and dilution (dispersion) effects on the detection can be reduced. Therefore, better results than existing methods should be expected.

In the work reported here, *p*-aminophenylphosphate and *p*-nitrophenylphosphate were used as the phosphate ester substrates to determine the added phosphate in water samples with amperometric and photometric detection, respectively. Their structures are shown below:
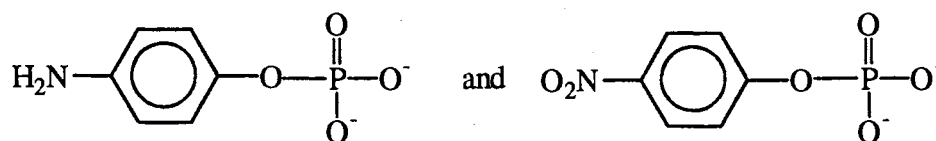
Two different bioreactor/detector units were used for the evaluation of the two different detection approaches, and the results from these two different methods have been compared. For a better understanding of how the determination approach works, the principles of inhibition are discussed in the section that follows.

Inhibition

Many substances alter the activity of an enzyme by combining with it in a way that influences the binding of substrate and/or its turnover number. Substances that reduce an enzyme's activity in this way are known as inhibitors.

An inhibitor that competes directly with a normal substrate for an enzyme active site is called a *competitive* inhibitor. The general model for competitive inhibition is given by the following reaction scheme:

$$E + S \underset{k_{-1}}{\overset{k_1}{\rightleftharpoons}} ES \xrightarrow{k_2} P + E$$

$$\begin{aligned} & + \\ & I \\ & \Updownarrow K_I \\ & EI + S \longrightarrow NO\ REACTION \end{aligned}$$
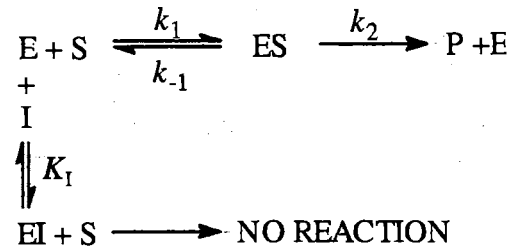
Here it is assumed that the inhibitor, I, binds reversibly to the enzyme E and is in rapid equilibrium with it, so that:

$$K_I = \frac{[E][I]}{[EI]} \tag{4.1}$$

In *uncompetitive* inhibition, the inhibitor binds directly to the enzyme-substrate complex ES, but not to the free enzyme:

$$E + S \underset{k_{-1}}{\overset{k_1}{\rightleftharpoons}} ES \xrightarrow{k_2} P + E$$

$$\begin{aligned} & + \\ & I \\ & \Updownarrow K'_I \\ & ESI \longrightarrow NO\ REACTION \end{aligned}$$
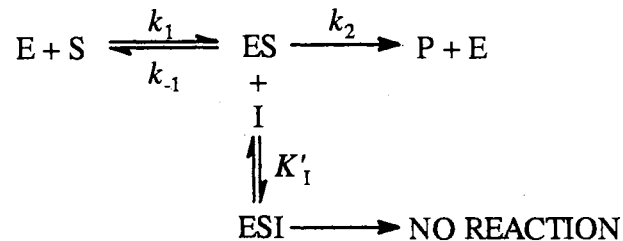
The enzyme-substrate-inhibitor complex has the dissociation constant:

$$K'_I = \frac{[ES][I]}{[ESI]} \tag{4.2}$$

If both the enzyme and the enzyme-substrate complex bind to the inhibitor, the following results:
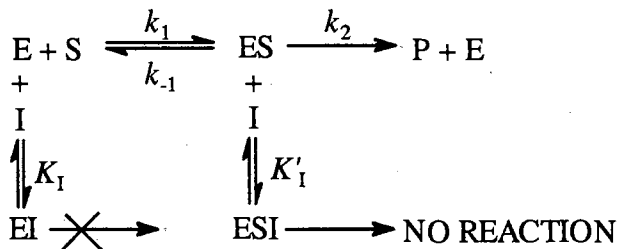
This phenomenon is known as *mixed* inhibition or *non-competitive* inhibition.

It is well known that the hydrolysis of phosphate esters catalyzed by alkaline phosphatase is subject to competitive inhibition by inorganic phosphate [81]. Therefore, only the mechanism of competitive inhibition is described in more detail here.

Because of the existence of EI, the total enzyme concentration is:

$$[E]_T = [E] + [EI] + [ES] \tag{4.3}$$

As discussed in the previous chapter, under steady-state conditions:

$$[E] = \frac{K_M[ES]}{[S]} \tag{4.4}$$

Rearranging Eq. (4.1) and substituting Eq. (4.4) into it:

$$[EI] = \frac{[E][I]}{K_I} = \frac{K_M[ES][I]}{[S]K_I} \tag{4.5}$$

Substituting the later two results into Eq. (4.3) yields:

$$[E]_T = [ES]\{\frac{K_M}{[S]}(1 + \frac{[I]}{K_I}) + 1\} \tag{4.6}$$

which can be rearranged to:

$$[ES] = \frac{[E]_T[E]}{K_M(1+\frac{[I]}{K_I})+[S]} \qquad (4.7)$$

Hence, the initial rate can be expressed as:

$$\upsilon_0 = k_2[ES] = \frac{k_2[E]_T[S]}{K_M(1+\frac{[I]}{K_I})+[S]} \qquad (4.8)$$

or

$$\upsilon_0 = \frac{V_{max}[S]}{\alpha K_M + [S]} \qquad (4.9)$$

where

$$V_{max} = k_2[E]_T \qquad (4.10)$$

and

$$\alpha = 1 + \frac{[I]}{K_I} \qquad (4.11)$$

Eq. (4.9) is the Michaelis-Menten equation with K_M modulated by α, a function of the inhibitor concentration (which will always be ≥ 1). The value of [S] at $\upsilon_0 = V_{max}/2$ is, therefore, αK_M.

Figure 24 shows the hyperbolic plot of Eq. (4.9) for various values of α. Note that as [S] $\rightarrow \infty$, $\upsilon_0 \rightarrow V_{max}$ for any value of α. The larger the value of α, however, the greater

V_{max}

v_0

$\dfrac{V_{max}}{2}$

α = 1 (no inhibitor)

Increasing [I]

α = 2

α = 4

V_{max}: maximum rate
[S]: substrate concentration
[I]: inhibitor concentration
K_I: enzyme-inhibitor complex dissociation constant
α = 1+[I]/K_I
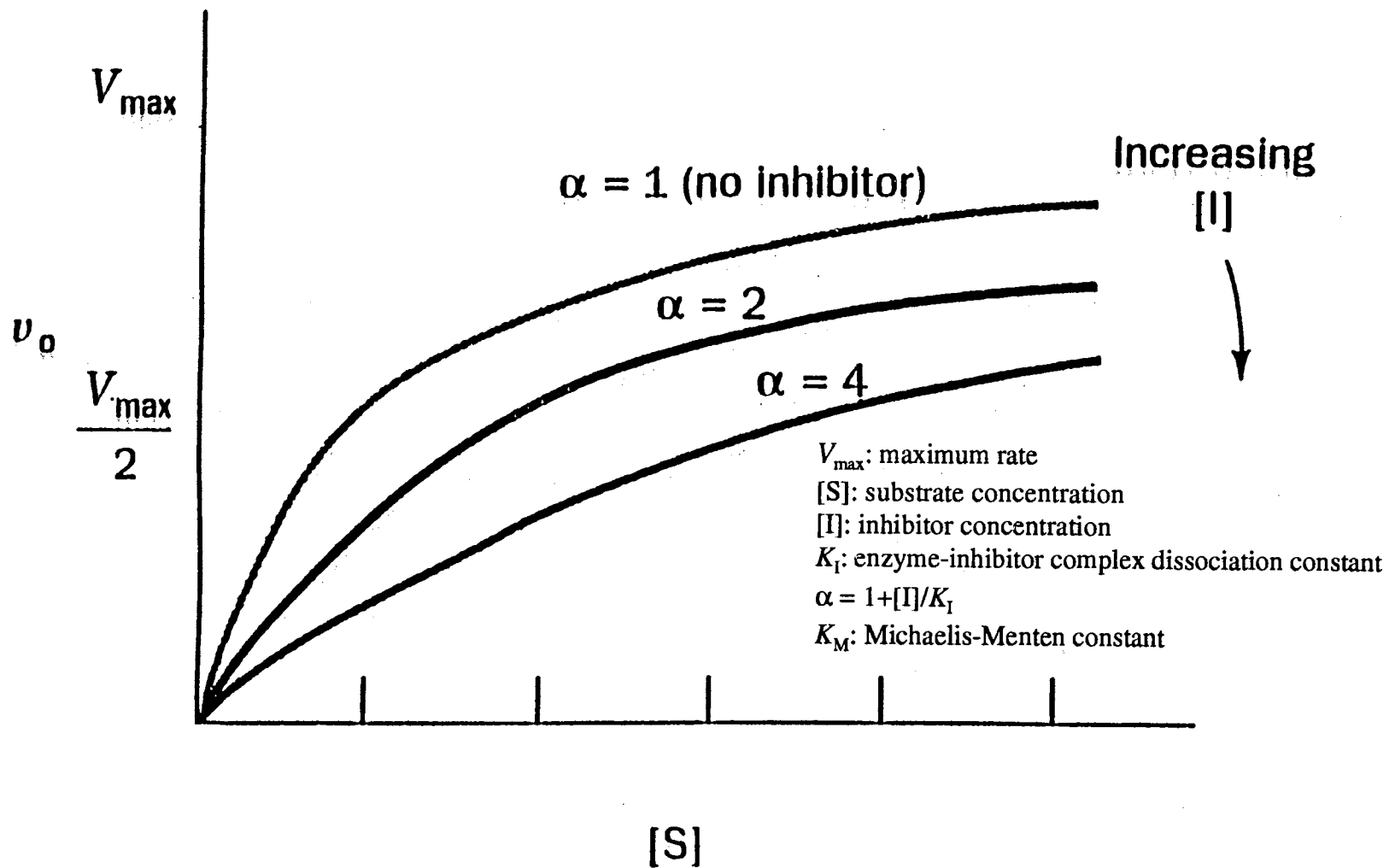K_M: Michaelis-Menten constant

[S]

Figure 24. Plot of V_{max} vs. [S] for Various α Values

[S] must be to approach V_{max}. Thus, the inhibitor does not affect the turnover number of the enzyme. Rather, the presence of I has the effect of making [S] appear to be more dilute than it really is. Conversely, increasing [S] shifts the substrate-binding equilibrium towards [ES]. Hence, there is a true competition between I and S for the enzyme's substrate-binding site, such that, their binding is mutually exclusive. Therefore, at a given substrate concentration [S], the inhibitor concentration can be determined by measuring the change in initial rate.

Because Eq. (4.9) can be rearranged to its double reciprocal form:

$$\frac{1}{\upsilon_0} = (\frac{\alpha K_M}{V_{max}})\frac{1}{[S]} + \frac{1}{V_{max}} \tag{4.12}$$

A plot of $1/\upsilon_0$ vs. $1/[S]$ is linear and has a slope of $\alpha K_M/V_{max}$, a $1/[S]$ intercept equal to $-1/\alpha K_M$, and a $1/\upsilon_0$ intercept equal to $1/V_{max}$ (Figure 25). The double reciprocal plots for a competitive inhibitor at various concentrations of I intercept at $1/V_{max}$; this is the diagnostic criteria for competitive inhibition as compared with other types of inhibition. The value of K_I can be found from Eq. (4.11) by determining the values of α at different inhibitor concentrations.

To have an accurate determination of the competitive inhibitor using a kinetic approach, the following factors need to be considered:

1. The inhibitor concentration, [I], should not be much less than the value of the enzyme-inhibitor dissociation constant, K_I. From Eq. (4.11), it can be known, that if $[I] \ll K_I$, $\alpha \rightarrow 1$, no more inhibition can be detected.

2. The substrate concentration, [S], should be as low as possible. Lower [S] values can make the αK_M term predominant in Eq. (4.9). That is, the change of initial rate, υ_0,

Figure 25. Plot of $1/v_o$ vs. $1/[S]$ for Various α Values

Labels within figure:

$1/v_o$

Increasing [I]

$\alpha = 4$

$\alpha = 2$

$\alpha = 1$ (no inhibitor)

$1/V_{max}$

V_{max}: maximum rate
[S]: substrate concentration
[I]: inhibitor concentration
K_I: enzyme-inhibitor complex dissociation constant
$\alpha = 1+[I]/K_I$
K_M: Michaelis-Menten constant

$-1/\alpha K_M$

0
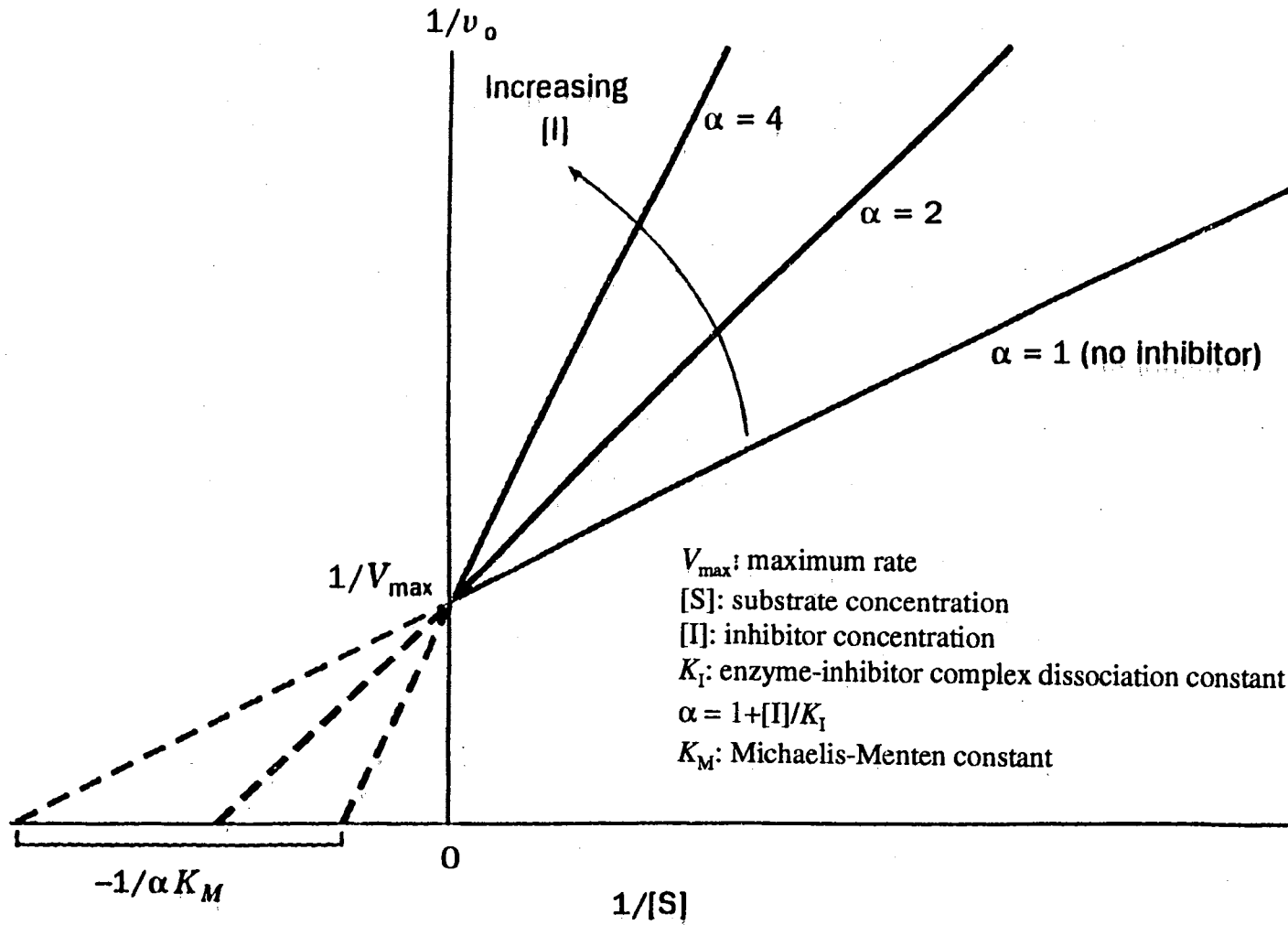
$1/[S]$

is more sensitive to the change in inhibitor concentration, [I]. The substrate itself, or its co-reactant(s), the product formed, however, should be concentrated enough to be sensitively detected.

In this work, *p*-nitrophenylphosphate and *p*-aminophenylphosphate were evaluated as two different substrates in the hydrolysis reaction catalyzed by alkaline phosphatase (AP). The products formed from these two substrates, *p*-nitrophenol and *p*-aminophenol, were detected photometrically and amperometrically, respectively. These two approaches are compared.

<div align="center">Experimental</div>

Preparation of the Bioreactor/Detector Units

In these studies, two types of bioreactor/detector cells were used with a UCF system for either photometric or amperometric detection. The photometric cell was the same as the one described in Chapter III, except that only one enzyme (AP) was used, and that this enzyme was immobilized on the rotating disk. The amperometric cell is illustrated in Figure 26. The body of the cell was made of Plexiglas. The ring electrode was formed by pressing a carbon paste (70% graphite and 30% light mineral oil) into an annular well at the top part of the cell. A copper wire was used to connect the carbon paste ring electrode to the potentiostat/amperometric detector unit. In this design, a magnetic bar was embedded into the rotating disk. The disk was 11 mm in diameter and 3 mm in thickness. The volume of the cell defined by the surface of the ring electrode and the rotating disk reactor was 113 μL.
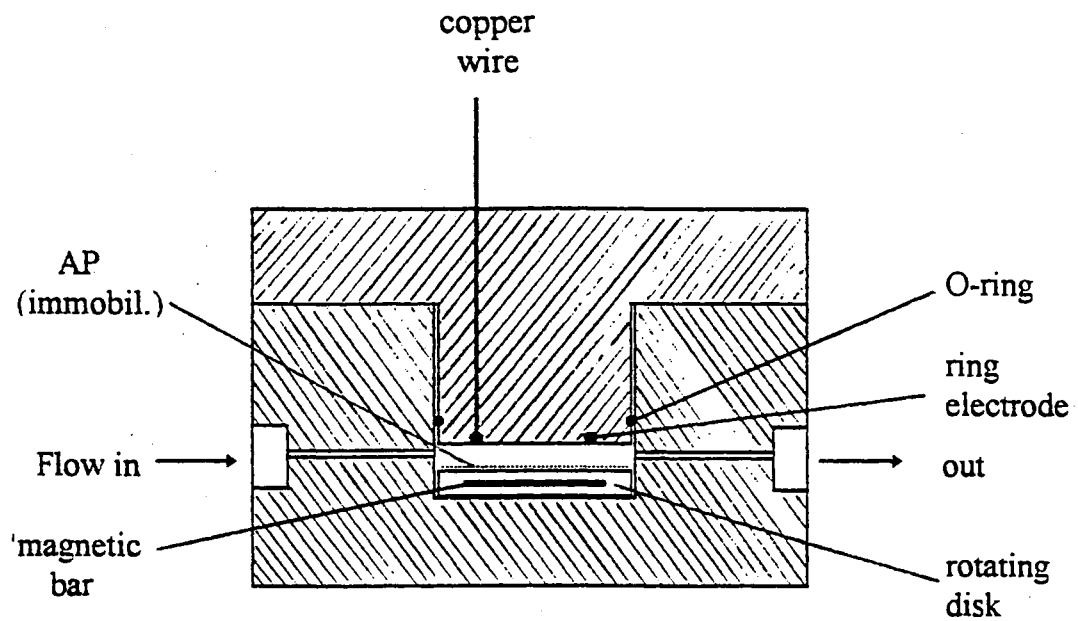
Figure 26. The Rotating Bioreactor/Amperometric Cell

The Unsegmented Continous Flow System

For photometric detection, the UCF system was exactly the same as the one used in Chapter III. For amperometric detection, the UCF system is illustrated in Figure 27. In this system the working electrode (WE) was a carbon paste ring electrode prepared as described above, the reference electrode (RE) was a Ag/AgCl reference electrode (3 M NaCl, from Bioanalytical Systems, West Lafayette, IN), and the auxiliary electrode (AU) was made of a stainless steel tube. A potentiostat/amperometric detection unit (Model LC-4B, Bioanalytical Systems, West Lafayette, IN) was used for potential control and current to voltage conversion and amplification. The readout device was a strip-chart recorder (Model 7127A, Hewllett Packard, St. Diego, CA). A microprocessor-controlled solution handling unit (FIAtron SHS-200, FIAtron Systems, Milwaukee, WI) was used for pumping, sample introduction, and for controlling the flow. The various type of tubing and the magnetic stirrer have already been described in Chapter III.

Enzyme Immobilization

The procedure for enzyme immobilization was the same as the one described in Chapter III. The enzyme used was alkaline phosphatase [EC 3.1.3.1] from bovine intestinal mucosa (type VII-NA, Sigma Chemical, St. Louis, MO) containing 27500 units in 1 mL of 3.2 M $(NH_4)_2SO_4$ solution (pH 7.0). Ten microliters of the enzyme suspension solution was diluted to 10 mL with 0.10 M Tris buffer solution (pH 8.0). Then 5 mL of the diluted enzyme solution was used for the preparation of the reactor. The preparation
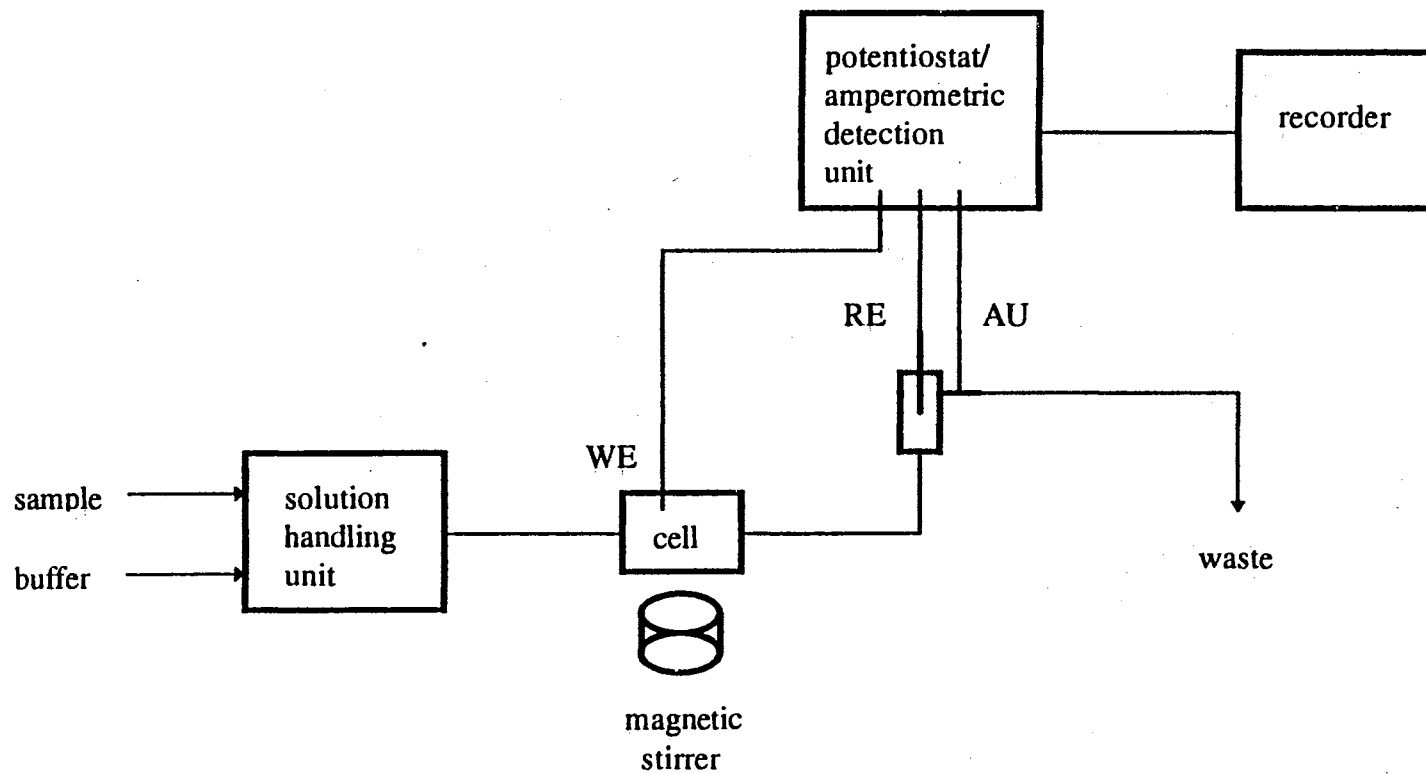
Figure 27. The UCF System with Amperometric Detection

was stored in Tris buffer solution (pH 8.0) and at 5 °C between uses, and it was stable for more than 5 months.

Preparation of Reagents and Samples

All chemicals used, except as noted, were of analytical reagent grade. The water used for solution preparation was deionized and further purified by distillation in an all-borosilicate-glass still with a quartz immersion heater. The p-nitrophenylphosphate (p-NPP) was from Sigma Chemical Co. (St. Louis, MO). The carrier solution was a 0.050 M carbonate buffer (pH 9.0).

p-Aminophenylphosphate (p-APP) was synthesized from p-nitrophenylphosphate (p-NPP) by hydrogenation as described by Thompson et al. [80]. Three grams of p-NPP were dissolved in 80 mL of degassed water, and the solution was quickly adjusted to a pH of 6.3 with 1.00 M hydrochloric acid. Eighty milligrams of Pd/C catalyst (Aldrich, No. 20,569-9) was added to the solution in a thick-walled vessel. The vessel was attached to a hydrogen shaker, purged three times with nitrogen gas, purged three times with hydrogen gas, and then shaken under 40 psi of hydrogen for 90 min. The vessel was flushed three times with nitrogen before removing it from the shaker. The catalyst was filtered from the solution, the water was removed by rotary evaporation at 100 °C , and impurities were removed by washing the solid with absolute ethanol. The cream-colored solid was heated at 100°C for 2 min to remove the remaining ethanol, and then stored at 4 °C. This synthesis was performed in the Hazardous Reaction Facility of the Chemistry Department with the help of Professor E.J. Eisenbraun.

Characterization of *p*-Aminophenylphosphate

Cyclic voltammetry was used to examine the electrochemical properties of the

substrates *p*-APP and *p*-NPP and of the products of the enzyme reactions. The cyclic

voltammetry of *p*-NPP and *p*-APP was performed to compare the electrochemical

properties of the two substrates. Cyclic voltammetric runs were performed with the aid of

a BAS-100 Electrochemical Analyzer (Bioanalytical Systems, West Lafayette, IN). The

working electrode was a carbon paste electrode (70% graphite and 30% light mineral oil),

the reference electrode was a Ag/AgCl, 3 M NaCl reference electrode from Bioanalytical

Systems, and the auxiliary electrode consisted of a Pt wire. After degassing under vacuum,

solutions of 2.0 mM *p*-APP and 2.0 mM *p*-NPP in 0.050 M carbonate buffer (pH 9.0)

were used for the characterization and comparison of the two detection methods. The

cyclic voltammetry of the substrates in the buffer were run first. Then, the cyclic

voltammograms of products (*p*-aminophenol and *p*-nitrophenol) formed from the AP-

catalyzed reactions were obtained after 2 min of adding AP to substrate-buffer solutions.

The scan rate used was 50 mV/sec.

Hydrodynamic Voltammetry of the UCF System
with *p*-Aminophenylphosphate

For the determination of phosphate using the UCF system with the rotating

bioreactor/amperometric cell, a hydrodynamic voltammogram (current vs. applied

potential under continuous-/stopped-flow conditions) was obtained. This was done to find

the optimum applied electrode potential under rotating hydrodynamic conditions; the

solution used for this purpose was 2.0 mM p-APP in 0.05 M carbonate buffer (pH 9.0).

The rotation speed was 840 rpm and the applied electrode potential was scanned from 50

mV to 320 mV (carbon paste vs. Ag/AgCl). The response is expressed as peak height

(mV) recorded at a fixed time interval (30 sec) from the point of stopping the flow.

Amperometric Determination of Phosphate Using
p-Aminophenylphosphate as Substrate

The amperometric determination of phosphate was carried out under the following

conditions:

1. the applied electrode potential was 300 mV against the Ag/AgCl reference;

2. the enzyme reactor was rotated at 840 rpm;

3. the time intervals for flushing, injecting the sample, and stopping the flow were

    60, 30, and 60 seconds, respectively.

The sample solutions were 1.0×10^{-7} M p-APP in 0.050 M carbonate buffer (pH 9.0) with

different concentrations of added phosphate. The rates of response from the amperometric

detector were measured by taking the slope of the leading part of the peak as described in

the previous chapter.

Photometric Determination of Phosphate with
p-Nitrophenylphosphate as Substrate

For the photometric determination of phosphate, a wavelength of 460 nm was

selected to detect the p-nitrophenol formed in the hydrolysis reaction:

$$O_2N-\!\!\langle\bigcirc\rangle\!\!-O-\overset{\overset{O}{\|}}{\underset{\underset{O^-}{\|}}{P}}-O^- + H_2O \xrightleftharpoons{\ AP\ } O_2N-\!\!\langle\bigcirc\rangle\!\!-OH + HO-\overset{\overset{O}{\|}}{\underset{\underset{O^-}{\|}}{P}}-O^-$$
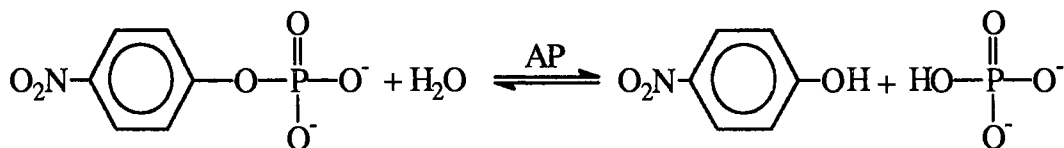
The sample solutions were 1.0×10^{-5} M p-NPP in 0.050 M carbonate buffer (pH 9.0) with different concentrations added phosphate. The rotating speed and time intervals were the same as for the amperometric detection described above.

Results and Discussion

Electrochemical characteristics of p-Aminophenylphosphate

The cyclic voltammograms of p-APP (Fig. 28) confirm that the expected compound has been synthesized, and that the compound behaves as expected in its AP-catalyzed reaction. The symmetric shape of the trace obtained by cyclic voltametry, Fig. 28, trace b, reveals an electrochemically reversible redox process for p-aminophenol, which is the product of the enzymatic reaction. The formal potential (the average of the anodic peak potential and the cathodic peak potential) for the reversible reaction was determined to be 0.020V against the Ag/AgCl reference electrode. The redox reaction on the surface of the electrode is:

$$H_2N-\!\!\langle\bigcirc\rangle\!\!-OH \xrightleftharpoons[+e^-]{-e^-} H_2N-\!\!\langle\bigcirc\rangle\!\!=O$$
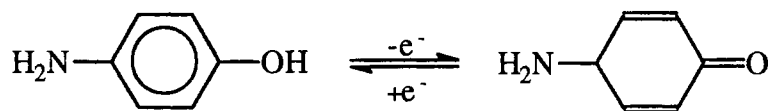
A literature value of 0.050 V has been reported [82]. In comparison with p-NPP, as shown in Fig. 29, trace b, and other substituted phenylphosphates [83,84], p-APP can be

93
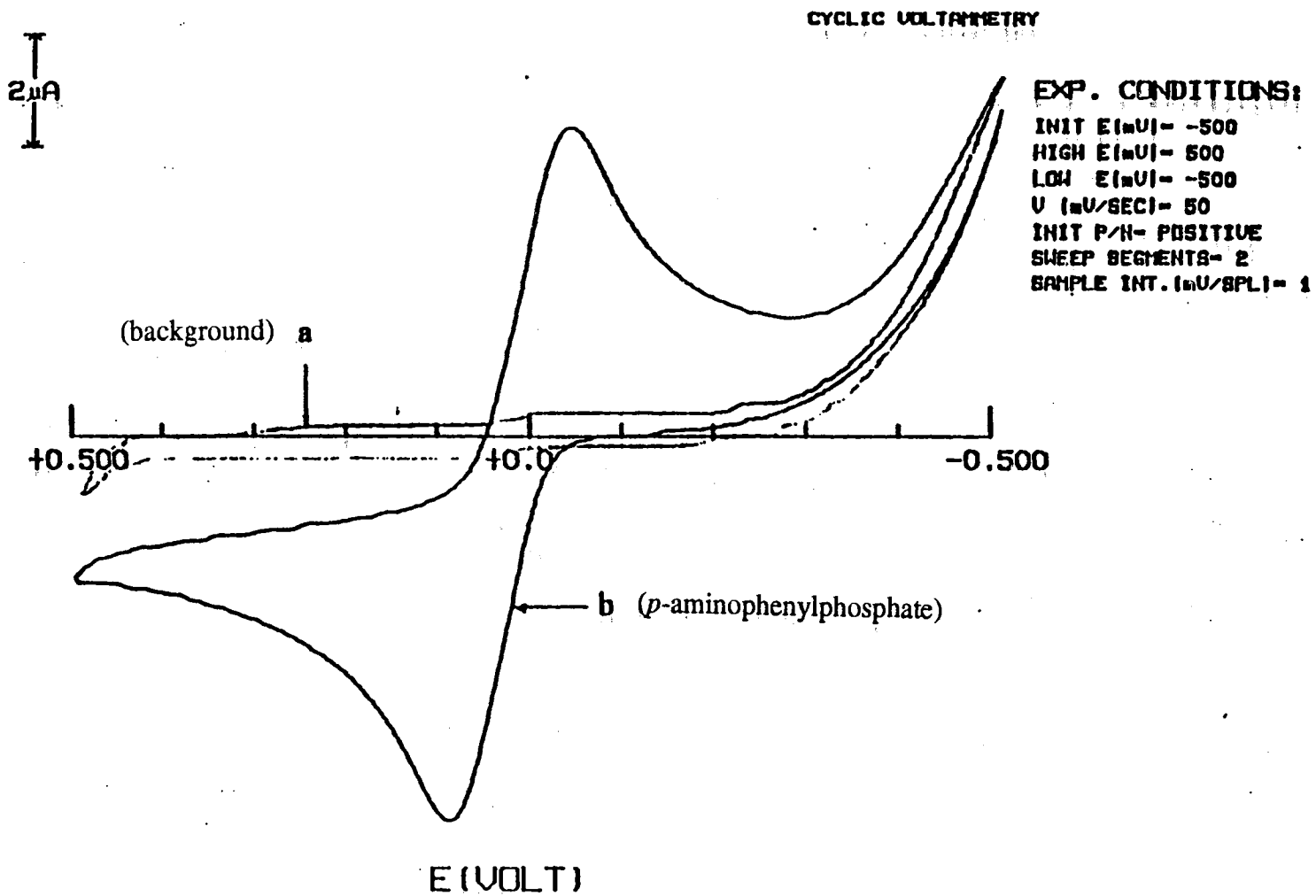
Figure 28. Cyclic Voltammogram of p-Aminophenylphosphate

2μA

EXP. CONDITIONS:
INIT E(mV)= -500
HIGH E(mV)= 500
LOW E(mV)= -500
V (mV/SEC)= 50
INIT P/N= POSITIVE
SWEEP SEGMENTS= 2
SAMPLE INT.(mV/SPL)= 1

(background) a

+0.500   +0.0   -0.500

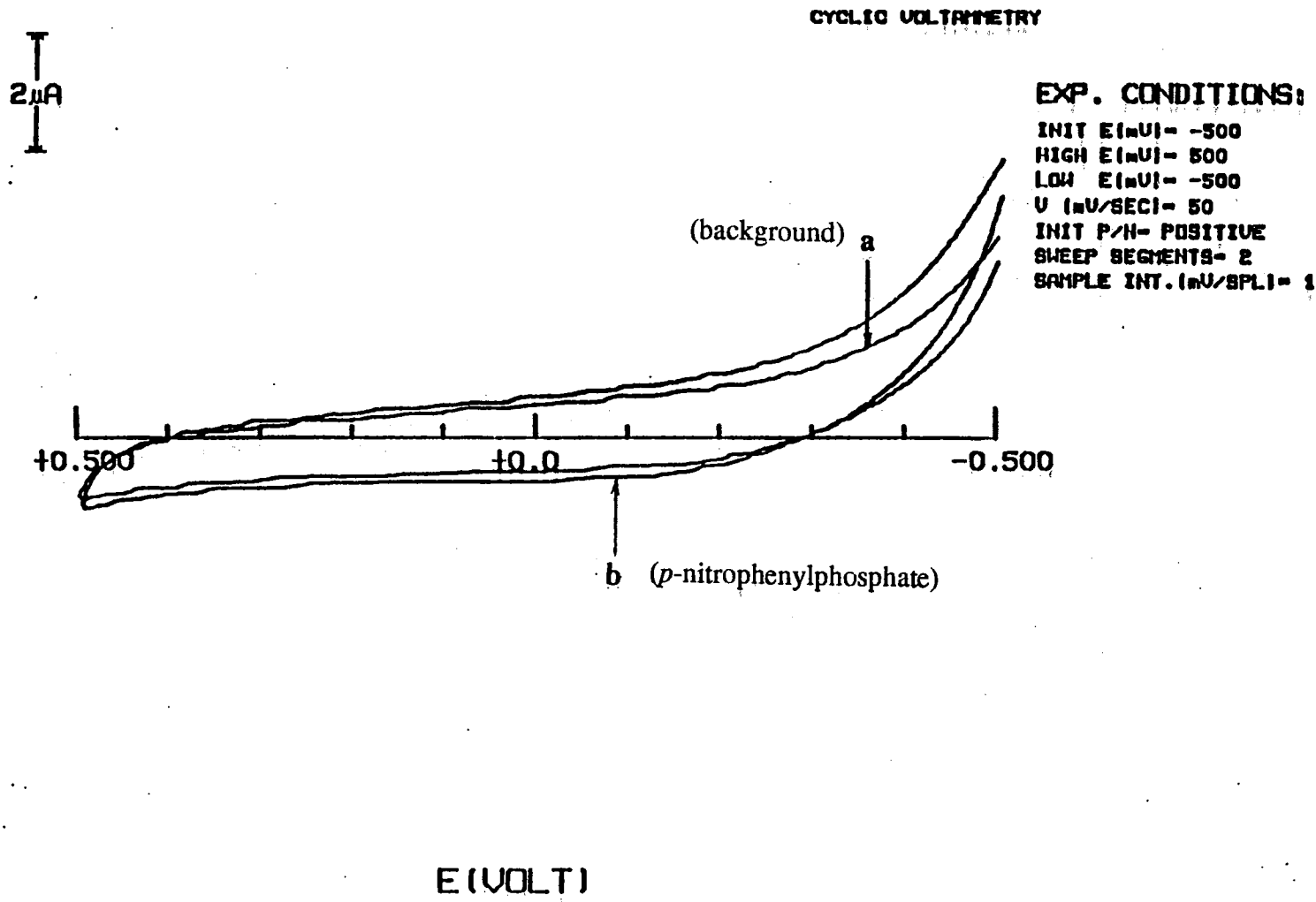b   (p-nitrophenylphosphate)

E(VOLT)

Figure 29. Cyclic Voltammogram of p-Nitrophenylphosphate

detected at much lower oxidation potentials, lower background currents, and lower limits of detection (1.0×10^{-7} M in this work). Trace a in both Figure 28 and figure 29 is for the background.

Effects of Cell Volume, pH, Substrate Concentration
and Reactor Rotation

As discussed in the previous chapter, the cell volume affects the limit of detection. Therefore, the volumes of the amperometric cell and the photometric cell were optimized by sliding the upper part of the cells up or down, to 113 μL and 330 μL, respectively. Differing from photometric detection which requires enough volume to pass the light, the amperometric cell volume can be smaller to obtain a relatively high concentration of detecting species (*p*-aminophenol). When the volume was smaller than 113 μL, however, resistance to injection as well as rotation was observed.

The effect of rotation on the limit of detection of phosphate was not determined, but rotation was needed to reduce the diffusional constraints in both detection methods, especially with the amperometric detection. With the use of amperometric detection, the rotation reduced diffusional constraints: 1) for the substrate and product to reach or to leave the immobilized enzymatic active sites, and 2) for the electrochemically active product to reach the electrode surface. A rotation speed of 840 rpm was used for both photometric and amperometric detection. Vibration of the rotating disk was encountered when the speed was higher than 840 rpm, impairing the detection processes.

It has been reported that the optimum pH for the hydrolysis of phenylphosphate is between 8-9, and that a lower pH helps with the inhibition [85,86]. However, a lower pH decreases the activity of alkaline phosphatase. Therefore, the enzyme had to be used in a basic environment. The commonly used buffers in the pH range of 6 to 8 are phosphate and Tris buffers. Obviously, phosphate buffers could not be used in this work because phosphate was the determined analyte. Tris buffers could not be used in this work either, because it is a phosphate acceptor which can introduce changes in the phosphate concentration. Consequently, a 0.10 M glycine buffer (pH 8.3) was used in this work to test the pH effect on inhibition. No significant change was found, however. Finally, a 0.050 M carbonate buffer was used in all subsequent measurements for phosphate determination.

In using the competitive inhibition approach to determine the inhibitor concentration, a lower substrate concentration needed to be used because it helps with the binding of inhibitor to the enzyme active site and makes the αK_M term predominant, as has been discussed previously. Therefore, in both amperometric and photometric detection, the values close to the lowest detectable substrate concentrations (1.0×10^{-7} M and 1.0×10^{-5} M) were used for the determination of phosphate.

Effect of Rotation of Reactor on the Applied Electrode
Potential for Amperometric Detection

Figure 30 is the hydrodynamic voltammogram of p-APP in 0.050 M carbonate buffer (pH 9.0) determined by using the rotating bioreactor/amperometric cell at a rotating speed of 840 rpm. This hydrodynamic voltammogram shows that the signal
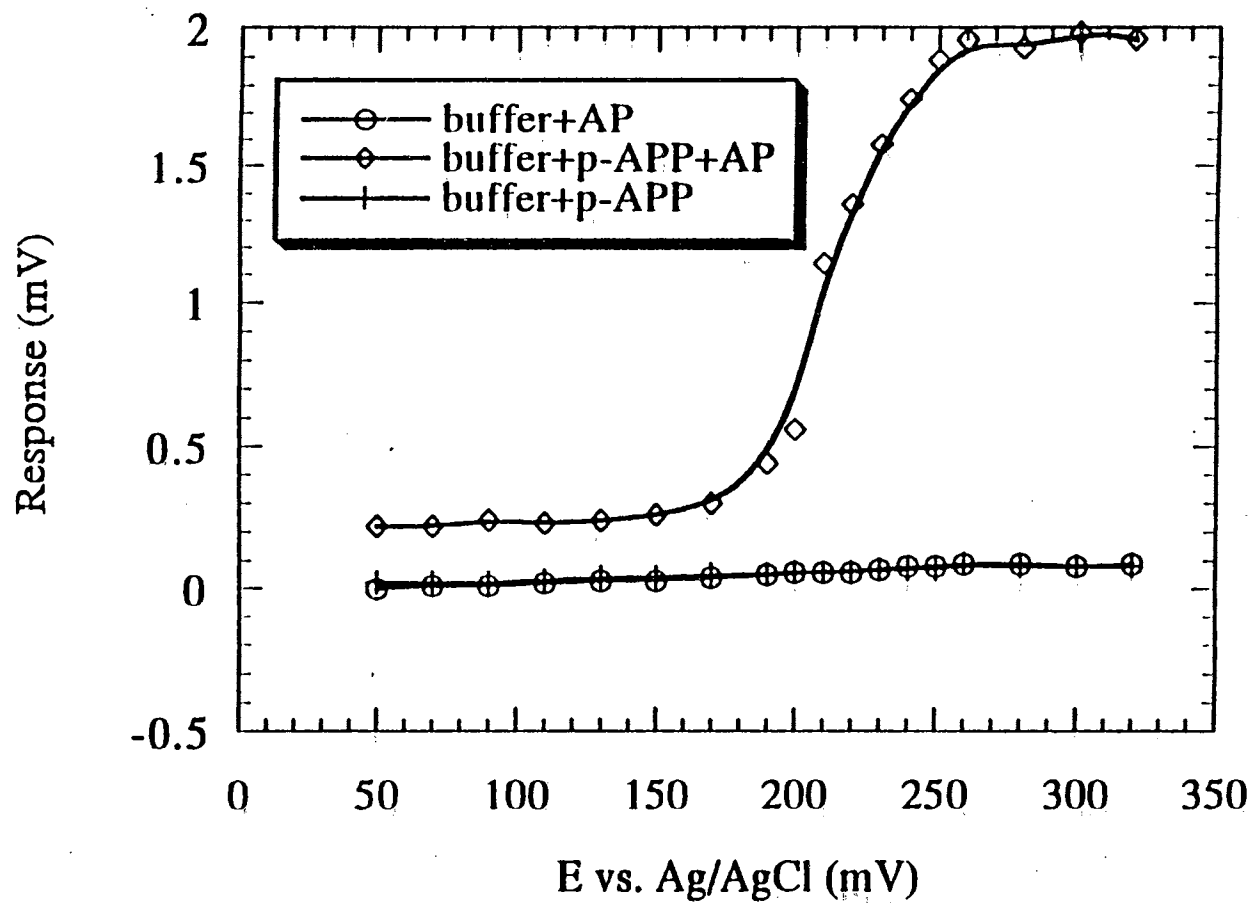
97

Figure 30. Hydrodynamic Voltammogram of p-Aminophenylphosphate
in the Bioreactor/Amperometric Cell

response reached a maximum after the applied electrode potential was higher than 250 mV vs. the Ag/AgCl reference. This was different from the formal potential of 20 mV obtained by cyclic voltammetry because of the influence of rotation and the different geometric shape of the electrochemical cells used in cyclic voltammetry and in hydrodynamic voltammetry. Therefore, to ensure amperometric detection, an applied electrode potential of 300 mV vs. the Ag/AgCl reference was used in all the amperometric detections used in these studies.

Determination of Phosphate Concentration

Results for the determination of phosphate using amperometric and photometric detection are presented in Table VII. For both amperometric and photometric detection, when the phosphate concentration was lower than 1.0×10^{-5} M, the rate of response did not change significantly. Therefore, the limits of detection for both detection methods were estimated to be 1.0×10^{-5} M. Comparing these two detection methods, amperometric detection was somewhat more sensitive than photometric detection because the change in the rate of response with phosphate concentration in amperometric detection is greater than that in photometric detection. The reasons for the poorer sensitivity of the photometric detection are the dispersion of the detecting species (p-nitrophenol), presumably due to the greater bioreactor/photometric cell volume (330 μL) than that of the bioreactor/amperometric cell (113 μL), and the relatively higher substrate concentration used. In addition, electrochemical detection is, in general, more sensitive than absorbance measurements. The limits of detection for both detection techniques are lower than those that have been previously reported (1.0×10^{-4} M) by Guilbaut [74],

TABLE VII

DETERMINATION OF PHOSPHATE WITH AMPEROMETRIC AND PHOTOMETRIC DETECTION

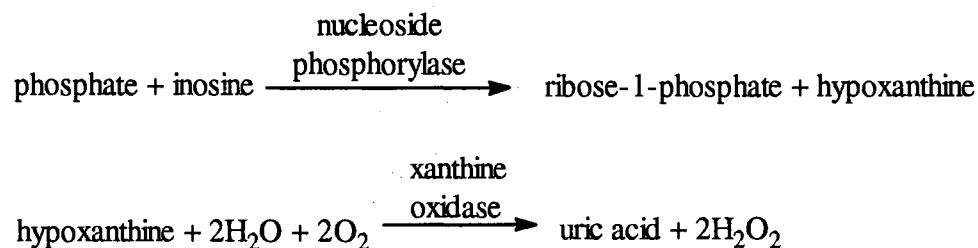| posphate concentration (M)	rate of response (amperometric)	rate of response (photometric)
0	67.9 ± 0.3	65.0 ± 0.5
1.0×10^{-6}	68.1 ± 0.4	65.0 ± 0.3
1.0×10^{-5}	63.3 ± 0.5	64.7 ± 0.3
1.0×10^{-4}	45.8 ± 0.3	54.2 ± 0.3
1.0×10^{-3}	26.8 ± 0.3	42.8 ± 0.4

* The determinations were based on 6 measurements at each concentration for both amperometric and photometric detection.

Cornel [75], and Weetall [76]. However, they still cannot be used for detecting phosphate

concentrations lower than the criteria suggested by the EPA (8.1×10^{-7} M phosphate, or

$25\mu g$ of phosphorus in 1L). Therefore, no real water samples were tested. The reason that

it was not possible to reach the criteria set by the EPA in this work can be traced to the

indirect nature of the approach employed. In indirect approaches, the limit of detection for

both amperometric and photometric detection were limited by the value of the AP-

phosphate dissociation constant K_I. As discussed previously, if [I] << K_I, $\alpha \rightarrow 1$, there is no

more inhibition detectable. A K_I value of 1.9×10^{-5} M has been reported in pH 8.0 Tris

buffer by Levine et al. [86]. Because a lower pH helps with the inhibition, as discussed

previously, the value of K_I at pH 9.0 in this work should be greater or equal to 1.9×10^{-5} M.

Therefore, when the inhibitor concentration was lower than 1.0×10^{-5} M, the rate of

response did not change for either amperometric or photometric detection. It could be

concluded that the limit of detection for the indirect approach cannot be much lower than

1.0×10^{-5} M. This work has shown that the design of the bioreactor/detector cells and the

UCF system improved the limit of detection from 1.0×10^{-4} M, obtained by using other

indirect enzymatic methods with the same enzyme, to 1.0×10^{-5} M. This is presumably

because the rotation reduced diffusion constraints in the cells, and the UCF system

provided a very precise reagent processing approach.

Conclusion

In this research, an indirect enzymatic approach was explored for the determination

of phosphate in aqueous solution. The approach is based on the inhibition by phosphate

of the hydrolysis reaction of phenyl esters, which is catalyzed by alkaline phosphatase.

Two different substrates, p-APP and p-NPP, were used with two different modes of

detection: amperometric and photometric, respectively. Therefore, two different

bioreactor/detector cells were used in conjunction with an UCF system. The results show

that amperometric detection provided better sensitivity than did photometric detection.

Although, both of the detection methods could not reach the EPA suggested limit for the

concentration of phosphate in water, they had better limits of detection than those

reported using the same enzyme but different substrates or different experimental

arrangements (reactor). This means that the design of the bioreactor/detectors and the

UCF system resulted in an improvement over existing indirect methods using the same

enzyme. For future study of the enzymatic determination of phosphate in water samples, a

direct approach should be attempted. For example, see the following coupled reactions:

$$\text{phosphate} + \text{inosine} \xrightarrow{\text{nucleoside phosphorylase}} \text{ribose-1-phosphate} + \text{hypoxanthine}$$

$$\text{hypoxanthine} + 2H_2O + 2O_2 \xrightarrow{\text{xanthine oxidase}} \text{uric acid} + 2H_2O_2$$

In the coupled reactions, 1 mole of phosphate in the first reaction leads to 3 moles of

electroactive species in the second reaction (1 mol of uric acid and 2 moles of H_2O_2).

Therefore, such a biological amplification could provide a sensitive amperometric

determination of phosphate. This could be envisioned by use of the rotating

bioreactor/amperometric cell and a UCF system described here.

EPILOGUE

The studies described in this dissertation demonstrate that unsegmented continuous flow (UCF) can be successfully employed for the determination of 1) the molecular diffusion coefficients of some Fe(II) complexes with ligands containing the =N-C=C-N= moiety, 2) glucose concentration in serum samples, and 3) phosphate in aqueous solutions.

In order to give a better description of UCF and its applications, the history of UCF, the important role of UCF in analytical chemistry, and the general conformation of UCF systems were reviewed first in this dissertation. Then, for each of the applications described in this research, the principles of the determinations, the design of the particular UCF systems, and the experimental procedures were discussed. At the end of each chapter, experimental results were compared with the existing methods and the experimental phenomena were discussed. In the enzymatic approaches, immobilized enzymes and rotating bioreactors were employed. The use of the rotating bioreactors reduced the diffusional constraints which are commonly observed when immobilized enzymes are used for the studies of biosensers. All the results obtained in this research confirm the advantages of using UCF in analytical chemistry: simplicity, reproducibility, small sample size requirement, accuracy, high sampling rate, low cost, and extreme versatility.

Unsegmented continuous flow has been increasingly recognized as a very powerful technique in analytical chemistry. The applications of unsegmented continuous flow have gone into many areas. This dissertation touches only a few of the many areas of UCF, but its contribution to UCF is of significance.

LITERATURE CITED

[1] P.E. Pungor, Zs. Fener and G. Nagy, *Anal. Chim. Acta*, **52**, (1970) 47.

[2] J.D. Frantz, P.E. Hare, *Carnegie Institution of Washington Year Book 72*, 700.

[3] H.U. Bergmeyer and A. Hagen, Frisenius Z. *Anal. Chem.*, **261**, (1972) 333.

[4] V.V.S. Eswara Dutt and H.A. Mottola, *Anal. Chem.*, **47**, (1975) 357.

[5] W.J. Blaedel, G.P. Hicks, *Anal. Chem.*, **34**, (1962) 388.

[6] J. Ruzicka and E.H. Hansen, *Anal. Chim. Acta*, **78**, (1975) 145.

[7] K.K. Stewart, G.R. Beecher and P.E. Hare, *Anal. Biochem.*, **70**, (1976) 167.

[8] H.A. Mottola, *Anal. Chem*, **53**(12), (1981) 1312.

[9] B. Karlberg and S. Thelander, *Anal. Chim. Acta*, **98**, (1978) 1.

[10] O. Astrom, *Anal. Chem.*, **54**, (1982) 90.

[11] H. Baadenhuijsen and H.E.H. Senuren-Jacobs, *Clin. Chem.*, **25**, (1979) 443.

[12] C.S Lim, J.N. Miller and J.W. Bridges, *Anal. Chim. Acta*, **114**, (1980) 183.

[13] G. Hohansson and L. Ogren, *Anal. Chim. Acta*, **145**, (1983) 71.

[14] J. Ruzicka, *Analyst*, **199**, Sept. 1994, 1925.

[15] H.A. Mottola, *Anal. Chim. Acta*, **180**, (1986) 26.

[16] G.E. Pacey, D.A. Hollowell, K.G. Miller, M.R. Straka and G. Gordon, *Anal. Chim. Acta*, **179**, (1986) 259.

[17] P. Dejardin, M.T. Le, J. Wittmer and A. Johner, *Langmuir*, **10**, (1994) 3898.

[18] H.A. Mottola and A. Hanna, *Anal. Chim. Acta*, **100**, (1978) 167.

[19] K. Matsumoto, J.J.B. Baeza and H.A. Mottola, *Anal. Chem.*, **65**, (1993) 636.

[20] W.C. Cardiner Jr., *Rates of and Mechanisms of Chemical Reactions*, Benjamin, New York, 1969, 165-70.

[21] J.C. Giddings, *Unified Separation Science*, Wiley, New York, 1991.

[22] A.J. Bard and L.R. Faulkner, *Electrochemical Methods: Fundamentals and Applications*, Wiley, 1980,127-134.

[23] H.R. Nahler and E.H. Cordes, *Biological Chemistry*, Harper and Row, New York, 2nd Ed., 1971.

[24] A. Fick, *Pogg. Annln*, **94**, (1855) 59.

[25] H.J.V. Tyrrell, *J. Chem. Educ.*, **41**, (1964) 397.

[26] A. Einstein, *Annln Phys.*, **17** (1905) 549.

[27] G.G. Stokes, *Mathematical and Physical Papers*, Vol.3, Cambridge University Press, 1903.

[28] H.J.V. Tyrrell and K.R. Harris, *Diffusion in Liquids: a Theoretical and Experimental Study*, Butterwouths, London, 1984, Chapter 5.

[29] A.J. Easteal, *Can. J. Chem.*, **68**, (1990) 1611.

[30] P. Stilbs, *Prog. NMR Spectrosc.*, **19**, (1987) 1.

[31] A. Sucheta and J.F. Rusling, *Electroanalysis*, **3**, (1991) 735.

[32] G. Denuault, M.V. Mirkin and A.J. Bard, *J. Electroanal. Chem.*, **308**, (1991) 27.

[33] G. Taylor, *Proc. R. Soc. London*, **219**, ser. A, (1953) 186.

[34] D. Betteridge, W.C. Cheng, E.L. Dagless, P. David, T.B. Gooad, D.R. Deans, D.A. Newton and T.B. Pierce, *Analyst*, **108**, (1983) 17.

[35] G. Gerhardt and R.N. Adams, *Anal. Chem.*, **54**, (1982) 2618.

[36] A. Griffiths, *Proc Phys. Soc.*, **219**, (1911) 190.

[37] J.G. Atwood and J. Goldstein, *J. Phys. Chem.*, **88**, (1984) 1875.

[38] D. Robinson, J.E. Anderson and J. Lin, *J. Phys. Chem.*, **94**, (1990) 1003.

[39] W.A. Boyle, R.F. Buchholz, H.A. Beal and J.L. McCarthy, *J Appl. Ploym. Scien.*, **42**, (1991) 1969.

[40] W. Loh, A.E. Beezer and J.C. Mitchell, *Langmuir*, **10**, (1994) 3431.

[41] W. Loh, C.A. Tonegutti and P.L.O. Volpe, *J. Chem. Soc. Faraday Trans.*, **89** (1), (1993) 113.

[42] J. Ruzicka and E.H. Hansen, *Anal. Chim. Acta*, **99**, (1987) 37.

[43] V. Ananthakrisgnan, W.N Gril and A.J. Bardhum, *AIChE. J.*, **11**, (1965) 1063.

[44] J.T. Vanderslice, K.K. Stewart, A.G. Rosenfeld and D. Higgs, *Talanta*, **28**, (1981) 11.

[45] J.T. Vanderslice, A.G. Rosenfeld and G.R. Beecher, *Anal. Chim. Acta*, **179**, (1986) 119.

[46] H. Bate, S. Rowland, J.A. Sirs and H.W. Thomas, *Brit. J. Appl. Phys. (J. Phys. D.)*, **2**, (1969) 1447.

[47] B. Carnhan, H.A. Luther and O.J. Wilkes, *Applied Numerical Methods*, Wiley, New York, 1969, 270.

[48] J.T. Vanderslice, G.R. Beecher and A.G. Rosenfeld, *Anal. Chem.*, **56**, (1984) 293.

[49] G. Gerhardt and R.N. Adams, *Anal. Chem.*, **54**, (1982) 2618.

[50] D. Robinson, *Ph.D. Dissertation*, Dept. of Chem., Boston College, Chestnut Hill, MA, 1990.

[51] M. Bonakdar, J. Yu and H.A. Mottola, *Talanta*, **36**, (1989) 219.

[52] D.S. Turnham, in G.J. Hills (Ed.), *Polarography 1964*, Vol. **1**, Macmillan, London, 1966, 535.

[53] I.M. Kolthoff and J.J. Lingane, *Polarography*, 2nd Ed., Interscience, New York, 1952.

[54] D. Harak, *Ph. D. Dessertation*, Dept. of Chemistry, Oklahoma State University, Stillwater, OK, August,1995.

[55] H.A. Mottola and H.B. Mark, Jr., *Anal. Chem.*, **56**, (1984) 96R.

[56] J. Raba and H.A. Mottola, *Anal. Biochem.*, **220**, (1994) 297.

[57] A. Kadish and D. Hall, *Clin. Chem.* **9**, (1965) 869.

[58] M. Nanjo and G.G. Guilbault, *Anal. Chim. Acta*, **73**, (1974) 367.

[59] H. Nilsson, A, Akerlund, and K. Mosbach, *Biochim. Biophys. Acta*, **320**, (1973)529.

[60] A.S.Keston, *Abstracts, 129th National Meeting of the American Chemical Society*, Dallas, TX, April 1956, p31C and 32C, Abstract No. **76**.

[61] G.E. Briggs and J.B.S. Halane, *Biochem. J.*, **19**, (1925) 338.

[62] H. Linweaver and D.J. Burk, *J. Am. Chem. Soc.*, **56**, (1934) 568.

[63] J. Konecny, in *Survey of Progress in Chemistry*, Vol. **8**, Acdemic Press: New York, (1977) 195.

[64] D.R. Walt and V.I. Agayn, *Trends in Analytical Chemistry*, Vol. **13**, No. 10, (1994)

425.

[65] J.J. Beeza Baeza, K. Matsumoto and H.A. Mottola, *Anal. Chim. Acta*, **283**, (1993) 785.

[66] L. Gorton and L. Ogrren, *Anal. Chim. Acta.*, **130** (1981) 45.

[67] E. Eisenstaedt, *J. Org. Chem.*, **3**, (1938) 153.

[68] L. Doldstein, Y. Levin and E. Katchalski, *Biochemistry*, **3**, (1964) 1913.

[69] L. Doldstein and E. Katchalski, *Fresenius'Z. Anal. Chem.*, **243**, (1968) 375.

[70] D.L. Massart, B.G.M. Vanseginste, S.N. Deming, Y. Michote and L. Kaufmam, *Chemometrics: A Textbook*, Elservier, Amsterdam, (1988) 41.

[71] D.G. Christian, *Analytical Chemistry*, 2nd Ed., Wiley and Sons, New York, (1977) 74.

[72] United States Environmental Protection Agency, Office of Water Regulations and Standards, Washington, D.C. 20460., *EPA* **440/5-86-001**, May 1, 1986.

[73] C.H. Fiske and Y. Subbarow, *J. Bio.Chem.*, **44**, (1925) 375.

[74] G.G. Guilbault and M. Nanjo, *Anal. Chim. Acta*, **78**, (1975) 81.

[75] N.W. Cornell, M.G. Leadebetter, and R.L. Weech, *Anal. Biochem.*, **95**, (1979) 524.

[76] P.R.N. Kind and E.J. King, *J. Clin. Pathol*, **7**, (1954) 322.

[77] H.H. Weetall and M.A. Jacobson, *IFS: Ferment. Technol. Today*, Proc **IV**, (1972) 361.

[78] A.P. Schaap, M.D. Sandison and R.S. Handley, *Tetrahedron Lett.*, **28**, (1987) 1159.

[79] J. Kulys, V. Razumas and A. Malimanskas, *Soviet Union Patent* **873121**, Oct. 15, 1981.

[80] R.Q. Thompson, G. C. Barone III, H.B. Halsall and W.R. Heineman, *Anal. Chem.*, **192**, (1991) 90.

[81] A. Garen and C. Levinthal, *Biochem. Biophys. Acta*, **38**, (1960) 470.

[82] H.T. Tang, G.E. Lunte, H.B. Halsall and W.R. Heineman, *Anal. Chim. Acta*, **214**, (1988) 187.

[83] K.R. Wehmeyer, M.J. Doyle, D.S. Wright, H.M. Eggers, H.B. Halsall and W.R. Heineman, *J. Liq. Chromatogr.*, **6**, (1983) 2141.

[84] M.J. Dolye, H.B. Halsall and W.R. Heineman, *Anal. Chem*, **56**, (1984) 2355.

[85] H.N. Frenley and P.G. Walker, *Biochem. J.* **104**, (1967) 1019.

[86] D. Levine, J. Reid and I.B. Wilson, *Biochem.*, Vol. **8**(6), (1969) 2374.

$\mathcal{2}$

VITA

Shaofeng Li

Candidate for the Degree of

Doctor of Philosophy

Thesis: BASIC AND APPLIED STUDIES WITH UNSEGMENTED CONTINUOUS FLOW SYSTEMS

Major Field: Chemistry

Biographical:

Personal Data: Born in Tianjin, P. R. China, May 16, 1958, the son of Hao Li and Lin Zhao.

Education: Graduate from Hepinglu Middle School, Tianjin, China, in July 1974; received Bachelor of Science Degree in Chemistry from Nankai University, Tianjin, China in January, 1982; completed requirements for the Doctor of Philosophy degree at Oklahoma State University in December, 1995.

Professional Experience: Engineer and Assistant Lab Manager, China National Research Center for Certified Reference Materials, Beijing, China, February, 1982 to July, 1990; Visiting Scholar, University of Manchester, England, September, 1985 to November, 1986; Teaching Assistant, Department of Chemistry, Oklahoma State University, August, 1990 to May, 1995; Technical Director, Analytical Products Group, Inc., Ohio, June, 1995 to present.